



Unione Europea



*Ministero dell'Istruzione,  
dell'Università e della Ricerca*



UNIVERSITÀ DEGLI  
STUDI DI SALERNO

## **FONDO SOCIALE EUROPEO**

**Programma Operativo Nazionale 2000/2006**

**“Ricerca Scientifica, Sviluppo Tecnologico, Alta Formazione”**

**Regioni dell’Obiettivo 1 – Misura III.4**

**“Formazione superiore ed universitaria”**

***Department of Industrial Engineering***

***Ph.D. Course in Industrial Engineering***

***Curriculum of Mechanical Engineering***

***(XVI Cycle-New Series, XXX Cycle)***

**Tesi di Dottorato in:**

### **ANALYSIS AND ENHANCEMENT OF RESIN FLOW IN LIQUID COMPOSITE MOLDING PROCESS**

**Supervisor**

*Prof. Pierpaolo Carlone*

**Ph.D. student**

*Felice Rubino*

**Ph.D. Course Coordinator**

*Prof. Ernesto Reverchon*

**2017/2018**



# List of Publications

F. Rubino, V. Paradiso, P. Carlone. Flow monitoring of Microwave pre-heated resin in LCM processes. Proceedings of the 20th International ESAFORM2017 Conference on Material Forming, Dublin, Ireland, 26-28th April 2017

Pierpaolo Carlone, Felice Rubino, Valentino Paradiso, Fausto Tucci. Multi-scale modelling and on-line monitoring of resin flow through dual scale textiles in liquid composite molding processes. The International Journal of Advanced Manufacturing Technology (2018).  
<https://doi.org/10.1007/s00170-018-1703-9>. ISSN: 1433-3015

V. Paradiso, F. Rubino, P. Carlone, G. S. Palazzo. Resin flow analysis in a microwave assisted liquid composite molding process. XIII Convegno dell'Associazione Italiana di Tecnologia Meccanica AITEM 2017 Pisa, 11-13 Settembre 2017.

Dragan Aleksendrić, Costanzo Bellini, Pierpaolo Carlone, Velimir Ćirović, Felice Rubino, Luca Sorrentino. Neural-Fuzzy Optimization of Thick Composites Curing Process. Materials and Manufacturing Processes. Under review.



# Summary

List of Publications .....	3
Summary .....	I
List of Figures.....	V
List of Tables.....	XI
Abstract .....	XII
Introduction .....	XIII
Chapter 1: LIQUID COMPOSITES MOLDING PROCESSES .....	1
1. Introduction to the Liquid Composites Molding processes .....	1
1.1 Vacuum Assisted Resin Infusion. ....	2
1.2 Resin Transfer Molding (RTM).....	3
2. Challenging Issues of LCM Processes .....	3
2.1 The Effect of Process Variables on LCM manufactured laminates .....	4
2.1.1 Void Content .....	4
2.1.2 Fibre Reinforcement .....	5
2.1.3 Resin Formulation .....	5
2.2 Strategies to improve the LCM processes .....	5
2.2.1 Injection Strategies for LCM.....	5
2.2.2 Cycle Time Reduction Techniques for LCM.....	6
2.2.3 Injection Gate Location.....	7
2.2.4 Injection Pressure .....	8
2.2.5 Preform Permeability .....	8
2.2.6 Resin Viscosity.....	8
2.2.6.1 Mould Temperature .....	8
2.2.6.2 Preform Preheating .....	9
2.2.6.3 Resin Preheating .....	9

2.2.7 Microwave Processing of Polymers .....	9
2.2.7.1 Microwave Cure.....	10
2.2.7.2 Microwave Preheating.....	11
2.2.7.3 In-Line Microwave Processing .....	11
Chapter 2: MICROWAVE HEATING.....	13
1. Microwave and heating mechanisms .....	14
1.1. Electrical Volumetric Heating .....	15
1.3. Ohmic heating .....	16
1.4. Radio frequency heating .....	16
1.5. Microwave heating .....	17
2. Mechanisms of Microwave Heating.....	18
3. Dielectric properties of materials .....	23
4. Microwave Hardware .....	24
4.1. Microwave Ovens .....	24
4.2. Magnetron .....	25
4.3. Multimode Microwave Ovens.....	27
4.3.1. Single Mode Microwave Ovens.....	28
4.3.2. Nomenclature for Single Mode.....	28
4.4. Wave Guides .....	30
4.5. Rectangular Applicators.....	30
4.6. Cylindrical Applicators .....	31
5. The microwave system. ....	31
5.1. Microwave generator .....	32
5.2. Security monitoring device .....	33
5.3. Wave guides and resonance cavity. ....	34
5.4. Using of the microwave generator.....	37
6. Preliminary tests of the in-line microwave heating system .....	39
6.1. Results of the preliminary tests on the first configuration .....	39
6.2. Results of the preliminary tests on the second configuration .....	41
6.3. Results of the preliminary tests on the third configuration .....	45
Chapter 3: FLOW FRONT MONITORING.....	47

1. Monitoring of the resin flow front and the resin curing in the LCM processes. ....	47
1.1 Resistive sensors .....	48
1.1.2. resin flow monitoring.....	48
1.1.2. resin cure. ....	51
1.2. SMART-weave sensors .....	52
1.2.1 Principle of working .....	55
1.3. Ultrasonic sensors .....	57
1.4. Fiber optic sensors.....	60
1.5. Temperature sensors.....	64
1.4. Pressure sensors .....	66
1.6. Electric time-domain reflectometry (E-TDR).....	66
1.7. Dielectrical analysis (DEA) .....	71
2. Experimental set-up for monitoring of the resin flow .....	76
2.1 The LCM Mold .....	76
2.2. Dielectric Sensors.....	78
2.3 Pressure Sensors and data acquisition devices.....	80
2.4. Data acquisition devices .....	81
2.5. Materials .....	81
2.5.1 Glass fiber reinforcement .....	81
2.5.2 Resin liquid system.....	82
Chapter 4: EXPERIMENTAL RESULTS .....	83
1. Infusion test of un-heating resin .....	83
1.1. Materials and Experimental procedure.....	83
1.2 Result of the Test 1.....	84
1.2. Result of the Test 2.....	86
2. In-line preheating infusion test: Resonance cavity 1.....	90
2.1. Materials and Experimental procedure.....	90
2.1 Experimental results .....	91
3. In-line preheating infusion test: Resonance cavity 2.....	95
3.1. Materials and Experimental procedure.....	95
3.1 Experimental results .....	97

4. In-line preheating infusion test: Resonance cavity 3 .....	100
4.1. Materials and Experimental procedure .....	100
4.2. Experimental results .....	100
BIBLIOGRAPHY .....	105
Appendix A: NUMERICAL SIMULATION OF THE RESIN FLOW .....	113
1. Modelling of the resin flow in the liquid composite molding processes.	113
2. The developed model of the micro-scale resin flow.....	115
3. Results of the simulation.....	117

# List of Figures

*Figure I.1: LCM manufacturing processes.*

*Figure I.2. LCM process chain.*

*Figure I.2. LCM process chain.*

*Figure I.3. a) Single stream injection system; b) Twin stream injection system.*

*Figure II.1. Schematic representation of the in-line microwave resin pre-heating system integrated with the LCM process.*

*Figure II.1. The electromagnetic spectrum.*

*Figure II.3. Random dipole orientation in uncharged, equilibrium state.*

*Figure II.4. Reorientation of dipoles by an applied electric field.*

*Figure II.5. Dipole vibration due to an alternating electric field.*

*Figure II.6. Microwave absorption characteristics for conductor, insulator and absorber.*

*Figure II.7. Schematic of components comprising a domestic microwave oven.*

*Figure II.8. Typical magnetron for common domestic microwave oven.*

*Figure II.9. Scheme of the conventional magnetron.*

*Figure II.10. Working fundamentals of a magnetron: a) schematic representation of electric and magnetic fields; b) action of the magnetic forces on the electrons and behavior of the charges.*

*Figure II.11. Schematic of components comprising a single mode microwave oven.*

*Figure II.12. Electric field pattern within a  $TE_{102}$  mode rectangular applicator.*

*Figure II.13. Electric field pattern within a  $TM_{020}$  mode cylindrical applicator.*

*Figure II.15.  $TE_{101}$  mode rectangular applicator.*

*Figure II.16.  $TE_{020}$  mode cylindrical applicator.*

*Figure II.17. Microwave generator.*

*Figure II.18. Detector MARTEK 500.*

*Figure II.19. a) Sketch of the tuner with the location of the three micro-screws; b) wave guide and tuner coupled.*

*Figure II.20. a) Resonance cavity; b) dimensions of the cavity.*

*Figure II.21. a) Front view b) rear view of the second cavity.*

*Figure II.22. Front view of the third cavity.*

*Figure II.23. Example of the measurement of power of the recipe listed in table II.2.*

*Figure II.24. Set up of the cavity 1 during the preliminary tests.*

*Figure II.25. Initial, final temperatures and temperature gradients achieved with the first cavity: the showed data are the average values obtained by the several tests performed with the same.*

*Figure II.26. Cavity 2: experimental set-up of the preliminary testing.*

*Figure II.27. Final temperatures and flow rates measured for Test 1 and Test 2 at different values of nominal power.*

*Figure II.28. Final temperatures and flow rates for Test 3 at different values of nominal power.*

*Figure II.29. Parameterized temperature gradients obtained with cavity 3at different values of power and flow rate.*

*Figure III.1. Circuit for measuring the sensor voltage  $V_s$  (scheme of lineal sensor).*

*Figure III.2. Typical response of lineal-voltage sensor for tow resin system.*

*Figure III.3. Response of a single point-voltage sensor when resin covers the poles.*

*Figure III.4. Variation of measured voltage during the curing process.*

*Figure III.5. Scheme of a SMARTweave sensor: the resistance network is formed by an excitation-sense pair (referred as sensor plane), with 3 excitation wires and 3 sense wires.*

*Figure III.6. Representation of the grid-like sensor system: the sensing threads are on a difference plane, so that they are perpendicular but not intersecting each other. A gap is formed between the wires that is the path with minimum resistance. At sensing gaps the resistance is measured.*

*Figure III.7. a) Electrically conductive threads are woven into the reinforcement fabric; b) the end of each threads can be easily displaced into the fabric in order to allow the clamping and the connection with the measuring device.*

*Figure III.8. Output voltage profile in a SMARTweave sensor: Resin IN and OUT refer to the voltage monitored at two distinct nodes, the inlet port and the vacuum point of the VARTM apparatus. Points a - c and points b - d refer to the peak values and zero voltage at inlet and vacuum point respectively.*

*Figure III.9. Representation of the 3D flow of the resin in a VARTM process with center inlet port.*

*Figure III.10. Response of an ultrasonic sensor: longitudinal sound velocity and relative attenuation versus of processing time trends.*

*Figure III.11. Ultrasonic measurement of preform impregnation and resin curing stage.*

*Figure III.12. Set-up of the optical fiber for measuring of the resin flow prior placing within the fiber preform.*

*Figure III.13a. Behavior of transmitted light in an optical fiber before the resin reaches the sensing point.*

*Figure III.13b. Behavior of transmitted light in an optical fiber after the resin reaches the bare spot.*

*Figure III.14. Typical signal from the optical fiber sensor.*

*Figure III.15. The optical fibers can be placed on different planes along the thickness of the laminate between the stacked fibers layers. The arrival of the resin on each sensing point is detected and the 3-D path can be reconstructed.*

*Figure III.16. Temperature profiles during the resin infusion in a RTM process in two different location of the heated mold: resin inlet point and mold periphery.*

*Figure III.17. Scheme of the E-TDR technique for flow monitoring:  $E_i$  and  $E_r$  are the voltage of emitted and reflected waves at a specific location respectively;  $Z_0$  is the characteristic impedance of the line;  $Z_d$  is the load or discontinuity impedance.*

*Figure III.18a. Example of planar E-TDR sensor response: voltage changes versus time trends.*

*Figure III.18b. Example of planar E-TDR sensor response: resin level measurement.*

*Figure III.19a. Scheme of E-TDR planar sensor.*

*Figure III.19b. Cross section of two wires sensor.*

*Figure III.20a. Scheme of the experimental setup for VARTM process.*

*Figure III.20b. Response of the TDR-F sensor to the arrival of resin flow at the sensing locations.*

*Figure III.21. Schematic representation of a parallel plate dielectric sensor integrated in a RTM tool.*

*Figure III.22. Dielectric monitoring of the resin fill front: capacitance as function of time.*

*Figure III.23. Dielectric measurement: a) correlation of dielectric property with the viscosity of the resin; b) correlation between the gelation and the ionic conductivity ; c) vitrification/full cure estimate by means of the dielectric data.*

*Figure III.24. Experimental setup: sensed die and acquisition system used in the flow tests.*

*Figure III.25. 3D sketch of the sensing mold.*

*Figure III.26. Drawings of the mold: a) bottom view of upper die; b) top view of lower die; c) Section A-A.*

*Figure III.27. a) 3D scheme of the designed shielding sensor; b) operating principles of a parallel plate dielectric sensors.*

*Figure III.28. Pressure sensor: Honeywell SSSDRNT100PAAA3.*

*Figure III.29. HM8118 LCR Bridge/Meter.*

*Figure III.1. Experimental and numerical results of the Test 1: a) pressure profiles; b) normalized capacitance and (extra-tow, intra-tow, and total) resin volume fractions; resin volume fraction when the resin arrive at the sensing locations c) S1, d) S2, and e) S3.*

*Figure III.2. Visual and experimental comparison of measure fill-front position.*

*Figure III.3. a) Normalized capacitance profiles, b) microstructure of a sample extracted in the region of the sensor S1, with evidence of the full saturation; c) microstructure of a sample extracted in the region of the sensor S3, with evidence of voids and unsaturated zones.*

*Figure III.4. a) Capacitance ( $C_s$ ) and dissipation factor ( $D$ ) during the curing stage at the sensor S1; b) resin degree of cure profiles evaluated in the sensing locations S1, S2 and S3 within the mold.*

*Figure III.5. Experimental set-up for the microwave in-line preheating tests with cavity 1.*

*Figure III.6. Pressure profiles at locations P2 and P3: comparison between the no-heating and preheating infusion tests.*

*Figure III.7. Normalized Capacitance measure by sensor S3: comparison between preheating and un-heating resin infusion test.*

*Figure III.8. Un-heated and preheated resin flow front advancement.*

*Figure III.9. Experimental set-up of the microwave in-line preheating tests with cavity 2.*

*Figure III.10. Result of the Test A: resin flow front progression for un-heating and preheating trials.*

*Figure III.11. Result of the Test B: a) resin flow front progression for un-heating and preheating trials; b) image of the composite laminate manufactured; micrographies of the laminate cross section in different location c) S1 and d) S3.*

*Figure III.12. Experimental set-up of the microwave in-line preheating tests with cavity 3.*

*Figure III.13. Microwave heating strategy.*

*Figure III.14. Resin flow front progression for un-heating and preheating trials.*

*Figure A.1. Microscopy observation of the manufactured laminates and 3D solid model of the representative volume element.*

*Figure A.2. Schematic of the domain and the applied boundary conditions.*

*Figure A.3 Streamlines of the inter-to flow in the representative volume element.*

*Figure A.4. Sink term variation as a function of the saturation.*

*Figure A.5. Sink term as a function of the inter-tow liquid pressure.*

*Figure A.6. Results of the regression analysis for the angular coefficient  $m(s)$ : a) third order polynomial model, b) fifth order polynomial model, c) seventh order polynomial model, d) exponential model.*

# List of Tables

*Table II.1. Constituents of microwave generator system.*

*Table II.2. Example of the power cycle executed by the microwave generator.*

*Table II.3. Average  $\Delta T$  at different power level achieved with the first cavity and for a heating liquid flow rate of  $7.8 \times 10^{-3}$  l/s.*

*Table II.4. Result of the heating trials for the Test 1 and Test 2.*

*Table III.1. Properties of the Polyester Resin.*

*Table A.1. Sink term parameters.*

# Abstract

The research activity was devoted to the study of the composite materials manufacturing processes. In particular, the liquid composite molding (LCM) processes were the object of the performed study. In recent years LCM processes have gained a widespread diffusion in different industrial fields, from civil to automotive and aerospace due to their several advantages compared to the conventional autoclave processes. However, some disadvantages related to a not uniform preform impregnation due to a local variation of the preform permeability, fibers bundles misalignment, that would results in dry zones or matrix richer areas, affect the LCMs limiting their usage in industrial full scale. Other limits are due to a limited pressure driving force as well as a reduced pressure compaction influencing the final volume fraction achievable with detrimental effects on the mechanical properties of the composite material product. A more deep knowledge of the phenomena involved in the manufacturing of the composite materials are required to implement proper control action on the parameters (e.g. pressure, resin flow rate, thermal cycle as well as inlet/vent locations) to optimize the process.

In order to improve the impregnation of the preform and reduce the time required to fully fill the mold cavity an in-line microwave preheating system was developed. The aims was to couple a microwave generator upstream the LCM mold to heat up the resin prior the entry into the mold. Indeed, the temperature increasing reduces the liquid viscosity allowing the resin to flow more freely through the dry preform. To perform a thorough study on the effectiveness of the proposed approach a laboratory scale apparatus for liquid composite molding processes was designed. The system was instrumented with ad-hoc designed sensors to monitor the resin flow during the process. Cheaper dielectric sensors are designed, produced and installed on the mold. A numerical model was also developed to simulate the resin flow through the fibers preform. The numerical model proved to be able to deal with the dual-scale nature of the textile preform commonly used in the LCMs, that are characterized by two different regions (inter- and intra-tow) with different values of permeability. The numerical outcomes were also used to validate the data obtained from the dielectric sensors. They demonstrated to be able to monitor the both the impregnation and the saturation of the fiber preform.

The developed microwave heating system proved to be effective to both reduce the total infusion time as well as improve the wetting of the fibers, achieving a more uniform impregnation with a limited amount of residual voids.

# Introduction

Liquid Composite Molding (LCM) processes are popular composite manufacturing methods which are used in the civil, aerospace, and automotive industry due their several advantages compared to other conventional production techniques like Autoclave processes. They include (but not limited to) net-shape production, high injection pressures, moderately low cycle times, simple tooling requirements as well as low VOx emissions to produce fiber reinforced polymer composites (FRPC). LCM have proved to be efficient for producing low-cost, high-quality and complex shaped composite parts. The LCM processes use a tailored stack of fibre reinforcements also known as preforms. Preforms, conventionally made of glass, carbon or Kevlar fibers, are usually manufactured from woven or stitched mats multiaxial orientated textile structures, or three dimensional weaves. The preforms can be produced exactly to fit the needs of the parts, designing the orientation and the arrangement of the fibers. Generally, it is possible to manufacture near net-shaped preforms and subsequently FRPC-parts. The term LCM summarizes different techniques, which present the same characteristics. Some of the most widespread LCM processing techniques are Vacuum Assisted Resin Infusion (VARI), and injection, e.g. Resin Transfer Molding (RTM), processes. Despite of the different developed techniques, the LCM processes essentially consists in several common stages. Initially the fiber preform is manufactured, as mentioned above. After the preform-manufacturing step, the preform needs to be saturated and impregnated during composite processing with a liquid matrix, a mixture of a polymeric resin and hardener. The matrix system replaces the air in the dry preform. The LCM processes start with placing the preform in a mold. The next step includes mold closing and preform compaction. After ensuring that the mold is closed the matrix impregnates the reinforcing structure. After the curing phase the part can be demolded and post processed. Combinations of composite manufacturing techniques, i.e. Vacuum Assisted Resin Transfer Molding (VARTM), are possible and used. Large scale components result in long distance flow paths determining several, e.g. long cycle times and increasing resin viscosity. To overcome these issues some techniques are developed, e.g. SCRIMP or ARTM, to improve the impregnation of the reinforcing structure. To date the LCM processes are still considered as “emerging” technologies compare to the well-established autoclave process that ensure high standard quality products, being their usage limited on an industrial full scale. Indeed, disadvantages affect the LCMs that can occur during processing along the whole process

chain. Several effects can be result of local variations of preform permeability, due to local differences in preform porosity or preform architecture. Race-tracking is a term which has been used to describe the deformation of the resin flow front. This effect can occur on edges, corners and other complicated areas in a mold. In order to eliminate these effects a careful mold design and a near net-shaped preform is needed. Low preform compaction and/or a high injection pressure can result in the effect of fiber wash out. Defects like matrix rich areas, bent or curved fibers and fiber buckling are leading to rim regions for those a mechanical post treatment, e.g. trimming, is necessary.

The effect of high speed processing on the mechanical properties and surface finish of RTM laminates has been investigated by several authors. Void content, reinforcement properties, and resin formulations have been shown to affect the quality of the laminates

Different strategies to improve the LCM processes in terms of improving of the products quality as well as reducing of cycle times and costs. These strategies can be related to different aspects of the process, such as the employed materials, tools as well as infusion/injection strategies.

The present research activity was devoted to the investigation of “In-line Resin Preheating” technique to improve the wettability of the fiber preform as well as reduce the overall impregnation time. Preheating of the resin system has a dual effect: it lowers the resin viscosity to facilitate flow and reduces the amount of heat that must be supplied by the heating apparatus to initiate polymerization. These factors promote reductions in both the impregnation and cure phases, resulting in an overall cycle time reduction. An in-line microwave resin preheating system basically consists in the heating of the resin during injection/infusion by means of a microwave system the provide the required heat to increase the resin temperature up to desired value. This technique is able to yield a true cycle time reductions, because it allows saving the time required to heat the resin before injection/infusion or flushing of the injection system after molding in the batch solution. The main challenge in the usage of in-line preheating system is related to the thermally sensitive nature of the thermosetting resin employed in the LCMs. A proper design of the microwave applicator is required to evenly heating the material. Indeed, under laminar flow conditions (that is the typical flow regime in the case of high viscosity liquids like the thermosetting resins) maximum velocity is developed along the flow axis, decreasing to zero at the wall of the transporting pipe. Uniform heating across the pipe diameter would cause an excessive heating of the liquid boundary layers at the pipe wall, with inadequate heating along the flow axis. It could results in a premature curing of the resin at the pipe wall or event the burning if the degradation temperature is exceeded.

The aim of the research activity was to investigate and developed a microwave system, including the microwave generator and the proper applicator, to preheat the resin prior the injection into the mold.

The study of the optimal solution has required the testing of different configuration of the microwave system, varying the geometry of resonance cavity and tuning the proper power-time cycle of the microwave source, as well as the simultaneously development of an sensing system integrated within the mould to monitor the composite manufacturing process. It also included the building up of a suitable numerical model able to predict the behavior of the resin during the infusion stage.

A laboratory scale sensing apparatus was designed and developed to reproduce a LCM manufacturing processes. The experimental system consisted in an aluminum mold with an inner cavity 3 mm deep. The little thickness of the manufacturable laminate and its bigger in-plane dimensions allow reproducing a monodimensional resin flow through the fiber bulk. The mold was instrumented with dielectric and pressure sensors. A video-camera was also mounted on the upper half-mold to perform a visual observation of the resin flow advancement independently of the experimental data provided by the sensors. The data from the pressure sensors coupled with the outcomes from numerical simulations were employed during a preliminary experimental campaign to validate the measurements obtained from the developed dielectric sensors. To this purpose, unreactive liquid system was employed and distinct process parameters configurations were adopted. The microwave system was carefully tested in order to evaluate the best configuration: preliminary heating tests were performed employing different resonance cavities and varying the flow rate within the pipe. The tests were needed to assess the proper microwave power and the exposition time of the resin to the electromagnetic field. The microwave system was set to provide a variable power during the infusion stage according to the decreasing resin flow rate.

In the first chapter a briefly description of the LCM processes is reported. The main features, drawbacks as well as the improvement strategies investigated in the recent years are debated. The second chapter is devoted to the microwave system. The main characteristics of a microwave generator and the working fundamentals are described. The developed laboratory-scale apparatus is also presented. The third chapter is focused on the monitoring system. The different techniques employed in the manufacturing of the composite materials are reported. Then, the dielectrical analysis fundamentals and the applications in LCM processes are described. The experimental apparatus, including mold, sensors and data acquisition system, is detailed in this chapter. In the four chapter the main results were reported and discussed. Then, proper conclusions about the research activity were drawn and debated.



# Chapter 1: LIQUID COMPOSITES MOLDING PROCESSES

## 1. Introduction to the Liquid Composites Molding processes

Liquid Composite Molding (LCM) processes are popular composite manufacturing methods which are used in the civil, aerospace, and automotive industry due their several advantages compared to other conventional production techniques like Autoclave processes. They include (but not limited to) net-shape production, high injection pressures, moderately low cycle times, simple tooling requirements to produce fiber reinforced polymer composites (FRPC) as well as low VOx emissions. LCM have proved to be efficient for producing low-cost, high-quality and complex shaped composite parts (Bickerton & Advani, 1999; Sozer, Bickerton & Advani, 2000). The LCM processes use a tailored stack of fibres reinforcements also known as preforms. Preforms, conventionally made of glass, carbon or Kevlar fibers, are usually manufactured from woven or stitched mats multiaxial orientated textile structures, or three-dimensional weaves (Bickerton & Advani, 1999). The preforms can be produced exactly to fit the needs of the parts, designing the orientation and the arrangement of the fibers. Generally, it is possible to manufacture near net-shaped preforms and subsequently FRPC-parts (Grieser, Rieber & Mitschang, n.d.; Weimer *et al.*, 2000b, 2000a). LCM processes are usually completed in several stages. Initially the fiber preform is manufactured, as mentioned above. After having finished the preform manufacturing step, it needs to be saturated and impregnated with a matrix system, a mixture of a polymeric resin and hardener. The matrix system replaces the air in the dry preform. The LCM processes start with placing the preform in a mold. The next step includes mold closing and preform compaction. After ensuring that the mold is closed, the matrix impregnates the reinforcing structure. After the curing phase the part can be demolded and post

## Chapter 1

processed (Bickerton & Advani, 1999; Kendall *et al.*, 1992). The term LCM summarizes different techniques, which present the same characteristics above described. Some of the most widespread LCM processing techniques are Vacuum Assisted Resin Infusion (VARI), and injection, e.g. Resin Transfer Molding (RTM), processes (see figure 1).

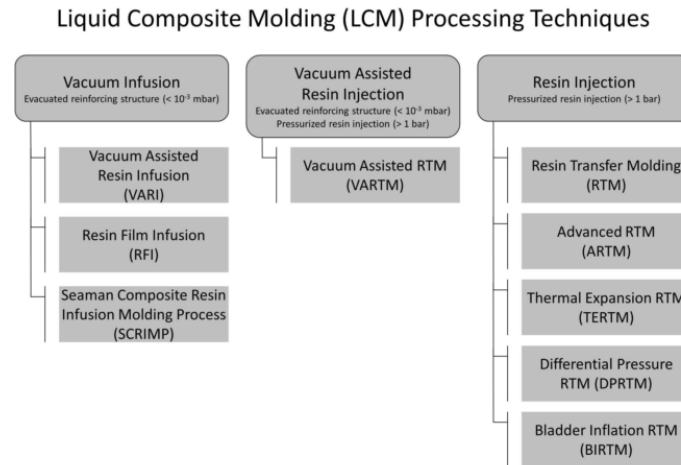


**Figure I.1:** LCM manufacturing processes (Schledjewski & Grössing, 2017)

Combinations of composite manufacturing techniques, i.e. Vacuum Assisted Resin Transfer Moulding (VARTM), is possible and used. Large scale components result in long distance flow paths determining several, e.g. long cycle times and increasing resin viscosity. To overcome these issues some techniques are developed, e.g. SCRIMP or ARTM, to improve the impregnation of the reinforcing structure (Becker & Mitschang, 2015).

### **1.1 Vacuum Assisted Resin Infusion.**

The VARI process is a simple and cost-effective technique to impregnate the dry reinforcement with a liquid resin system. A predefined preform is draped in a one-sided mold. It is covered by a peel ply, a distribution medium (plastic tubes and spiral hoses) and a vacuum bag. Around the mold, the vacuum bag is fixed with sealant tape, which also seals the cavity. By applying the vacuum within the vacuum bag, the preform gets compacted by ambient pressure. After opening a valve in the infusion tube, the resin flows under the vacuum bag and infiltrates the reinforcing bulk. After a complete impregnation, the valve is closed and the matrix system cures. The curing process can be aided by using a curing oven or a heating system. The maximum part sizes that can be handle with the VARI are limited by the maximum pressure difference of  $\Delta P < 1$  bars per injection points that can be

applied. Flow distribution medium and more injection points, placed along the part length are, are usually employed to overcome these limits, preventing the detrimental premature gelification of resin prior the complete impregnation of preform, and allow the infiltration of larger reinforcing structures, e.g. rotor blades of a wind energy plant. Different infusion strategies, like point, ring and line gates, make possible to control the infusion time and the flow impregnation progression. The mold manufacturing and the used equipment for a VARI are due to the requirements comparatively cost- effective. The process limitations are low fiber volume contents, generally  $< 50\%$ , a higher amount of voids due to the limited compaction action exerted by the ambient pressure, low quantities about up to 2000 parts/year as well as thickness restrictions of the part (Schubel, 2010; Modi *et al.*, 2009).

### ***1.2 Resin Transfer Molding (RTM)***

The RTM process, in contrast to the VARI process, utilizes a closed mold for processing FRP-parts. The two mould halves are usually mounted on a mold carrier, which ensures, with its closing force, a closed cavity during fluid injection. In contrast to VARI, no additional consumables are required. After placing the preform in the mould cavity the mold is closed, the preform is compacted to the final part thickness, and the liquid resin system is injected into the mould by a designed pressure or mass flow. After a successful impregnation, the mold halves can be heated in order to accelerate the curing reaction. The process cycle time depends on the part size, the part geometry, the part complexity and of course the injection strategy. As a result of full automated RTM processes, process cycle times between 5 – 25 minutes and a quantity of  $> 50000$  per year can be reached. The reinforcing structure has a huge and direct impact on the matrix flow behavior in the mold. The filling strategy i.e. the position of the injection and vent points of the mold, play a key role for the process success. Thus, the mold filling behavior should be considered during the mold design and mold development phase using numerical filling simulations in order to eliminate the very expensive trial-and-error procedure. The investment costs (a mold carrier, an injection unit, and a complex two-part mold) for RTM processing are more expensive compared to the VARI process. (Kendall *et al.*, 1992).

## ***2. Challenging Issues of LCM Processes***

Disadvantages for LCM can occur during processing along the whole process chain (see figure 2). Several effects can be result of local variations of preform permeability, due to local differences in preform porosity or preform architecture. The Race-tracking describes a deformation of the resin flow front that can occur on edges, corners and other complex areas in the mold. In order to eliminate these effects a careful mold design and a near net-shaped preform

## Chapter 1

is needed (Bickerton & Advani, 1999; Grieser, Rieber & Mitschang, n.d.). Low preform compaction and/or a high injection pressure can result in the effect of fiber wash out. Defects like matrix rich areas, bent or curved fibers and fiber buckling are leading to rim regions for those a mechanical post treatment, e.g. trimming, is necessary (Grieser, Rieber & Mitschang, n.d.).

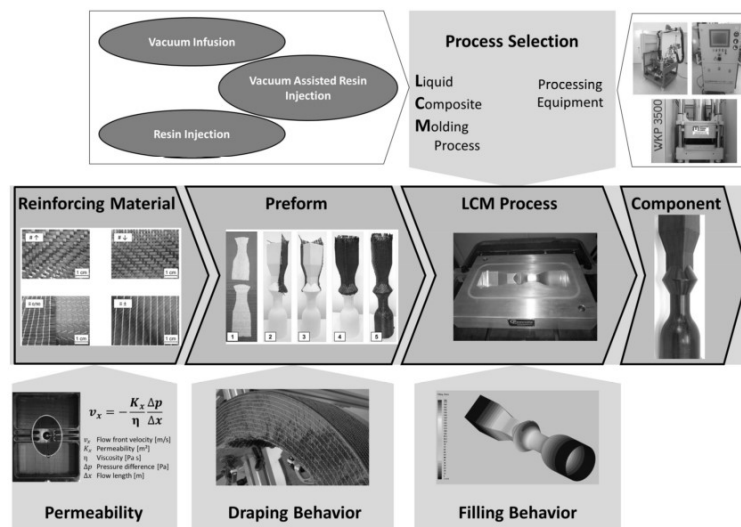


**Figure I.2.** LCM process chain

### 2.1 The Effect of Process Variables on LCM manufactured laminates

The effect of process variables on the mechanical properties and surface finish of RTM laminates has been widely investigated. Void content, reinforcement properties, and resin formulations have been shown to have a significant influence on the quality of the laminates.

#### 2.1.1 Void Content

Two mechanisms have been identified that promote voids formation in composites (Lundstrom & Gebart, 1994). Gas discharge into the resin due to the chemical reaction between the resin and catalyst is one cause of voids. A second mechanism for void formation is the mechanical entrapment of air during mold filling. This situation occurs when the longitudinal resin flow front (macro flow) exceeds the lateral flow of resin into the fiber bundles (micro flow). Macro flow is responsible for displacing the air within the reinforcement (wet-through), while micro flow allows the resin to wet and bond with the individual fibers (wet-out). Lundstrom and Gebart (Lundstrom & Gebart, 1994) stated that void content dropped significantly when a vacuum was drawn at injection, or pressure was applied during cure. Patel et al. (Patel,

## Liquid Composites Molding Processes

Perry & Lee, 1991) showed that low injection pressures increased the tensile strength of unidirectional reinforced polyurethane laminates. They attributed this result to improved micro flow for better fiber wet-out during the longer impregnation phase. These researchers also recorded higher tensile strengths for high temperature moldings as a result of enhanced wet-out due to lower viscosity, and greater chemical bonding between the fiber sizing and the resin.

### 2.1.2 Fiber Reinforcement

Young and Tseng (Young & Tseng, 1994) related fibre configuration to the degree of fibres wetting. They concluded that large bundle sizes in bidirectional woven roving reinforcements created flow channels between the bundles. Low filling speeds were necessary to allow sufficient wet-out without rapid advancement of the flow front down the channels. Fabrics with smaller fiber bundles could be filled faster with improved fiber wet-out. Moldings produced with unsaturated polyester resin and CFRM reinforcement coated in an unsaturated polyester sizing agent, produced the highest strength laminates due to good bond formation at the interface.

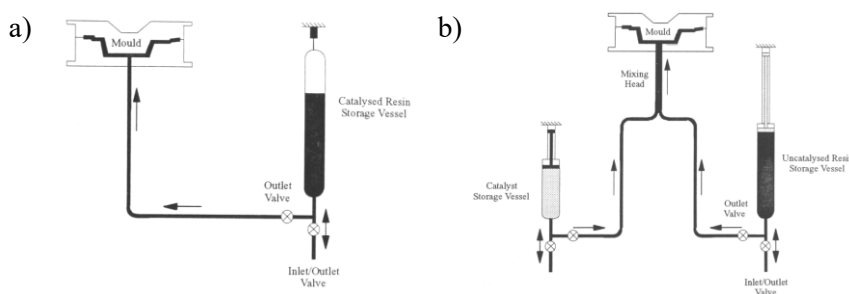
### 2.1.3 Resin Formulation

Lindsey (Lindsey, 1994) showed that increasing the catalyst concentration from 1 % to 3% (by mass) in polyester resin not only reduced cycle times, but also improved the strength of CFRM reinforced laminates. Furthermore, the addition of calcium carbon filler to polyester resin was determined to affect laminate mechanical properties. Rudd et al. (Rudd & Kendall, 1992) showed that increasing the filler content up to 50 phr increased the laminate mechanical properties, with decreases in properties occurring at higher concentrations

## 2.2 Strategies to improve the LCM processes

### 2.2.1 Injection Strategies for LCM

Figures I.3 illustrates the single stream and twin stream injection techniques typically used in liquid composite molding processes.



## Chapter 1

**Figure I.3.** a) *Single stream injection system;* b) *Twin stream injection system.*

SRIM is constrained to twin stream injection by nature of the chemically reactive resin systems. The resin and hardener streams remain separate until impingement mixing near the injection gate. Most RTM resin systems are thermally activated making twin stream injection possible, but not essential. The principal advantage of a twin stream delivery system is that the resin and catalyst components are non-reactive, and therefore, insensitive to temperature until mixing at the injection gate. Preheating large volumes of each component to increase resin reactivity is possible using simple conduction heating devices, although precise temperature control would be difficult to achieve. Highly reactive resin systems can be used with the qualification that the mold is filled, and fiber wet-out is sufficient, before the resin gels. Twin stream injection systems prevalent in industry for producing large components commonly are driven by reciprocating pumps. Pressure variations occur during the pump stroke using these systems. Karbhari et al. (Danideh & Sadeghzadeh, 2013)(Karbhari *et al.*, 1992) showed that decreasing the length of the pump stroke reduced the pressure variations and improved the mechanical properties of the laminate. Pulsed delivery of the individual streams leads to inaccurate dosing and has prompted the following investigators to implement constant volume, lance driven injection systems.. Measured resin quantities can be mixed before molding and stored in a pressure vessel. Delivery of the resin into the mold under constant pressure results in cavity pressures that are typically lower than for a reciprocating pump system (Kendall *et al.*, 1992). The primary disadvantage of single stream injection is that the pre-mixed resin is thermally sensitive. Resins with low reactivity at ambient temperature must be used to prevent premature cure within the storage vessel before injection has been completed. Single stream systems are dependent upon heat to initiate the polymerization reaction. Normally, heat is provided by the mold. Thermal quench at the injection gate due to cold resin entering the hot mold hinders the heat transfer capacity of the mold and extends cycle time. Preheating the resin to reduce mold quench is an obvious solution, however, the thermal sensitivity of the resin warrants special treatment to prevent premature cure within the injection system (Hill, 1993).

### 2.2.2 Cycle Time Reduction Techniques for LCM

Several authors have identified the process variables that affect cycle time and have suggested techniques to reduce this time. The interaction between process parameters makes isolation of a single factor difficult. Karbhari et al. (Karbhari *et al.*, 1992) performed a Taguchi study to quantify the interaction of several molding parameters including reinforcement types, mold

temperature, and injection strategies. They found that a short pump stroke had the greatest influence on the tensile, flexural, and shear properties of composites. From a broader standpoint, their work proposed a methodology to define a robust processing window for RTM. Other investigators have varied a single parameter then analyzed the resulting changes to the process. Cycle time comprises both the impregnation and cure phases. Most process models separate the phases into two separate events for simplicity (Kendall *et al.*, 1992) Resin flow during impregnation has been described by the Darcy relationship:

$$Q = \frac{KA}{\mu} \frac{dp}{dx} \quad (I.1)$$

Where the resin flow rate (Q) is proportional to the preform permeability (K), the flow area (A), and the pressure gradient (dp/dx), but inversely proportional to the resin viscosity ( $\mu$ ). Typically, reductions in the impregnation time will promote overall cycle time reductions. The cure phase consists of heat transfer into the stationary resin at the end of impregnation, followed by heat generation from the exothermic polymerization reaction. The rate of this reaction ( $d\alpha/dt$ ) is often expressed by the Kamal and Sourour expression (Kamal & Sourour, 1973):

$$\frac{d\alpha}{dt} = (k_1 + k_2\alpha)^m(1 - \alpha) \quad (I.2)$$

Where  $\alpha$  is the degree of cure and the kinetic constants are  $k_1$  and  $k_2$ . The end of the cure phase (and cycle time) can be defined as being equal to a pre-established percentage of conversion. Several RTM process variables that influence cycle time are discussed below.

### 2.2.3 Injection Gate Location

Gebart *et al.* (Gebart, Gudmundson & Lundemo, 1992) determined that the impregnation time was influenced strongly by the injection gate location. Three injection techniques were used to fill a square plaque mold including center pin gate injection, edge, and peripheral gate injection. Peripheral injection was approximately three times faster than edge injection and ten times faster than center injection as a result of a larger flow area for the resin. Lower impregnation times were assumed to result in proportional reductions in the cycle time. Rudd and Kendall (Rudd & Kendall, 1991) reported similar results for equivalent gating strategies. Peripheral and edge injection also reduced mold quench by increasing the area of the mold being subjected to cold incoming resin. Local cooling was limited, and the overall cycle time was reduced (Rudd & Kendall, 1992). However, the authors concluded that the pressure on the mold was greatest during peripheral injection, and least for center injection. Overfilling the mold increased the hydrostatic pressure and

## Chapter 1

caused significantly higher in-mold pressures during exotherm. High pressure, particularly in shell molds, could result in resin leakage, clamp damage, localized mold distortion, or part thickness variations.

### *2.2.4 Injection Pressure*

Increasing the pressure of a constant pressure injection system reduces the impregnation time. This results from an increased forcing pressure gradient is countered by a higher resin viscosity as in-mold heating of the flowing resin is decreased. Rudd et al. (Rudd, Owen & Middleton, 1990) concluded that the injection pressure affected the impregnation time to a greater extent than the cycle time since thermal quench was distributed over a larger portion of the mold. One disadvantage of high injection pressure is mold deflections. Selection of injection pressures beneath the mold damage threshold has been controversial. Some manufacturers argued that a low injection pressure improves fiber wet-out, while others claimed high pressure is necessary to purge air from the mold (Young & Tseng, 1994)

### *2.2.5 Preform Permeability*

Preform permeability is governed by fiber architecture and volume fraction. Highly permeable preforms reduce the restriction of resin flow, lowering the impregnation time. Peterson and Robertson (Peterson & Robertson, 1991) determined that for a given fiber volume fraction, increasing the fiber diameter increased reinforcement permeability, reducing the impregnation time. Increasing fiber bundle diameter also increased the resin flow rate, but void formation was a dominant effect.

### *2.2.6 Resin Viscosity*

Reducing resin viscosity improves resin flow through the preform, in turn lowering the impregnation time for constant pressure injection systems. Resin viscosity can be reduced by several means including mold temperature increases, preform preheating, and resin preheating. The influence of each of these parameters is described below.

#### *2.2.6.1 Mold Temperature*

Increasing the mold temperature heats the resin to a greater extent as it flows through the mold, reducing viscosity and shortening the impregnation phase. In addition, the cure phase can be reduced significantly by increasing the mold temperature since gel times across the mold are reduced. Thermal quench occurs when cold resin enters the hot mold, cooling the preform and mold. Kendall (Rudd & Kendall, 1992) determined that the overall cycle time was dictated by thermal quench at the injection gate. Perry et al. (Perry *et al.*, 1992) investigated the relationship between mold material and cycle time. The

## Liquid Composites Molding Processes

use of high thermal conductivity molds such as aluminum and chromed copper, shortened the cycle time compared to epoxy tooling, as a result of faster heat up after thermal quench, and a more even temperature distribution across the mold. In addition, peak exothermic temperatures were lower in the high conductivity molds since heat could be removed more effectively from the mold surface

### 2.2.6.2 Preform Preheating

Preheating the preform to the mold temperature (110° C) prior to injection under constant pressure was shown to reduce the impregnation time by 15% and the cycle time by 40% compared to molding produced with a colder preform (50°C) (Rudd, Owen & Middleton, 1990). The warm preform lowered the resin viscosity for improved flow, contributing to a reduction in impregnation time. Furthermore, the temperature within the mold cavity at the end of impregnation was greater so that the time to heat the quenched laminate back to mold temperature was reduced.

### 2.2.6.3 Resin Preheating

Preheating lowers the resin viscosity to facilitate flow, and reduces the amount of heat that must be supplied by the mold to initiate polymerization. These factors promote reductions in both the impregnation and cure phases, resulting in an overall cycle time reduction. Several techniques have been used to preheat the resin. Rudd et al. (Rudd, Owen & Middleton, 1990) fitted a heater jacket to the resin storage vessel to raise the temperature from 20°C to 55°C. A molding produced with preheated polyester resin reduced both the impregnation and cycle times by 20%. Hill (Hill, 1993) produced a similar result by preheating polyester resin in a domestic microwave oven to 60°C for a 50% reduction in cycle time. However, these cycle time reductions did not include the time required to heat the resin before injection or flushing of the injection system after molding. Subsequently, Hill developed a sophisticated in- line microwave resin preheating system that yielded true cycle time reductions, since the resin was heated during injection. Using this microwave system, a 35% reduction in cycle time by preheating resin to approximately 46°C was demonstrated.

### 2.2.7 Microwave Processing of Polymers

The time required to heat the stationary thermosetting resin at the injection gate to the activation temperature of the initiator dominates the cycle time (Rudd, Owen & Middleton, 1990). Industrial acceptance of microwave processing over conventional heating methods is increasing since microwave heating features high power density applicators, improved thermal control,

## Chapter 1

and reduced equipment size. Microwave processing is common in the rubber industry where extruded rubber is heated to the vulcanization temperature in a microwave oven in a continuous process. The food preparation industry has developed continuous microwave heating processes with the additional advantages of greater sanitation and pasteurization capabilities (Metaxas & Meredith, 1983). Industrial microwave systems dedicated to FRP processing are less developed although research in the following areas has been reported.

### 2.2.7.1 Microwave Cure

An early application of microwave cure in the composites industry was presented by Strand (Strand, 1980) who showed a thirty-fold reduction in the cure time of an iron-oxide filled epoxy resin. Glass fiber reinforcement impregnated with the resin was placed in a microwave transparent mold. The mold was located in a multimode oven for curing. The dielectric loss factor of the epoxy mold was relatively low compared to uncured liquid epoxy resin so that it absorbed only a small amount of the microwave power. The uncured resin, however, readily absorbed the microwave power and the cure time was reduced. Strand used the same technique to cure a polyester resin. Boey et al. (Boey, Gosling & Lye, 1993) modified an autoclave for microwave curing of glass reinforced epoxy components. Laminates were placed in a single-sided mold, vacuum bagged for consolidation, then placed in an autoclave that had been sealed to prevent microwave leakage. Microwaves were emitted from a horn directed towards the composite. A PC controlled stepper motor moved the horn along an X-Y plane over the surface of the component. Dosage levels were controlled by altering the microwave power or the traversing speed of the horn so that laminates of varying thickness could be cured more evenly. The addition of glass reinforcement into neat resin systems causes no microwave processing difficulties since most glasses are virtually transparent to microwave energy. However, use of carbon fiber reinforcement complicates microwave processing. Typically, the carbon fibers are longer than the microwave wavelength so that reflection occurs when the fibers are placed parallel to the electric field, and absorption when the fibers are oriented perpendicularly. Lee and Springer (Woo Il Lee & Springer, 1984) considered this to be a limitation for microwave processing of structural components since the carbon fibers would have a multidirectional orientation. Subsequently, Drzal et al. (Drzal, Hook & Agrawal, 1991) determined that the heated carbon fibers initiated cure in the epoxy by thermal conduction, with the advantage of improved interfacial bonding. The effects of microwave processing on laminate properties is disputed. Yue and Boey (Boey & Yue, n.d.) measured a 50% increase in the tensile modulus of epoxy by microwave curing as opposed to conduction curing. Hawley et al. (Hawley & Wei, 1991) claimed improved flexural properties for epoxy composites but did not quantify their results. Marand et al. (Marand, Baker & Graybeal, 1992)

concluded that microwave processing led to a lower degree of cure and was expected to result in inferior mechanical properties.

#### 2.2.7.2 Microwave Preheating

Thermoplastic materials that do not possess a dipolar structure normally can not absorb microwave power. However, thermoplastics such as polyethylene and polyphenylene sulfide have been preheated by mixing a microwave absorbing additive (N-ethyl toluenesulfonamide) into the matrix. The additive promotes localised heating to allow processing of the thermoplastic without degrading its mechanical properties (De Meuse & Ryan, 1993). Costigan and Birley (Costigan & Birley, 1988) batch preheated SMC in a multimode oven prior to compression molding. The viscosity of the charge was reduced and flowed more readily, implying that a lower capacity press could be used. Furthermore, the temperature drop across the mold was reduced, lowering cycle times. The tensile strength of the laminate increased proportionally with the charge preheat temperature. The authors attributed this result to less fiber reorientation, more even cure, and reduced thermal stresses.

#### 2.2.7.3 In-Line Microwave Processing

Methven and Ghaffariyan (Methven & Ghaffariyan, 1992) developed a cylindrical applicator to process glass FRP reinforcement bars for concrete by pultrusion. Heat was transferred efficiently to the resin so that the die length could be reduced with a corresponding decrease in frictional forces. As a result the glass fiber reinforcement could be pulled through the die more rapidly, and larger cross section parts could be produced, compared to the conventional system. In-line preheating of thermally sensitive liquids is more complex. Under laminar flow conditions, maximum velocity is developed along the flow axis, decreasing to zero at the wall of the transporting pipe. Uniform heating across the pipe diameter would heat the boundary layers at the pipe wall excessively, with inadequate heating along the flow axis. Apart from study of Hill and Johnson, (Hill, 1993; Johnson, 1995), no microwave preheating system for thermally sensitive resins has been discovered in the literature.

## Chapter 1

# Chapter 2: MICROWAVE HEATING

The purpose of this research was to estimate and characterize the effects of resin microwave preheating on the resin infusion process and quantify the resulting changes in terms of infusion time required and level of preform saturation. The idea consists in coupling a microwave system with the laboratory scale apparatus for the composite resin infusion manufacturing process. The microwave system, comprising microwave generator, waveguides and applicator, heat up the liquid resin coming for the vessel prior entering into the mold. The resin flow pass through the resonance cavity within a PTFE tube that is transparent to the microwave, so that it does not alter the electro-magnetic field. The temperature of the resin increases and consequently a reduction of the viscosity is experienced. It allows the liquid resin to flow more freely through the fiber preform

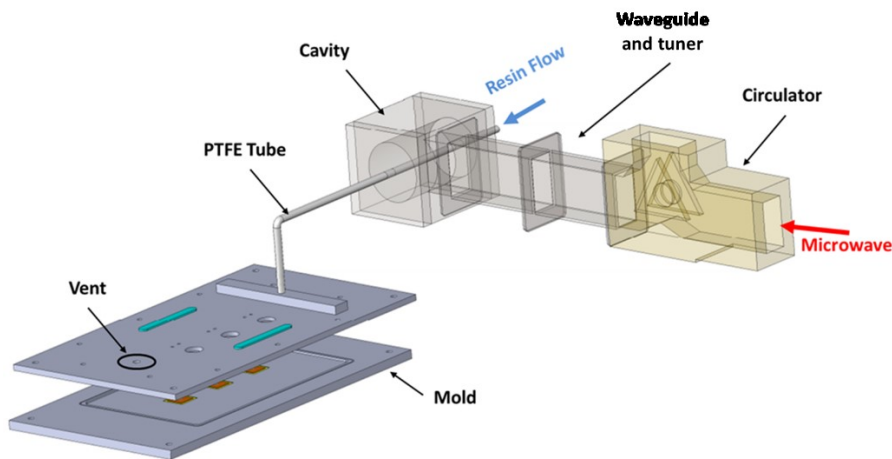


**Figure II.1.** Schematic representation of the in-line microwave resin pre-heating system integrated with the LCM process.

## Chapter 2

This chapter briefly described the materials, the equipment and methods adopted to perform the study. The resin infusion system and the instruments used to delineate between the effects of ordinary process and resin preheating are defined. The hardware employed to integrate the resin preheating system into the resin infusion cycle is described. The methods adopted to develop and evaluate the performance of the preheating system is detailed and discussed.

### **1. Microwave and heating mechanisms**

Microwave heating as an industrial process is a technique which was originally conceived about sixty years ago. The advent of the magnetron during the Second World War presented engineers and scientists a unique challenge to put such a device for generating microwaves into successful use. The main challenge to face was related to the lack of appropriate equipment and the lack of data on dielectric property of the materials, which were considered as candidates for microwave heating. During the late forties and early fifties, many efforts was paid to obtain reliable data on material properties. The work of von Hippel on the properties of many organic and inorganic materials in the frequency region  $100 < f < 10^{10}$  Hz has formed a solid basis for the establishment of radio frequency and microwave energy techniques in industry (Von Hippel, 1995). In addition, there have been significant developments on the design of magnetrons, power supplies and ancillary equipment, giving greater reliability to this new technique. The engineering aspects of many applications in terms of scale-up, continuous operation, automatic control, etc., have considerably improved since the original days.

In recent years, interest has grown rapidly in extending the application of microwave energy to process new engineered materials, including ceramics, polymers, composites, and chemicals due to the many benefits of microwave processing, the increased knowledge about the fundamentals of the microwaves and their interaction with the materials as well as the availability of novel production techniques.

The use of microwave energy provides clean, rapid, and efficient heating over a wide range of temperatures (up to 2000 °C or more), as well as a higher flexibility over conventional processing methods. Microwave processing is fundamentally different from conventional heating because electromagnetic energy is directly transferred to and absorbed by the processed material. This energy is converted into heat within the material and thus provides energy savings by eliminating the large thermal mass of conventional furnaces. Because of microwaves are a penetrating radiation, materials exposed to them are heated from the inside and they can be heated more uniformly than conventionally heated materials without high temperature gradient between the surfaces and the core of the material. This is particularly desirable for low

## Microwave Heating

thermal-conductivity materials, such as polymers and ceramics. This method enables internal moisture to be removed from wet solids, as well as internal gases generated during binder burnout. Because of microwave heating mechanisms are different from conventional heating processes, processing equipment and processing conditions present new challenges that have to be dealt with.

It is important to define the frequency ranges for which the terms microwave and radio frequency will be subsequently used (see figure II.2). At frequencies below 100 MHz, where conventional open wire circuits are used, the technique of industrial processing will be referred to as radio frequency heating. At microwave frequencies (above 500 MHz), wired circuits cannot be used and the power is transferred to the applicator containing the material to be processed in waveguides. This technique will be referred to as microwave heating. In between, there exists a diffuse regime where the equivalent circuit representation for the two techniques blend together and become difficult to differentiate.

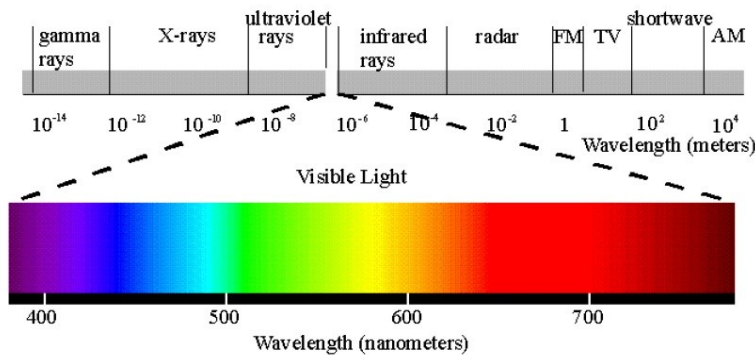


**Figure II.1.** *The electromagnetic spectrum*

### **1.1. Electrical Volumetric Heating**

By electrical means, volumetric heating is possible wherein all the infinitesimal elements constituting the volume of a workload are each heated individually, ideally at substantially the same rate. The heat energy injected into the material is transferred through the surface electromagnetically, and does not flow as a heat flux, as in conventional heating. The rate of heating is no longer limited by thermal diffusivity and surface temperature, and the uniformity of heat distribution is greatly improved. Heating times can often be reduced to less than 1% of that required using conventional techniques, with effective energy variation within the workload less than 10% (Meredith, 1998). Any material can be heated directly by electrical volumetric heating provided that it is neither a perfect electrical conductor nor a perfect insulator, implying that the range extends from metals to dielectric materials which

## Chapter 2

could be considered quite good insulators. No single electrical techniques is effective in all cases and there are four methods used in practice, classified by the effective electrical resistivity and physical properties of the work piece.

### ***1.2. Conduction and induction heating***

These processes are used for heating metals with low resistivity and involve passing a heavy current through the workload to cause  $RI^2$  heating. The current may pass between physical electrical connections to the workload (conduction, or resistance, heating). The electrical frequency used ranges from direct current (DC) to 60 Hz. Alternatively the workload may form the secondary of a step-down transformer in which the induced electric and magnetic field (EMF) causes the References heating current to circulate (induction heating), with electrical frequency of 50 Hz to about 30 kHz.

### ***1.3. Ohmic heating***

Ohmic heating is a conduction heating technique for liquids and pumpable slurries; it consists of equipment for passing an alternative current through the liquid between electrodes. Aqueous solutions, in particular, are almost always sufficiently conductive to permit a high power density to be dissipated, because dissolved salts provide ions as charge carriers. Ohmic heating invariably uses a power-frequency supply (50-60 Hz) and is extremely efficient as a converter of energy to heat in the workload, with efficiency of conversion over 95%.

### ***1.4. Radio frequency heating***

When the workload has high resistivity, the voltage required to pass sufficient current for a practical power-dissipation density becomes prohibitive at the low frequency used for conduction heating. This problem can be overcome by increasing the frequency to the range 1-100 MHz, most often 27.12 MHz, one of several internationally agreed frequency for the purpose. Typical applications are plastics (welding and forming), wood (seasoning and gluing), textiles, paper and board (drying), food (post-baking/drying) and ceramics (drying). The workload is placed between electrodes in the form of plates or rods, to which is applied a high voltage (usually several kV) at the chosen high frequency. Radio-frequency (RF) heating has been used in the industry since the 1930s and has grown to a substantial and important industry (Meredith, 1998).

### ***1.5. Microwave heating***

Intensive research during the Second World War into high-definition radar led to the development of microwave frequency (500 MHz to 100 GHz), and in particular the magnetron valve as a microwave generator of very high power output with exceptional efficiency (Meredith, 1998). In the post-war years further development resulted in microwaves being used for heating, especially for domestic purposes, but also significantly in industry, where there are some important advantages compared with processing at lower frequencies. Modern industrial-microwave-heating systems are used for a diversity of process in the food industry, tempering and thawing, continuous baking, vacuum drying, pasteurization and sterilization, and in ceramic, rubber and plastic industries, as well as many specialized processes in the chemical industry where there is great interest in vacuum processing. Contemporary equipment has very high reliability and running costs are competitive with other heating methods, especially when the advantages of volumetric heating are included. Moreover, high-power magnetrons, although initially expensive, are now rebuilt after normal end of life at a cost representing less than 10% of the energy they use. In industry, microwave heating is performed at frequency close to 900 MHz or at 2450 MHz, the frequencies are chosen by international agreement with the principal aim of minimizing interference with communication services. Most of the materials which can be heated at RF, can be also be treated at microwave frequencies together with some others which are difficult with RF because of their low loss factor. Because microwave heating operates at a much higher frequency than RF, the applied electric field strength is less, so the risk of arcing is less. The higher power density of heating can also be used, resulting in physically smaller plant. However the penetration depth is less at microwave frequencies than for RF, and, with the shorter wavelength giving greater prominence to standing waves, the uniformity of heating may be inferior. The overall efficiency of microwave heating systems is usually very high because of the exceptional efficiency of high-power magnetrons (85% at 900 MHz, 80% at 2450 MHz). Because of microwave frequencies have very short wavelength (33.3 cm at 900 MHz, and 12.2 cm at 2450 MHz), the used electrical techniques differ greatly from RF heating: RF equipment uses conventional electrical components such as inductors and capacitors, with open conductors for the electrical connections. Microwave equipment cannot use these components because their size is comparable with the operating wavelength; under these conditions the components behave anomalously and the circuits would radiate most of the energy into space. Instead, microwave heating uses waveguides (hollow metal tubes) to convey power from the magnetron to the heating oven (more frequently called applicator). The applicator may have many forms but is almost invariably based on a closed metal structure, with an access door or small open ports to allow the workload to pass through in a continuous flow.

## 2. Mechanisms of Microwave Heating

In order to be heated the materials are exposed to the microwaves and they absorb electromagnetic energy. Basically, the microwave heating can occur by means of three mechanisms. The generally best-known mechanism is the excitation of a molecule covered with dipole moment. It is based on the polarization of the charges in a dielectric material under the action of an electric and on the inability of the molecules to follow the reversals of the electric field (Metaxas & Meredith, 1983). In an equilibrium state, the dipoles are oriented randomly within a non-metallic material (Figure II.3). The application of an alternate electric field forces the dipoles to be reoriented in a direction opposite to the field (Figure II.4). The reorientation energy is stored by the dipoles as potential energy while the field is applied. The energy absorption from the microwave field is the more intense the nearer the resonance rotation of the molecule lies at the frequency of the microwave.

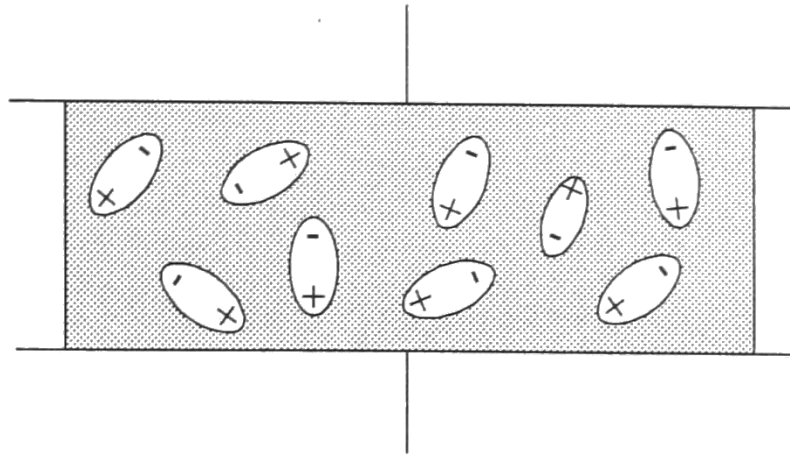


**Figure II.3.** *Random dipole orientation in uncharged, equilibrium state*

## Microwave Heating

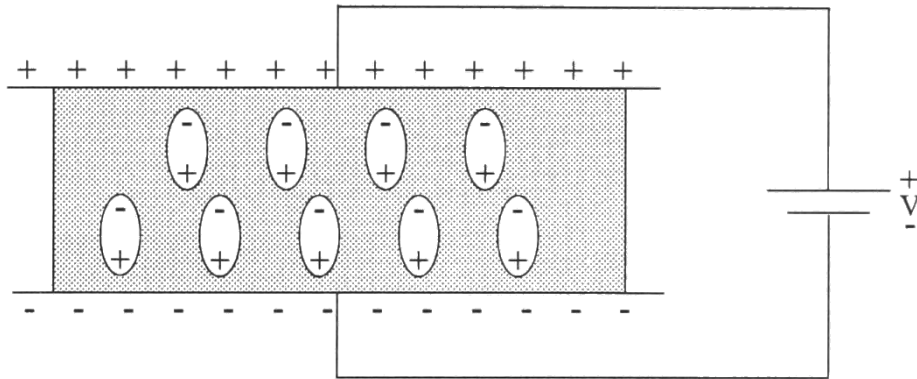


**Figure II.4.** *Reorientation of dipoles by an applied electric field*

Once the electric field was removed, the dipoles relax to a new equilibrium position; the stored energy is released and transferred to the system in the form of heat. Reversing the polarity of the electric field forces the dipoles to rotate at 180° angle. The interference with neighboring molecules determines a delay of the dipole orientation with the electric field and generates heat within the sample (Figure II.5) (Tinga & Nelson, 1973).

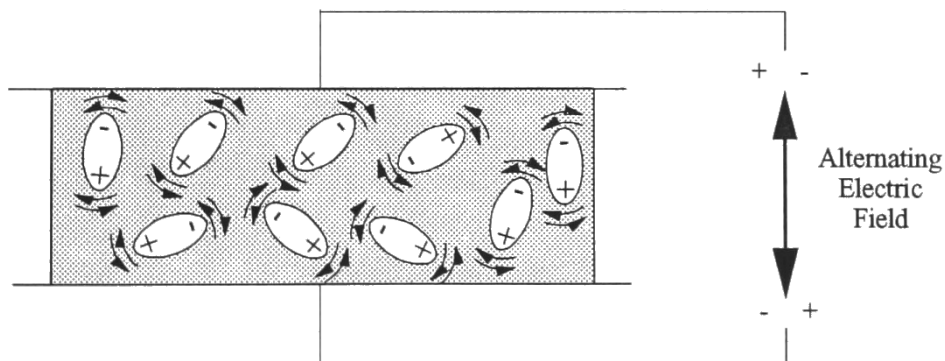


**Figure II.5.** *Dipole vibration due to an alternating electric field*

Heating in the electromagnetic field also happens, if there are free ions in the product. This sort of heating takes place in electrolytes, but also in many glass or ceramic materials. A third possibility of coupling is the magnetic absorption, however, having little importance in industry apart from the fact that such materials are often being used in absorptive locks for a damping of microwave energy. Conductive materials, like metals also interact with the microwaves; in this case, the penetration depth of the microwave is only a few micrometers, thus almost no energy is being absorbed from the microwave field due to the small resistance of these materials, i.e. the microwaves are

## Chapter 2

being reflected at the metallic surface. The ability of any material to absorb microwave energy is being expressed by its dielectric loss factor, which is combined with the dielectric constant. This dielectric loss factor depends on the type of material, frequency and temperature. To describe the heating potential of a material, the complex dielectric constant ( $\epsilon^*$ ) can be expressed as:

$$\epsilon^* = \epsilon' - j\epsilon'' \quad (\text{II.1})$$

The dielectric constant ( $\epsilon'$ ) influences the amount of energy that can be stored in a material in the form of electric fields, while the loss factor ( $\epsilon''$ ) is a measurement of how much energy the material can dissipate as heat. Material property tables often list the loss tangent ( $\tan \delta$ ) which is equivalent to the ratio  $\epsilon''/\epsilon'$ .

The relative permittivity (also called dielectric constant,  $\epsilon'$ ) is a dimensionless number that stands for the ability of the dielectric material of refracting (i.e. changing in direction and magnitude) or absorbing the lines of electric field entering the surface of the material, analogously with the refractive index for optical materials (Metaxas & Meredith, 1983). Relative permittivity is a multiplying factor by which the capacitance of a vacuum capacitor would be increased if instead it were filled with a dielectric material of that permittivity. To better clarify the meaning of the permittivity, the simple alternative current (AC) theory can be used: capacitor of value  $C$  connected to a sinusoidal generator of voltage  $V$  at angular frequency  $\omega$ , the current  $I$  that can be detected is expressed by the eq. (2.2):

$$I = j \cdot V \cdot \omega \cdot C \quad (\text{II.2})$$

The operator symbol  $j$  signifies that the sinusoidal current leads the voltage by precisely  $90^\circ$ , and because there is no component of the current flowing in phase with the voltage there is no net power dissipation. Consider now the capacitor  $C$  as a parallel-plate capacitor for which the capacitance value is well-known and given by the eq. (2.3):

$$C = \frac{A\epsilon_0\epsilon'}{d} \quad (\text{II.3})$$

Where  $\epsilon^*$  is the complex relative permittivity of the dielectric material filling the space between the plates,  $A$  is the area of one plate and  $d$  is the spacing between the plates. Supposing the permittivity having an imaginary component, it is could be written as the eq. (2.1). Then the current  $I$  is expressed in eq. (2.4):

$$I = V\omega \frac{A\epsilon_0}{d} (j\epsilon' + \epsilon'') \quad (\text{II.4})$$

## Microwave Heating

The first term in parenthesis shows the component of current in phase quadrature with the voltage as it would be with a loss capacitor, but the second term is a component in phase with the applied voltage, and therefore representing power dissipation. This power dissipation P is given by the

$$P = \operatorname{Re}(VI) = V^2 \omega \frac{A \epsilon_0}{d} \epsilon'' \quad (\text{II.5})$$

The term  $\epsilon''$  clearly quantifies the power dissipation in the capacitor having a dielectric filling with relative permittivity defined by eqs. (2.1-2.5) and it is called the “loss factor” of the dielectric. The “loss angle”  $\delta$  is another term used to quantify the lossiness of a dielectric. This the angle by which the resultant current differs from the ideal  $90^\circ$  phase angle relative to the voltage and it could be determined from the eq. (2.6):

$$\delta = \tan^{-1} \frac{\epsilon''}{\epsilon'} \quad (\text{II.6})$$

As previously mentioned, microwaves are a specific form of electromagnetic radiation that occupies a bandwidth of the spectrum between 300 MHz and 30 GHz. Electromagnetic energy is comprised of orthogonally related magnetic and electric field components that propagate as sinusoidal waves. The electric field produces dipole reorientation that ultimately heats the dielectric material. The magnitude of the electric field (E) is related to the amount of microwave power (P) that a volume of dielectric material (V) can absorb, as illustrated by the following equation (Metaxas & Meredith, 1983):

$$P = 2\pi f E^2 \epsilon_0 \epsilon'' V \quad (\text{II.7})$$

Where f is the microwave frequency. Some very important features of dielectric heating equation are particularly evident from eq. (2.7):

- a) The power density dissipated in the workload is proportional to frequency where the other parameters are constant. This means that the volume of workload in the oven may be reduced as the frequency rises, resulting in more compact oven.
- b) The power density is proportional to the loss factor.
- c) For a constant power dissipation density the electric field stress E reduces with f. Then if  $\epsilon''$  remains constant with frequency the risk of voltage breakdown reduces as the chosen operating frequency rises.
- d) In practice the value of  $\epsilon''$  varies with the frequency, generally, but not always  $\epsilon''$  rises with the frequency. It also varied with temperature, moisture content, physical state (solid or liquid) and composition. All these may change during processing, so it is important to consider  $\epsilon''$  and also  $\epsilon'$  as variables during the process.

## Chapter 2

Microwave power can also be related to the temperature rise ( $\Delta T$ ) in a material for a given heating period ( $t$ ) as (Metaxas & Meredith, 1983):

$$P = \frac{m}{t} C_p \Delta T \quad (\text{II.8})$$

Where  $m$  is the mass and  $C_p$  is the specific heat capacity of the sample. Combining eqs. (2.7) and (2.8) leads to an expression for a uniform temperature rise in a sample heated by an electric field:

$$\Delta T = \frac{2\pi f t E^2 \epsilon_0 \epsilon''}{\rho C_p} \quad (\text{II.9})$$

Where  $\rho$  is the material density. It is evident from Equation 10 that the dielectric loss factor ( $\epsilon''$ ) enables heating of a material, regardless of its thermal properties. Low conductivity materials, such as thermosetting resins, can be heated uniformly by microwaves avoiding large thermal gradients through the material. In addition, the temperature rise within the sample is proportional to the oscillation frequency of the electric field. Because of absorption, the electromagnetic fields decrease as the wave passes through the material. In the absence of reflected waves in the material, the field intensity exponentially decays with distance from the surface. Because the power absorbed in an elemental volume of material is proportional to the power flux density flowing through it, the power dissipation also falls exponentially from the surface. The rate of decay of the power dissipation is a function of both the relative permittivity  $\epsilon'$  and the loss factor  $\epsilon''$ . The "Penetration depth"  $D_p$  is defined as the depth into the material at which the microwave power has been attenuated to 37% ( $1/e = 0.368$ ) of its initial value and it is given by the eq. (2.10) (Metaxas & Meredith, 1983):

$$D_p = \frac{\lambda_0}{2\pi\sqrt{2\epsilon'}} \frac{1}{\sqrt{\left[1 + \left(\frac{\epsilon''}{\epsilon'}\right)^2\right]^{0.5} - 1}} \quad (\text{II.10})$$

When  $\epsilon'' \leq \epsilon'$  eq. (2.10) simplifies in:

$$D_p = \frac{\lambda_0 \sqrt{\epsilon'}}{2\pi\epsilon''} \quad (\text{II.11})$$

The penetration depth is a very important parameter for a workload because it gives an immediate first-order indication of the heat distribution within it.

### 3. Dielectric properties of materials

Knowledge of dielectric data is essential in the design of heating systems because it enables estimates to be made of the power density and associated electric-field stress and equally important to the microwave- penetration depth in the material. It will be appreciated from the following that there can be substantial variation from the norm for a given material, and so it is desirable that measurements be made of each specific material to be processed. Materials may be classified into three groups, i.e. conductors, insulators and absorbers, as illustrated in Figure II.6.

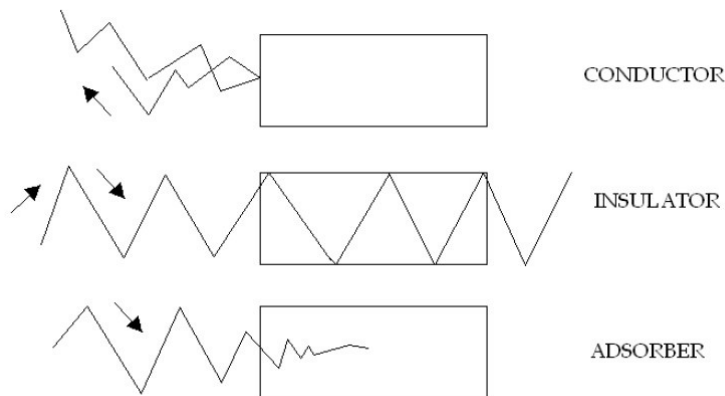


**Figure II.6.** *Microwave absorption characteristics for conductor, insulator and absorber.*

Materials with a high conductance and low capacitance (such as metals) have high dielectric loss factors. As the dielectric loss factor gets very large, the penetration depth approaches zero. Materials with this dielectric behavior are considered reflectors. Materials with low dielectric loss factors (insulators) have a very large penetration depth. As a result, very little of the energy is absorbed in the material, and the material is transparent to microwave energy. Because of this behavior microwaves transfer energy most effectively to materials that have dielectric loss factors in the middle of the conductivity range. In contrast, conventional heating transfers heat most efficiently to materials with high conductivity. The dielectric properties of materials vary widely, not only with composition, but also with density, temperature and frequency:

- a. Variation of the permittivity with moisture content: liquid water is strongly polar in its structure, causing readily to adsorb microwave energy and convert it into heat. Therefore, the variation of  $\epsilon$ , in particular  $\epsilon''$  with moisture content, plays an important role in the design of microwave heating/drying devices. For this a major effort was devoted to

## Chapter 2

establishing the variation of  $\epsilon'$  and  $\epsilon''$  with moisture for many industrial materials encountered in manufacturing industry, such as paper, board, foodstuffs, leather, wood and textiles.

- b. Variation of  $\epsilon''$  with temperature: the loss factor increases with temperature since the physical binding reduces and the dipoles are freer to re-orientate (Metaxas & Meredith, 1983). For hydrations above 25% the loss factor decreases with increasing temperature.
- c. Variation of  $\epsilon''$  with frequency: the measurement of the relaxation response of  $\epsilon'$  in a particular industrial material, is not in itself of particular significance other than to point out the relative values of the loss factor  $\epsilon''$ , at the various allocated frequencies. However, industrial use of microwaves calls for operation at discrete frequencies within given bands carefully selected so as not to interfere with other frequencies in use in telecommunications, defense and maritime applications.

Dielectric property data are important because they give values of the loss factor,  $\epsilon''$ , which controls, along with other parameters such as the dielectric field and the frequency, the power that can be dissipated in a given material volume. Alternatively, for a given power dissipation,  $\epsilon''$  controls the rate of rise of temperature. The larger the loss factor the easier the material absorbs the incident microwave energy. As a general practical rule, loss factors less than 2 require very high electric field strengths in order to ensure a reasonable rate of rise of temperature in the material; such low loss factor would almost certainly require fundamental mode resonant applicators as distinct from travelling wave or multimode applicators. On the other hand, loss factors of greater than 5 might present depth of penetration problems, in that because the material is highly absorptive to microwave radiation, most of the incident energy is absorbed within the first few millimeters, leaving the internal parts little affected. This causes non uniformities of heating which for in- depth heating are totally unacceptable. Therefore loss factors between the limits  $2 < \epsilon'' < 5$  would be presented by materials which, in general are good candidates for microwave heating applications.

## 4. Microwave Hardware

### 4.1. Microwave Ovens

Figure II.7 is a schematic representation of the components comprising the domestic microwave oven and is typical of all microwave heating systems. The power is converted to high voltage by a transformer then supplied to the magnetron that is used to produce microwaves providing efficient high power output at a stable frequency.

## Microwave Heating

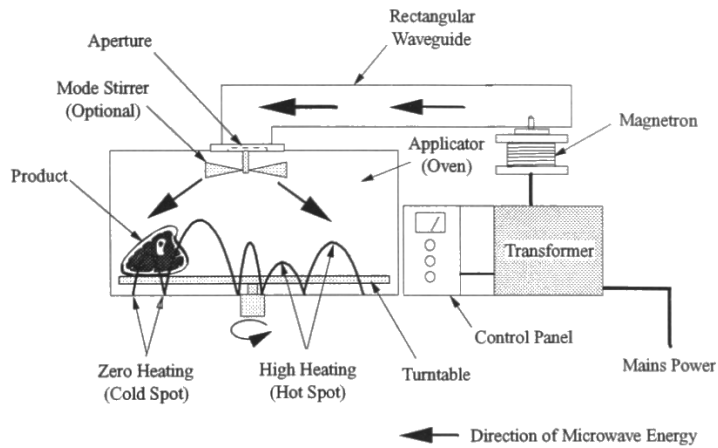


**Figure II.7.** Schematic of components comprising a domestic microwave oven (Johnson, 1995)

### 4.2. Magnetron

The magnetron (figure II.8) converts the direct current in high frequency (approximately 2.45 for common domestic usages) electromagnetic waves, the power is extracted from the magnetron via an antenna and launched into a rectangular metallic waveguide for transmission. The magnetron is basically constituted by a cylindrical shaped anode, made of copper or another high temperature resistance metallic alloys, with a coaxially drilled hole (called “interaction space”) on the circular surface. A wire, generally made of nickel, is placed within the hole and act as a cathode (see figure II.8). On the anode, around the central hole, several similar holes, called resonators, are drilled separated from each other by a short distance. A small slot is cut between the resonators and the interaction space (see figure II.9).

## Chapter 2



**Figure II.8.** Typical magnetron for common domestic microwave oven

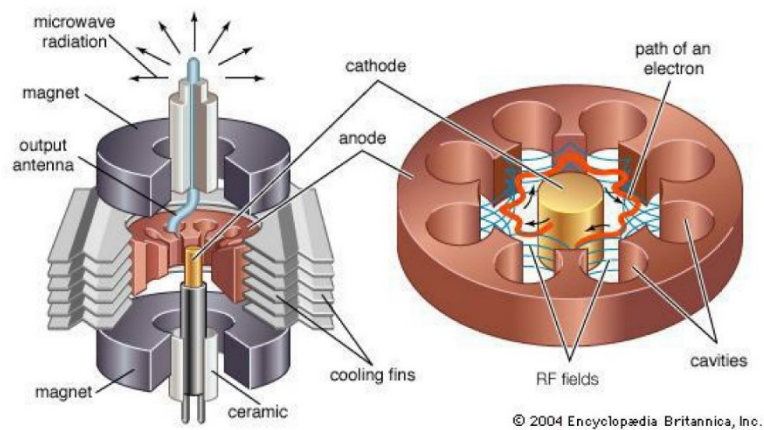


**Figure II.9.** Scheme of the conventional magnetron

The magnetron is called a "crossed-field" device in the industry because both magnetic and electric fields are employed in its operation, and they are produced in perpendicular directions so that they cross. The applied magnetic field is constant and applied along the axis of the circular device illustrated. The power to the device is applied to the center cathode which is heated to supply energetic electrons. Electron from filament would, in the absence of the magnetic field, move radially to the outside ring anode which surrounds it. Electrons are released at the center hot cathode by the process of thermionic emission and have an accelerating field which moves them outward toward the anode. The axial magnetic field exerts a magnetic force on these charges, which is perpendicular to their initially radial motion, and deflects them to in the sense shown in the figure II.10a, so they tend to be swept around the circle.

## Microwave Heating

As these electrons sweep toward a point where there is excess negative charge that charge tends to be pushed back around the cavity, imparting energy (“pumping”) to the oscillation at the natural frequency of the cavity. This driven oscillation of the charges around the cavities leads to radiation of electromagnetic waves, the output of the magnetron (figure II.10b).

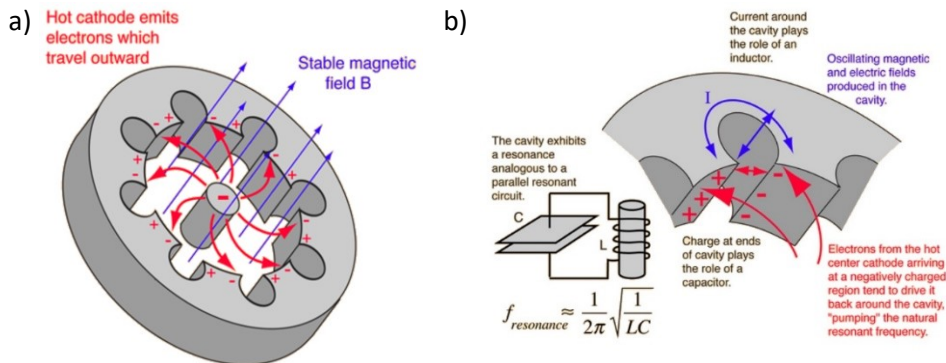


**Figure II.10.** Working fundamentals of a magnetron: a) schematic representation of electric and magnetic fields; b) action of the magnetic forces on the electrons and behavior of the charges.

Little wings are mounted externally the anode and act as heat exchanger to dissipate the generated heat. The magnetron is powered with high voltage direct current and works in manual or automatic mode. Microwave energy propagates along the waveguide to the oven, or applicator, where the product is heated. An applicator is a conductive metallic enclosure with a small aperture in one wall through which microwaves enter. Microwaves are reflected off the walls of the applicator, combining with incident microwaves to form a standing wave, termed a mode. The mode includes both electric and magnetic field components, however, only the electric field component contributes to the heating of a dielectric material as shown in eqs (2.7 and 2.9). So that, referencing to a mode concerns only the resonating electric field that is equivalent to the heating profile within an applicator.

### 4.3. Multimode Microwave Ovens

A domestic microwave oven (Figure II.7) is a multimode oven because of its large volume supports several coincident modes. The mode shape determines the heating profile within the oven. Maximum heating occurs when the product is situated at a mode peak (antinode), with zero heating at a node. The heating profile within a domestic oven is non-uniform due to an uneven modal distribution. Localized hot and cold spots can develop within this kind of applicators in relation to the mode amplitude at a particular location. For this reason, the product is often placed on a turntable and is

## Chapter 2

exposed to a series of hot and cold spots to provide a uniform heating. In addition, a rotating metallic fan is used as mode stirrer modifying the modes within the applicator and then providing another aid to heat the product more uniformly.

### 4.3.1. Single Mode Microwave Ovens

Figure II.11 is a schematic of a typical single mode heating system. The components of this system are similar to those in a domestic microwave oven (Figure II.7), with the addition of a circulator. A circulator allows incident microwave power from the magnetron to pass through it. Reflected power is diverted by the circulator to a water load, protecting the magnetron and ensuring a more stable output frequency. Non-reflected microwave power enters the single mode applicator. Compared to multimode ovens, the volume of a single mode applicator is reduced so that a unique standing wave, or mode, is excited. Knowledge of the mode shape permits locating the product at the point of maximum heating (antinode). Since the balance of microwave power is directed into a single mode, heating is more concentrated than for multimode ovens. As a result, low loss factor dielectric materials can be heated rapidly within single mode applicators.

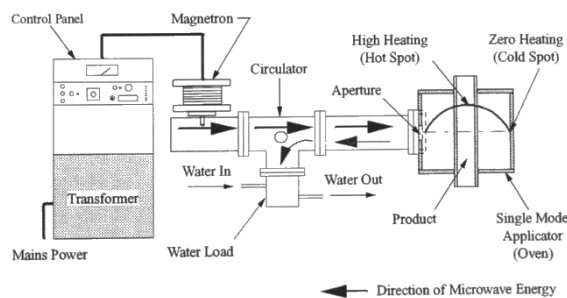


**Figure II.11.** Schematic of components comprising a single mode microwave oven (Johnson, 1995)

### 4.3.2. Nomenclature for Single Mode

An infinite number of mode profiles can be established within an applicator depending upon its geometry. Single mode applicators, or ovens, are typically rectangular or cylindrical. A specific mode profile is represented by a proper notation to distinguish between applicators operating in different modes.

The notation defines the electric or magnetic field transverse to the direction of propagation within a waveguide, and has been extended to describe stationary fields within single mode applicators. Modes are classified as transverse electric (TE) or transverse magnetic (TM) and by means of three numerical subscripts " $l$ ", " $m$ " and " $n$ " (Smyth, 1955). Orthogonal coordinates are used to classify modes within rectangular applicators. The

## Microwave Heating

subscripts  $l$ ,  $m$ , and  $n$  are related to the number of half wavelengths in the  $x$ ,  $y$ , and  $z$  directions as defined in Figure II.12.

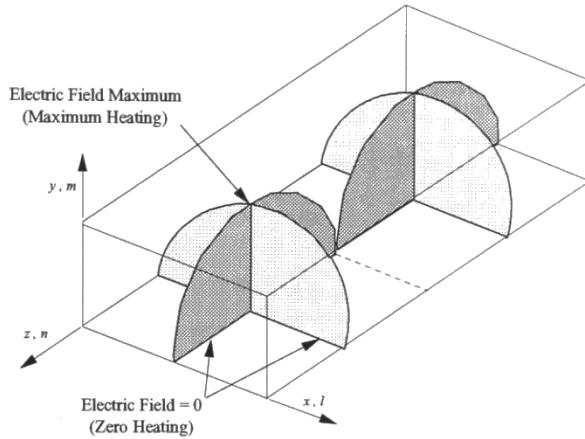


**Figure II.12.** *Electric field pattern within a  $TE_{102}$  mode rectangular applicator)*

For example, the electric field profile within the  $TE_{102}$  mode rectangular applicator is characterized by a single half wavelength along the width ( $x$ ,  $l$ ) of the rectangular section. The heating rate is constant along the height of the applicator ( $y$ ,  $m$ ) since no variation in the electric field occurs in that direction. Finally, two half wavelengths are produced along the length of the applicator ( $z$ ,  $n$ ). Mode profiles within cylindrical applicators are defined using cylindrical polar coordinates. The subscripts  $l$ ,  $m$ , and  $n$  are related to the  $\Phi$ ,  $r$ , and  $z$  directions as defined in Figure II.13.

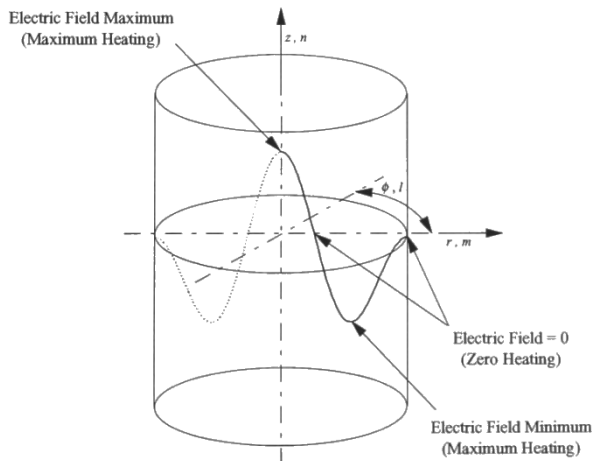


**Figure II.13.** *Electric field pattern within a  $TM_{020}$  mode cylindrical applicator.*

## Chapter 2

The  $l$  coordinate designates the number of full wavelengths in the electric field along the circumference ( $\Phi$ ) of the applicator. The  $m$  coordinate specifies the number maximums and minimums occurring in the electric field between the axis and wall of the applicator. Variation in the electric field along the length of the applicator ( $z$ ) is denoted by the  $n$  subscript. For example, the  $TM_{020}$  mode is characterized by one maximum and one minimum along the radial direction ( $r$ ) so that  $m = 2$ . No circumferential or lengthwise variations are excited in the  $TM_{020}$  mode for even heating along these coordinates.

### 4.4. Wave Guides

The wave guides (or applicators) direct the electromagnetic wave into the resonant cavity which the load are placed in. They basically consist in a metallic tube, with rectangular or circular section.

### 4.5. Rectangular Applicators

Figure II.15 shows a  $TE_{101}$  mode rectangular applicator. The product is heated as it flows through a PTFE pipe oriented perpendicular to the applicator. PTFE absorbs little microwave power due to its low loss factor ( $\epsilon'' = 0.0003$ ) so that the balance of the microwave energy is transferred to the product. Heating materials that have different dielectric properties shifts the resonant frequency of the mode within the applicator, and likewise, the heating profile. A proper designed tuner (a double plunge tuner in the depicted scheme) mounted at the edge of the metallic wave guide realigns the resonant frequency with the magnetron output frequency, correcting the problem. The tuning capability of rectangular applicators permits a variety of materials with different dielectric properties to be heated effectively. The heating profile is virtually uniform across the pipe diameter making this system unsuitable for heating catalyzed resins with laminar flow properties. Excessive heat at the pipe wall could cause premature resin polymerisation within the PTFE pipe (Hill, 1993).

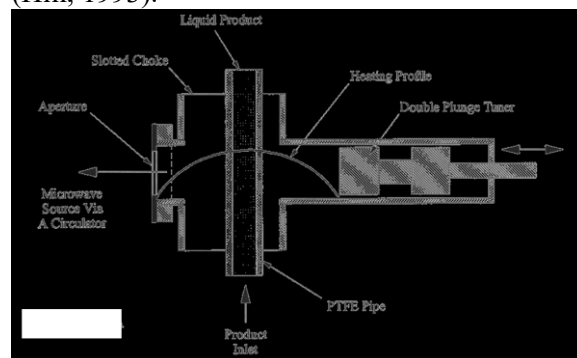


**Figure II.15.**  $TE_{101}$  mode rectangular applicator

#### 4.6. Cylindrical Applicators

Figure II.16 shows a cylindrical applicator. The product is heated as it flows through a PTFE pipe located concentrically along the applicator. The diameter of the applicator is calculated for resonance in a particular mode based on the dielectric properties of the product. As a result of its fixed geometry, heating within the cylindrical applicator is limited to materials with similar dielectric properties. The advantage of cylindrical applicators is that the modes (such as the  $TM_{020}$ ) suitable for heating thermally sensitive materials can be established.

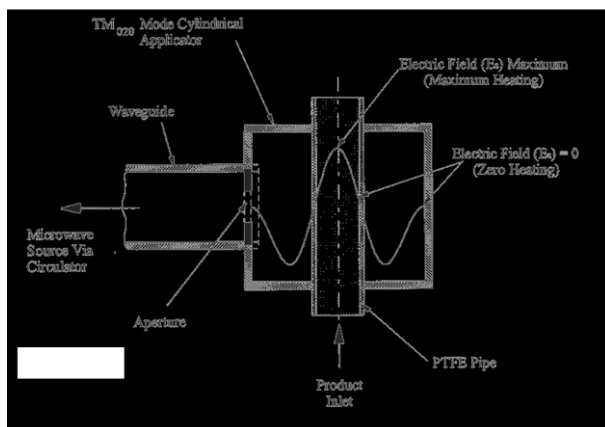


**Figure II.16.**  $TE_{020}$  mode cylindrical applicator

The profile of the electric field in the cylindrical shaped resonance cavity determine a zero heating condition (or at least a low intensity of electric field) on the walls of the PTFE tube and a maximum electric field along the pipe axis where the resin velocity is greatest. It allow preventing an over-heating of the heat catalyzed resin and providing a uniform heating of the liquid in the PTFE pipe. The heating performance of a single mode applicator is optimized by an iterative tuning and coupling procedure. Tuning involves matching the natural resonant frequency of the desired mode within the applicator to the magnetron output frequency. Coupling is performed to maximize the transferal of microwave energy from the waveguide into the applicator. A fully optimized applicator will resonate at the magnetron output frequency with all of the available microwave energy being directed into the applicator for heating.

#### 5. The microwave system.

In the present paragraph, the developed laboratory scale microwave system is detailed. The hardware, comprising the magnetron, the wave-guides, the

## Chapter 2

resonance cavities and the ancillary tools, was described. In order to evaluate the optimal configuration of the system able to perform the proper heating of the working fluid several preliminary trials have been carried out on the stand-alone microwave system detached from the LCM apparatus. The designing stage has involved the choice of the geometry of the resonance cavity and the tuning of the source power according to the variable flow rate of the liquid system during the infusion. For this reason, three distinct configurations have been considered and tested. Three cylindrical applicator of different length were designed. The aim was to vary the exposition time of the heating liquid to the microwaves resulting in (once defined a specific flow rate) different temperatures achievable. In addition, the proper strategy for the source power vs time profile that will be applied during the composite manufacturing processes has been investigated. To do that, previous experimental trails provided the data regarding the resin flow propagation through the fiber preform within the mold and the flow rate that established during the infusion. The data allowed to estimate the amount of energy that should be provided to the liquid system in order to obtain the wanted temperature at the exit of the applicator avoiding either detrimental overheating either ineffective heating of the resin.

### 5.1. Microwave generator

The main elements of the microwave system is the generator (Figure II.17).

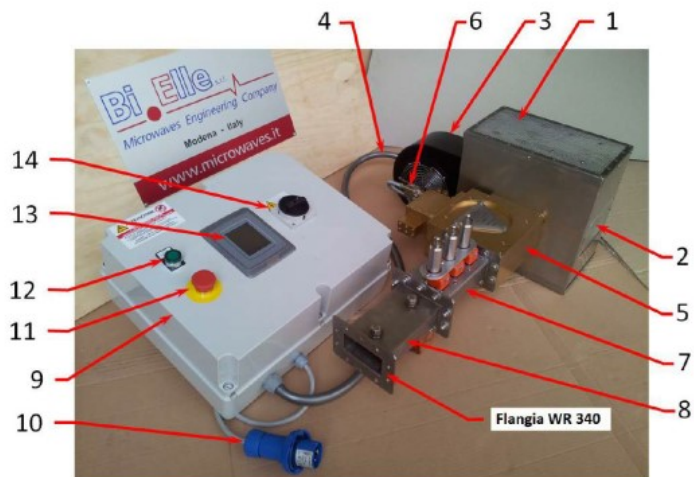


**Figure II.17.** Microwave generator.

The main elements that compose the apparatus as provided by the manufacturer ACQ BIELLE are:

## Microwave Heating

- a. A 2 kW Magnetron Head (n° 1), with WR340 wave guide, placed inside an AISI 304 stainless steel box. The magnetron is equipped with a thermo-switch for the control of temperature. The switch interrupts the energy supply as the temperature reaches a threshold value, set by the operator, in order to prevent superheating and failures of the equipment.
- b. Centrifugal fan (n° 3) for the forced air cooling of the Magnetron Head.
- c. Insulator (or circulator) (n°5) with water cooling stream at the exit of the waveguide, inside the magnetron head. The insulator allows the microwave from the magnetron to pass through it, the reflected microwave are deflected to a water load that absorbs the radiation and preserve the correct working of the magnetron.
- d. Tuner (n°7): a rectangular WR 340 wave guide, 170 mm length, equipped with three micro-screw. The micro-screws control three adjustable pins that come out from the inner wall inside the wave guide. The pins alter the propagation path of the microwave, allowing the modification of the microwave mode.
- e. Wave guide (n° 8), 170 mm length, placed at the end of the tuner.
- f. Control panel (n°9): it contain the electronic equipment to manage and control the microwave generator

Other ancillary elements are listed in table II.1.

**Table II.1.** *Constituents of microwave generator system*

	Elements
1	Magnetron Head
2	CE plaque
3	Centrifugal fan
4	Electric connection cable
5	Insulator
6	Sensing diode
7	Tuner
8	Wave guide
9	Control Panel
10	Electric plug (220V)
11	Emergency stop switch
12	Auxiliary switch
13	Touch screen control panel
14	Main switch

## 5.2. Security monitoring device

The safety usage of the system is guaranteed by means of using of a detector, able to measure the wasted power density in the surrounding area.

## Chapter 2

The employed device, MARTEK500 (figure II.18), detects three distinct range of emission, signaled with three different colored warning light.



**Figure II.18.** *Detector MARTEK 500*

The green light indicates a safety working condition with measured power density below the  $0.1 \text{ W/m}^2$ . The yellow light stand for a condition with a limited risk, the dispersed power density is approximately equal to  $0.5 \text{ W/m}^2$ . The red light indicates a critic situation for the operators' health, with a power density above  $1 \text{ W/m}^2$ . To limit that the dispersion of microwaves in the environment, it is necessary containing the radiation inside the system (wave guides and resonance cavity) using a proper reflective sealant at the joints between the different elements.

### **5.3. Wave guides and resonance cavity.**

The propagation of the microwave from the magnetron to the resonance cavity takes place through two rectangular shaped wave guide made of stainless steel AISI 304 (figure II.19). Each wave guide is equipped with two external flanges at both ends for the reciprocal connection and the joining with the circulator and the cavity. The AISI 304 is good conductor and allows to minimize the radiation losses. Once connected, the two wave guides have a total length of 340 mm.

## Microwave Heating

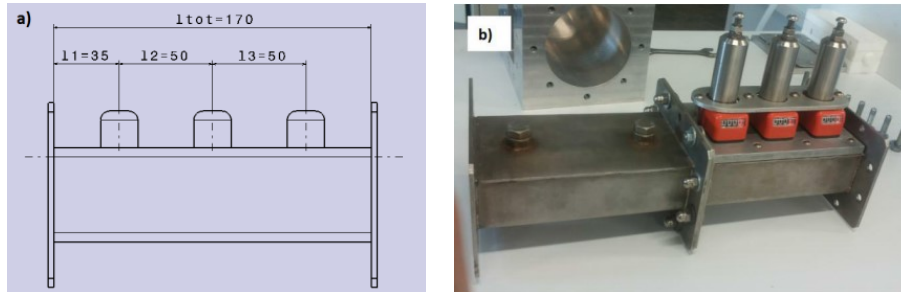


**Figure II.19.** a) Sketch of the tuner with the location of the three micro-screws; b) wave guide and tuner coupled

The tuner presents three copper “fingers”, 12 mm diameter, which can extend inside the wave guide until a maximum penetration depth of 20 mm. These fingers act like capacitors or inductors modifying the propagation path of radiation and then minimizing the reflected power. The micro-screws are evenly spaced by 50 millimeters, the external screws are far from the connection flanges 35 mm. The geometry of rectangular wave guides, with the shorter side being the half of the longer one, 43 mm and 86mm respectively, allow the establishing of a single mode ( $TE_{10}$ ) microwave. The single mode is conventionally used in low power applications and maximize the transfer of electromagnetic energy.

Three cylindrical cavities have been considered in the present research activity:

1. Cavity 1 (Figure II.20): 100 mm diameter cylindrical cavity, machined within an aluminum cube of  $150 \times 150 \times 150 \text{ mm}^3$  dimensions. A rectangular inlet section was machined on the side of the cube (see figure II.20b) for the microwaves from the wave guides. The cavity is closed by two aluminum plate, 20 mm thick. Two holes, 12 mm in diameter, were drilled on the plates for the housing of the PTFE tube. The plates are perfect conductor, like the cavity, and prevent the dispersion of the radiation in the environment. The cavity is 150 mm in length.

## Chapter 2

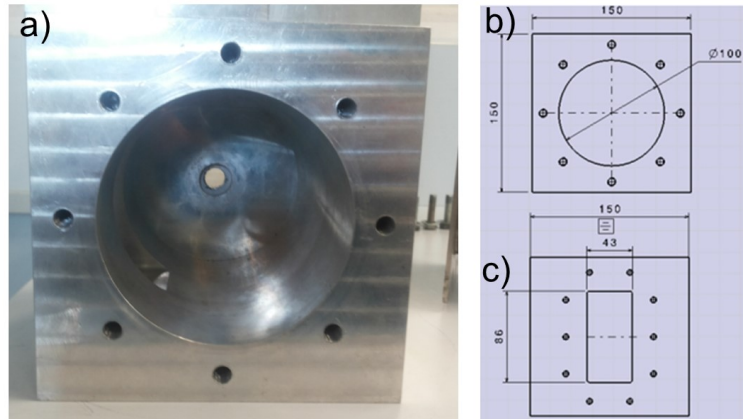
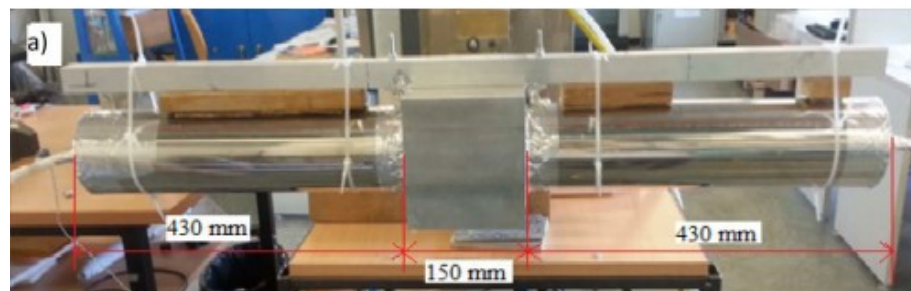


**Figure II.20.** a) Resonance cavity; b) dimensions of the cavity

2. Cavity 2 (figure II.21): the second cavity has a cylindrical shaped and was obtained adding to the first cavity two stainless steel pipes 430 mm length. So that, the total length of the cavity was approximately 1 meter. The pipes have the same length to preserve the symmetry of the exposition of the product to the radiation and an inner diameter of 100 mm in order to properly fit with the first cavity. The second cavity allow to significantly increase the exposition time of the heating liquid to the microwave. So that, once fixed the flow rate a higher temperature increasing can be obtained at the same power compared to the first cavity according to the eq.(2.8). A 12 mm diameter PTFE tube, with inner diameter of 10 mm, was placed inside the cavity. To ensure the correct alignment of the longer tube with the cavity four PTFE disks (two disks for each tube) were machined and put inside the steel tubes at the both ends. The disks were drilled at the center for the housing of the tube.



## Microwave Heating



**Figure II.21.** a) Front view b) rear view of the second cavity

3. The third cavity has a total length of 610 mm and was made adding two stainless steel pipes at the ends of the first cavity. The pipes are the same that were employed to create the second cavity. If the aim of the second configuration was to maximize the yield of the system, obtaining the maximum temperature gradient at fixed microwave power, with the third cavity the objective was to realize a tunable system able to vary the supplied power according to the evolution of the resin infusion process. This aspect will be better debated in the following sections.

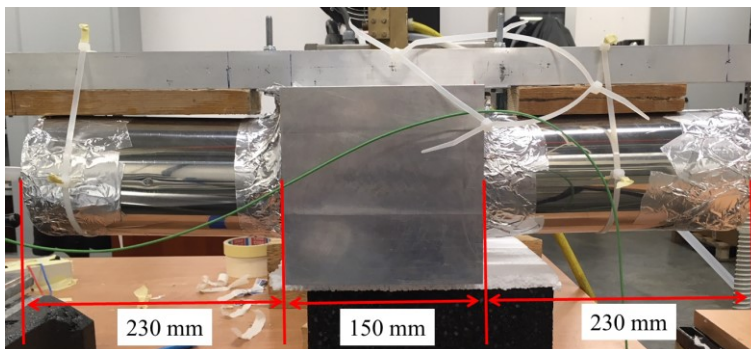


**Figure II.22.** Front view of the third cavity

### 5.4. Using of the microwave generator

The microwave generator can be set to operate in automatic or in manual mode. In manual mode the operators set the power of the magnetron and the microwave system will work at fixed regime until the stop switch is activated by the operator. In the automatic mode, the operator compiles a program (also called “recipe”), the PLC controller installed on the system will perform the power cycle and will stop the magnetron as soon as the last instruction has been executed. The “recipe” is basically a list of instructions (or steps) executed by the generator, each step, compiled by the operator, consists of a set of two data, the nominal power of the magnetron and the duration of the

## Chapter 2

single step. The system allows to monitor in real time different parameters of the generator:

- a. Nominal Power: it is the power of the magnetron as it is set by the operator.
- b. Actual Power: it is the power at the exit from the head of the magnetron. It is calculated from the nominal power taking into account the losses inside the system due to the actual behavior of the components (magnetron, internal wave guides, etc...).
- c. Reflected Power: it is the power that is not absorbed by the liquid and is reflected back to the magnetron through the waveguides. It is measure by a diode mounted on top of the circulator.
- d. Output power: it is the power absorbed by the material. It is calculated subtracting the reflected power from the actual power.
- e. Step: the monitor on the control panel shows in real time the step that is currently executing by the system
- f. Magnetron temperature: it is the temperature experienced by the magnetron and detected by the thermo-switch mounted inside the magnetron head. The switch acts as the temperature reaches a threshold value (fixed at 120 °C) to prevent potential superheating of the generator.

The system is completed by a DAQ to acquire the data during the working. The acquisition system records the data concerning the power (nominal, reflected and actual), the current step and the current cycle time. An example of the programmable “recipe” and the data obtainable from the DAQ are depicted in the table II.2 and Figure II.23.

**Table II.2.** *Example of the power cycle executed by the microwave generator*

	Nom. Power [W]	time [s]
Step 1	500	60
Step 2	1000	60
Step 3	1500	60
Step 4	2000	60
Step 5	0	25
Cycle time		265

## Microwave Heating

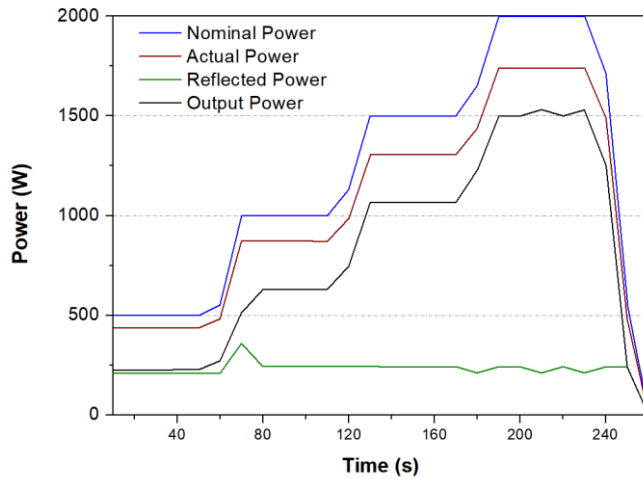


**Figure II.23.** Example of the measurement of power of the recipe listed in table II.2

## 6. Preliminary tests of the in-line microwave heating system

Several preliminary trials have been performed to investigate the behavior of the hypothesized pre-heating configurations, evaluating benefits and drawbacks. The tests were needed to assess the achievable temperature increases with the three cavities varying the input power and the flow rate of the liquid. All preliminary tests were carried out using only the microwave system, detached for the LCM apparatus. The un-catalyzed resin were employed for these trials in order to avoid the unwanted polymerization of the resin. It also allows to reuse the resin after the proper cooling and degassing and it make easily to clean the apparatus after each test and re-arrange the set-up for the subsequent trials.

### 6.1. Results of the preliminary tests on the first configuration

In the following, the main results of the preliminary tests on the cavity 1 were reported. The total length of the PTFE tube exposed to the radiation was equal to 150 mm, the same length of the cavity (see Figure II.24). The flow rate of the liquid resin was set at 0.0083 l/s, corresponding to an average value of the flow front speed within the tube of 0.11 m/s. Each trial were performed setting the automatic mode of the microwave generator. The power cycle adopted is similar to the one depicted in the table II.2. The temperature at the exit of the cavity was measured by means of a thermocouple connected with a digital multimeter that provide in real time the current value of the resin temperature. From the data of the thermocouple the temperature gradient between the inlet and the exit of microwave cavity can be calculated.



**Figure II.24.** *Set up of the cavity 1 during the preliminary tests.*

The initial temperature of the liquid was measured equal to 26.5 °C, while the maximum temperature was 31.5 °C at 2000 W of the nominal power (figure II.25). The temperature increase is almost linearly proportional to the supplied power. The highest temperature gradient achievable with this configuration was 5.7 °C.

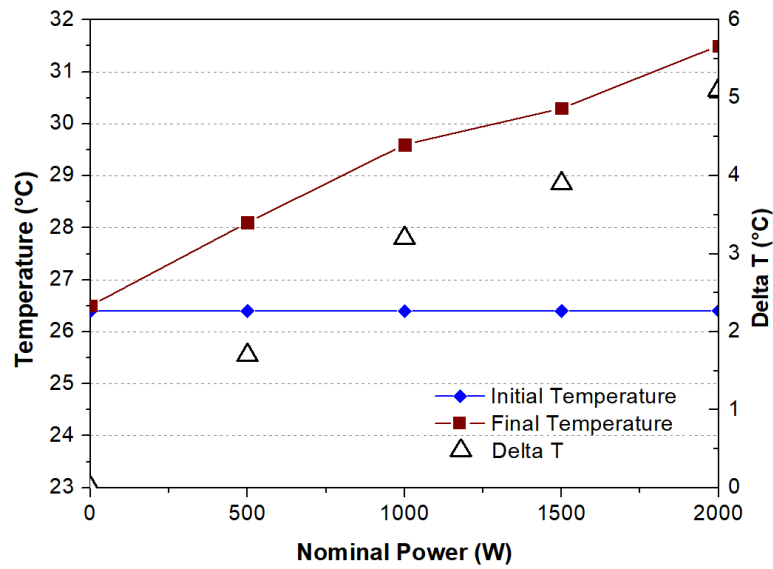


**Figure II.25.** *Initial, final temperatures and temperature gradients achieved with the first cavity: the showed data are the average values obtained by the several tests performed with the same.*

## Microwave Heating

The first cavity was also tested reducing the flow rate of the heating fluid. The aim was to reproduce the flow conditions that could be established during the infusion stage. Indeed, the flow rate of the resin significantly varies during the impregnation of the preform, starting from high values at the beginning of the infusion and exponentially decreasing as the process continues. The values of flow rate and the decay profile were assessed by means of the other infusion tests performed at room temperature. The flow rate for this second set of trials was set equal to  $7.8 \times 10^{-4}$  l/s, corresponding to a flow velocity within the tube of 0.01 m/s. This resulted in an exposition time of the heating resin of approximately 15 s. The table II.3 summarizes the temperature gradients obtained at different values of the nominal power.

**Table II.3.** Average  $\Delta T$  at different power level achieved with the first cavity and for a heating liquid flow rate of  $7.8 \times 10^{-3}$  l/s

Nominal Power [W]	$\Delta T$ [°C]
200	5.3
500	8.5
1000	14.5
1200	16.4
1500	22.1

The maximum temperature reached during the test was 48.6 °C at 1500 W of nominal power, which is suitable for the resin system used for the resin infusion. Indeed, if on the one hand a significant reduction of the viscosity can be obtained, on the other hand the temperature experienced by the resin is not able to promote a potential premature cure of the catalyzed resin within the cavity. No further significant increases of resin temperature have been obtained using a power above the 1500 W, therefore for the sake of brevity the relative measurements have not been reported. Observing the reported results, it can be argued that the first cavity can be used to successfully heat the resin. Therefore, experimental trials of the resin infusion process have been performed adopting this configuration. The result of the campaign will be showed in the chapter 4. The main drawback observed in the first cavity is related to the high power level required to achieve the wanted temperature. Indeed, values generally between 1500 and 2000 W (the maximum level allowed by the microwave generator) have been necessary. The system as designed is proved to be not cost-effective and it does not allow any further regulation.

### **6.2. Results of the preliminary tests on the second configuration**

The second configuration was developed in order to improve the efficiency of the heating system. The longer cavity allows to increase the exposition time

## Chapter 2

of the heating liquid being equal the nominal power and the liquid flow rate compared to the first configuration. The figure II.26 shows the set-up for the testing of the cavity 2. The microwave system was connected to the vacuum pump that applied the pressure to drive the liquid resin from the vessel, through the microwave cavity to a reservoir for the re-use of the resin. The circuit is composed by two twin streams controlled by two valves. The first stream connects the microwave system to the LCM mould it is used only in the infusion tests, during the preliminary trials the valve is kept closed. The second stream connects the PTFE tube directly to the resin reservoir, it is used for the testing of microwave heating.

The twin stream circuit is also employed during the infusion tests. The working of the circuit will be detailed in the dedicated section.

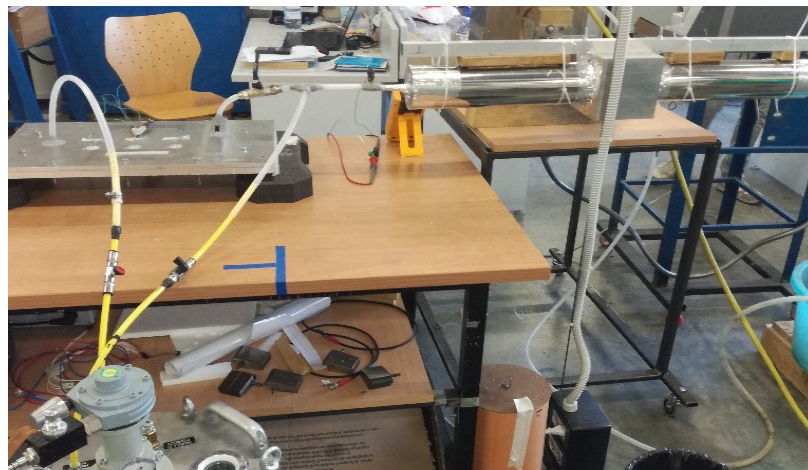


**Figure II.26.** *Cavity 2: experimental set-up of the preliminary testing*

Three distinct sets of trials were carried out varying the flow rate. The distinct values of the flow rate were obtained introducing a localized pressure drop by means of the valve that can be set in three different configurations:

1. Fully open: the valve is completely open and no pressure drop is realized. The flow rate reaches the maximum value allowed by whole circuit, taking into account the driving pressure applied by the vacuum pump and the pressure drops that can be occurred within the pipe and at the connections. The configuration refers to Test 1 (see figure II.27 and table II.4).
2. Partially open: the valve is kept half-open. Localized pressure drop results in a reduction of flow rate. The configuration refers to Test 2.
3. Almost closed: the valve is almost totally closed. The flow rate significantly reduced approaching the typical values that were establishing during the fibers impregnation when the resin flow is fully developed, after the first transient stage characterized by high flow rate. This configuration refers to Test 3 (see figure II.28)

## Microwave Heating

For Test 1 e 2, considering the relative high values of the flow rate that were detected, only the trials performed at high power have resulted in significant temperature increasing. Indeed, power levels below the 500 W did not provide appreciable results, thus the relative data were not reported.

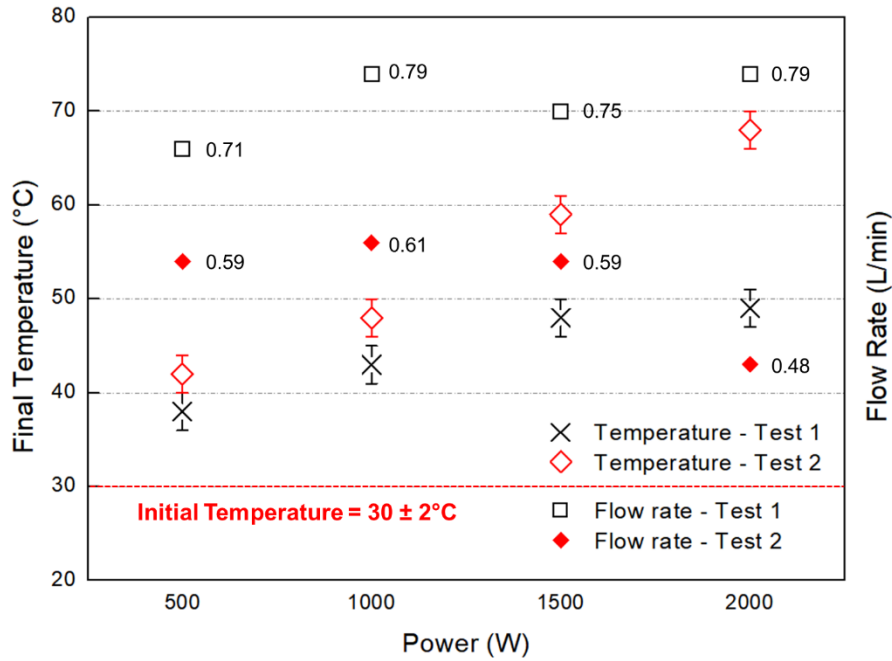


**Figure II.27.** Final temperatures and flow rates measured for Test 1 and Test 2 at different values of nominal power.

Table II.4 summarizes the temperature measured during the trials of Test 1 and Test 2. The temperature gradients achieved were also listed. As can be seen, the temperature increases obtained with the cavity 2 are significantly higher than the one achieved for cavity 1 at equal input power. Indeed, for low flow rates a  $\Delta T$  of approximately  $40^{\circ}\text{C}$  can be reached corresponding to a temperature at the exit of cavity of  $68^{\circ}\text{C}$  for a flow rate of  $0.48\text{ L/min}$  (see Test 2) and a  $T_f$  of  $50^{\circ}\text{C}$  in case of fully open valve. These values are significantly higher than the first configuration where the maximum temperature gradients detected were  $5^{\circ}\text{C}$  and  $22^{\circ}\text{C}$  for the highest flow rate (approximately  $0.5\text{ L/min}$ ) and the lowest one ( $\approx 0.05\text{ L/min}$ ) respectively.

Chapter 2

**Table II.4.** Result of the heating trials for the Test 1 and Test 2.

	Nominal Power [W]	Ti [°C]	Tf [°C]	ΔT [°C]
Test 1	500	28	38	10
	1000	29	43	14
	1500	29	48	19
	2000	28	49	21
Test 2	500	29	42	13
	1000	28	48	20
	1500	29	59	30
	2000	29	68	39

The cavity 2 was also tested for lower flow rate values (Test 3). The result of the preliminary tests were depicted in Figure II.28. The flow rate detected during the trials was significantly lesser than the Test 1 and 2. Therefore, according to the eq.(2.8), the final temperatures experienced by the heating liquid were higher. Indeed output temperature between 60 °C and 70 °C were observed for nominal power of the microwave generator that ranged between 200 W and 600 W. For the established flow conditions in the Test 3 power above the 600W resulted in a detrimental overheating of the resin. For this reason, the results of the trials performed at high power levels were not reported.

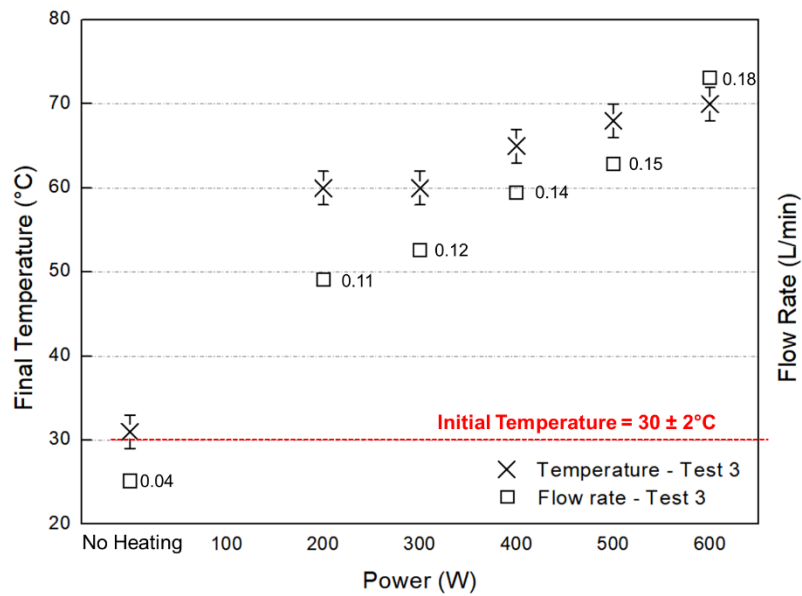


**Figure II.28.** Final temperatures and flow rates for Test 3 at different values of nominal power.

## Microwave Heating

The outcomes of the preliminary tests allowed to design the heating strategy adopted in the infusion experiments.

### 6.3. Results of the preliminary tests on the third configuration

The cavity 3 was also tested performing several experimental trials. The heating liquid flow rate was varied from approximately 1 L/min, typical values for the first stage of the infusion, to values of 0.1 L/min (see figure II.29) representing the steady value that establishes in the main stage of the process after the first transient. The figure II.29 shows the data obtained for the experimental campaign.

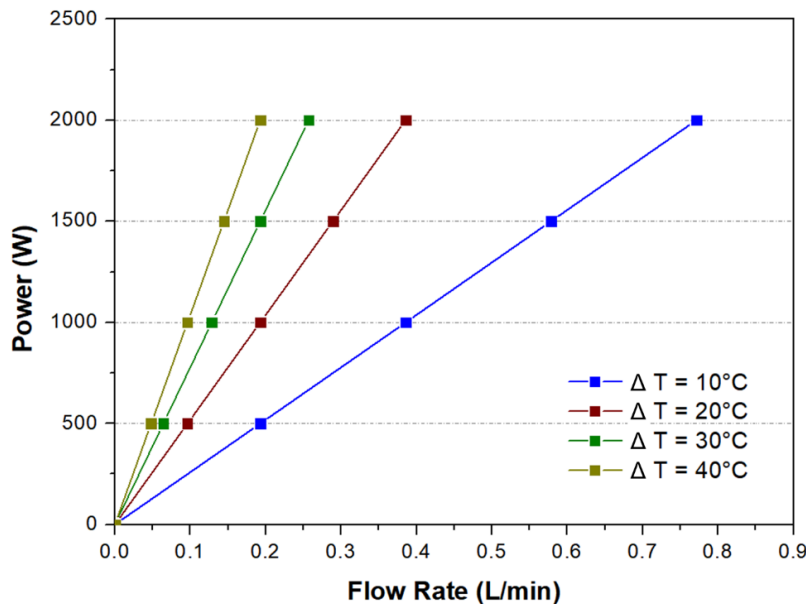


**Figure II.29.** Parameterized temperature gradients obtained with cavity 3 at different values of power and flow rate.

As can be seen, different  $\Delta T$  can be achieved for distinct experimental conditions. Considering for example a wanted temperature gradient of 20 °C, it can be obtained adopting different values of nominal power according to the variation of the flow rate during the infusion (see eq.(2.8)). At high flow rates ( $\approx 0.4 - 0.5$  L/min), the power required to heat up the liquid of 20 °C is 2000 W. As the flow rate drops the required power decreases, so at 0.1 L/min only 500 W are needed to keep the liquid at the same temperature. The cavity 3 seems

## Chapter 2

to be fail with the high flow rate conditions, where only a temperature rise of 10 °C can be achieved. To overcome this disadvantage a proper strategy of heating during the resin infusion process should be designed.

Observing the data from the preliminary tests for the cavity 1 and 2, it can be argued that the wanted resin final temperature can be obtained with a few microwave parameters combinations. Indeed, the cavity 1 in case of high flow rate can be provide a temperature increasing of only 5 °C and thus it probably will not able to sufficiently preheat the resin in the first stage of the infusion. Then, when the flow rate drops the cavity 1 provide an interesting  $\Delta T$  of approximately 22°C. However, it requires the maximum level of power allowed by the microwave generator resulting in a lesser cost-effective solution.

Conversely, the cavity 2 can provide significant temperature increases at different values of flow rate. Therefore, it can potentially produce the wanted output temperature of the resin system during the whole infusion stage. The main observable drawback is due to the fact that when low values of flow rate are established the risk of overheating increases even for the lowest power levels.

Cavity 3 appears a suitable solution for the microwave heating system. It allows the operator to have a reasonable flexibility to regulate the system.

# Chapter 3: FLOW FRONT MONITORING

The investigation of the effectiveness of the microwave heating to improve the impregnation of the fibers during a LCM process requires the design of a proper experimental set-up. For this reason a complete sensing apparatus to reproduce on a laboratory scale the resin infusion process have been developed and realized. The system consists of a metal mould to manufacture a flat composite laminate and a set of sensors to monitor in real time the evolution of process parameters. The acquired data allow to trace the flow of the resin through the fiber perform. Pressure and dielectric sensors have been chosen coupled with a video-camera to an independent visual observation. The designing of the apparatus required the choice of the other ancillary devices. All details concerning the developed LCM system were illustrated in the chapter.

For the sake of clarity, a brief digression about the several monitoring techniques and the sensor employed in the LCM composite manufacturing monitoring was reported. Then more attention was paid on the dielectric monitoring. The fundamentals of the dielectric analysis, focusing on its use in the composite manufacturing field, are briefly described. Then, the designed experimental apparatus is detailed.

## **1. Monitoring of the resin flow front and the resin curing in the**

### **LCM processes.**

Liquid composite molding such as resin transfer molding (RTM) is a versatile and attractive process for high volume, high performance, and low cost manufacturing of polymer composites. However, at present, many trial and correction cycles are still required before one can manufacture a successful part within certain requirements increasing the global processing costs. This has established an urgent need for improving the LCM. Automation allows real-time adjustments to the manufacturing process to

## Chapter 3

account for part to part variability and to produce more uniform and high quality composite parts. It also is a suitable means to reduce manufacturing cycle time and costs. The study of controlling the processes by means of in-situ sensors is the first step to deal with toward the automation. Sensors for liquid composite molding have been the subject of an intense research activity in the recent year. Embedded and non-embedded sensor were developed for the LCMs, such as RTM, VARTM and SCRIMP. The non-embedded sensors have to be placed outside the mould, these included but not limited to ultrasonic sensors, video recording and linear variable differential transformer (LDVT). These sensors have the advantage of a minimum interference with the mold and the work piece. However, they require a visual access through the mold making them suitable for a limited class of process, like VARTM or SCRIMP, while they cannot be adopted in case of metal mold and high temperature and pressure conditions. Embedded sensors include pressure transducers, dielectric sensors as well as fiber optic sensors. These sensors are able to measure the flow front, pressure, resin viscosity and degree of cure. On the other hand, they remain in the finished parts and therefore they potentially are a source of structural defects. At this regard, it is preferable to place the sensors on the inside surfaces of the mold to limit the interferences with the resin flow. In the follow, some of the most used sensors in the LCM processes are detailed.

### ***1.1 Resistive sensors***

#### *1.1.2. Resin flow monitoring*

Resistive sensors (Lawrence *et al.*, 2002; Danisman *et al.*, 2007; Barooah, Berker & Sun, 2003) use either point or lineal conductor probes to detect arrival and curing of the resin. The sensor basically consists of a pair of closely placed conductive wires with a small fixed gap between them (see Figure III.1). In a lineal sensor, the electrodes are placed on the mold wall, the resin flow along the wires.

## Flow Front Monitoring

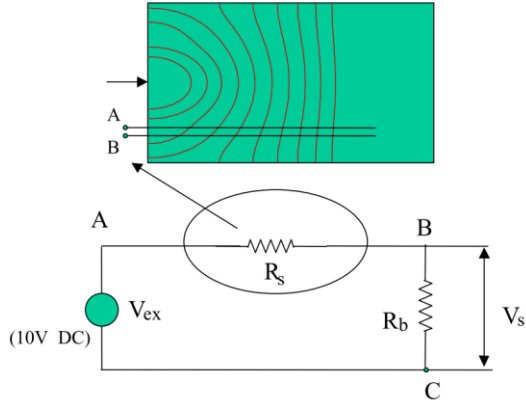


**Figure III.1.** Circuit for measuring the sensor voltage  $V_s$  (scheme of lineal sensor).

At the beginning of the process, the medium between the two electrodes B and C is the dry fabric preform, which is in contact with the sensor. The electrical conductance of this material is practically zero, therefore voltage measured between the electrodes is zero. When the resin reaches the sensor, infiltrating the free space between the wires, the two wires are connected by a conductive medium, the resin. When there is no resin, the resistance between the wires,  $R_s$ , is infinite. As the wetted length of the wires increases, electrical resistance between the probes,  $R_s$ , decreases significantly. Consequently, the output voltage between points B and C,  $V_s$ , in the circuit shown in Figure III.1 goes up according to the constitutive equation:

$$V_s = \frac{R_b}{R_b + R_s} V_{ex} \quad (\text{III.1})$$

Where  $R_b$  is a fixed resistance and  $V_{ex}$  is the constant excitation voltage. In both point- and lineal-voltage the  $V_s$  is measure continuously to monitor the resin flow during the mold filling and the cure.

The sensor detect what fraction of the wires length was covered by the resin. The actual position of the flow front was evaluated by monitoring the ratio between the measured output voltage  $V_s$  and the maximum voltage,  $V_{s,max}$ , that can be read when the wires are fully covered:

$$r(t) = \frac{V_s(t)}{V_{s,max}} = \frac{L_{wet}}{L} \quad (\text{III.2})$$

Where  $L_{wet}$  and  $L$  are the length of sensor wires covered with the resin and the total length respectively. Obviously the lineal sensors have to be accurately calibrated measuring the  $V_{s,max}$  before the usage. The resistance  $R_s$  linearly depends on the ratio  $f(\rho, s)/L_{wet}$  where  $f(\rho, s)$  is a function of the gap,  $s$ ,

### Chapter 3

between the wires and  $\rho$  is the electrical resistivity of the resin. Hence, the output voltage  $V_s$  is proportional to the  $L_{wet}/f(\rho, s)$ . However, the resistance of typical RTM resin between the probes is in the order of hundreds of MegaOhms. Therefore, the voltage change upon the resin arrival can be so low that electrical noise caused by other equipment can interfere with the measurements. Moreover, to correctly design the sensor and accurately measure the  $V_s$ , the fixed resistance  $R_b$  should be chosen as close as possible to the  $R_s$  (the resistance of the polymer). Figure 2 shows the typical response of a lineal sensor when the resin reaches the electrodes (Barooah, Berker & Sun, 2003).

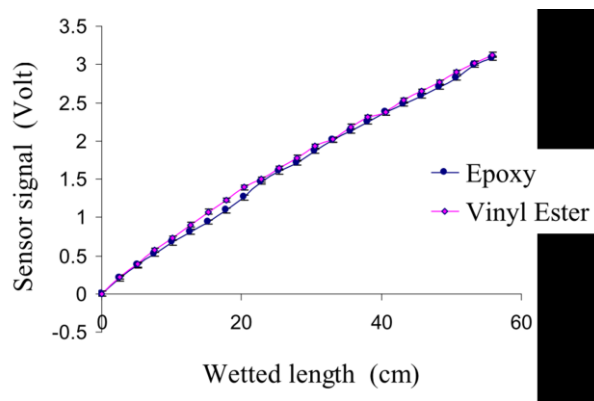


**Figure III.2.** Typical response of lineal-voltage sensor for tow resin system

As can be argued, the main advantage of the lineal sensor is that the signal is continuous in time. Having continuous sensor signals represents a more desirable condition to have a real-time feedback control. If the sensor system is point type, information on the resin flow is only available at certain instants when the flow front reaches the sensor. When the flow is in between two sensors, no further information is available about its state, and the controller cannot update its actions. A continuous signal, as one provided by lineal sensors, allows the controller to update its action far more frequently.

Compared to the single point-voltage sensors that can only detect the arrival of the resin, the lineal one can monitor more accurately the resin flow. However, they are some relevant disadvantages:

- a) The sensor can detect the fraction of wires covered by the resin and not the exact section wetted. It could result in wrong evaluation of the data in input and then the outcome might mislead the users. Indeed, the experiments Danisman et al (Danisman *et al.*, 2007) proved that the sensors are sensitive to the total wetted length of the wires independently is the resin evenly covers them or covers multiple sections. In both cases, if the total length is equal the output voltage will be the same.

## Flow Front Monitoring

- b) The sensors have to be accurately calibrated, measuring the value of  $V_{s,max}$  when the wires are fully covered and estimate the proper form of the function  $f$ . Several experiments are required to do that.
- c) The wires are placed on the surface of the wall. Despite of they are very thin, they can affect the structure of the fiber preform and cause a disturbance of resin flow. Indeed, the effective permeability at the preform-sensors interface might be different from the bulk preform.
- d) The sensors generally can be used once.
- e) The sensors must be removed after the process and it can be troublesome. The surface of the final part could have some irregularities after the detachment of the sensors. Alternatively, the sensors can be left on the surface, however they could cause stresses concentration on the component and affect the performances and the duration

Because of the major issues of the lineal sensors, the point sensors are more widely employed.

### 1.1.2. resin cure.

In a point-voltage sensor, the electrodes are very close to each other, and resin touches only the tip of the electrodes. Thus, a point-voltage sensor detects the arrival of resin at a point and the voltage changes from zero to a final value almost instantaneously. Many sensors have to be used to a detailed monitoring of flow. Figure III.3 shows the typical response of a point-voltage sensor.

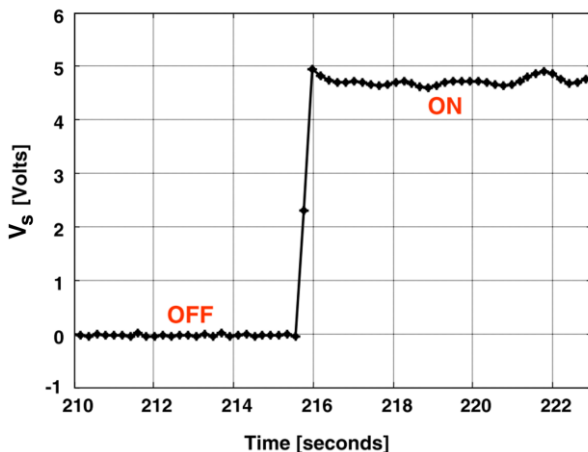


**Figure III.3.** Response of a single point-voltage sensor when resin covers the poles (Danisman *et al.*, 2007).

Initially the poles of the sensors are in contact with the dry preform and the output voltage is practically zero. When the resin flows in the mold cavity

## Chapter 3

reaches the sensors, it covers the poles closing the circuit. So, the voltage reaches almost instantaneously the final values. To compensate the minor sensitivity in the flow monitoring, a large number of point sensors mounted together on the mold surface to form a grid of sensors are usually employed. It allows to reconstruct the flow front of the resin during the filling (Danisman *et al.*, 2007; Lawrence *et al.*, 2002).

As mentioned, the resistive sensor can also be used to monitor the curing process. Usually  $V_s$  decreases during resin cure due to the increasing of measured resistance  $R_s$ . The voltage readings gradually decrease and drop to the zero level when the full cure is achieved (figure III.3). By monitoring the output voltage  $V_s$ , the user can determine the corresponding electrical resistivity of the resin and decide when open the mold.

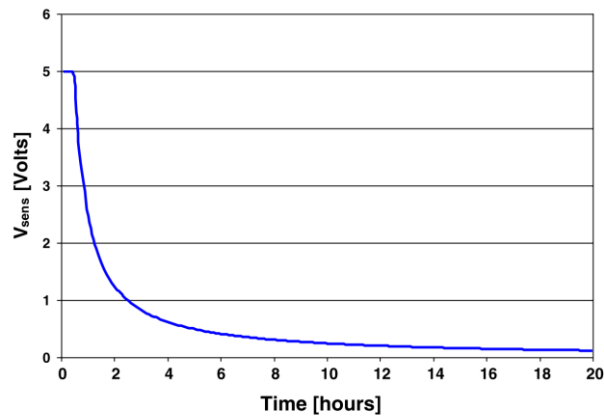


**Figure III.4.** Variation of measured voltage during the curing process (Danisman *et al.*, 2007).

At this regard, the evaluation of a critical value of  $V_s$  (or  $R_s$ ) corresponding a full-cure state (or at least a state in which no issues could be resulted by the demolding of composite part) of the resin has to be done previous the actual use of the sensor (Danisman *et al.*, 2007). Indeed, after the  $V_s$  drops below this critical value one can demold the composite part safely without occurring of warps or deformations on the product. For the evaluation of an optimal demolding time, different mechanical and physical tests should be performed on composites samples demolded at different values of  $R_s$  allowing to build an accurate relationship between the degree of cure and the electrical resistivity and better calibrating the sensors.

### 1.2. SMART-weave sensors

SMARTweave (Sensor Mounted As Roving Threads) (Fink *et al.*, 1995; Bradley *et al.*, 1998) sensors is a based direct current sensing that measure the

## Flow Front Monitoring

changes in the conductivity of resin between excitation and sense leads working like the resistive sensors, except for that the probes are the junctions a grid composed by conductive wires separated by non-conductive dry fabric layers (see Figure III.5) (Bradley *et al.*, 1998). The electrically conductive threads even if placed in a grid-like configuration, do not intersect, they simply overlap one another. So that where two wires overlap each other, instead of a physical contact between them there is a vacant space, called “sensing gap”. The ends of each wire is connected to a data acquisition device that measures the electrical signal existing in the sensing gaps between the perpendicular threads. The signal that can be measured are basically resistance, capacitance as well as dielectric properties.

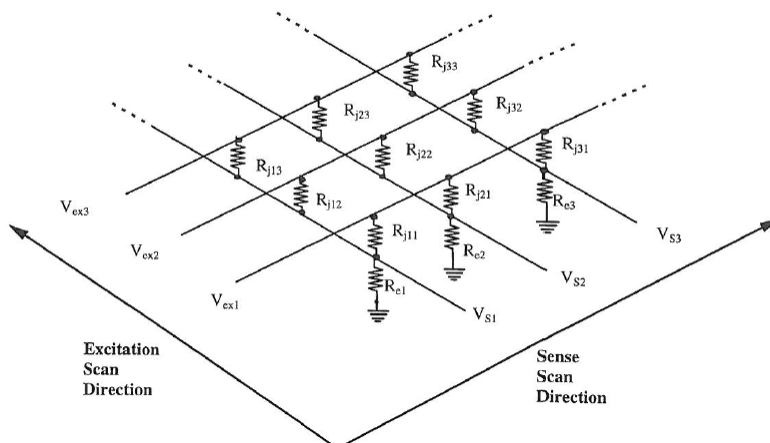


**Figure III.5.** Scheme of a SMARTweave sensor: the resistance network is formed by a excitation-sense pair (referred as sensor plane), with 3 excitation wires and 3 sense wires.

Before the resin infiltrates the dry preform, the excitation and sense wires are disconnected and the junction has an indefinite resistance, especially in the case of glass fibers. The resin system commonly employed in the manufacturing of composite materials has an electrical resistance ranging from approximately  $10^6$  to  $10^{11}$  ohms in its liquid state; while when it is fully cured the electrical resistance increase up to  $10^{15}$  ohms. As the resin flows within the fabric preform, it fills the sensing gap between the conductive wires forming a conducting path across the grid junctions; a measurable finite resistance is then established. This resistance indicates that the resin has reached a specific location. Therefore, changes from the initial indefinite reading to a finite value of resistance allow to determine the resin flow front location. In addition, from measuring the resistance between the gaps the resin cure progress can be controlled. Indeed, as the resin cures, it exhibits an

### Chapter 3

increase in electrical resistance. Hence, the readings of measured resistance allow to estimate the curing rate and the amount of cure of the resin at each sensing location.

The sensor system is embedded into the materials during the manufacturing and remains integrated in the part after the process is completed. Therefore, the materials of the conductive threads must be carefully chosen in order to not affect the behavior of resin system during the manufacturing process and not alter the properties of the final composite part. Sensor materials may include materials that are conventionally used as reinforcement, therefore graphite or metal-coated glass fibers can be adopted as sense threads. Generally speaking, any electrically conductive material manufactured into a thin fiber is suitable to be employed in the sense grid, so aluminum, copper, lead as well as conductive polymers materials can be chosen (Walsh, 1993).

The sensor threads may be used alone, placing them on top and bottom the bulk preform (see figure III.6) or may be woven into a fabrics layer and placed between reinforcement the layers especially in case of thicker composite parts when more than a pair of excitation-sense leads are needed (see figure III.7) (Walsh, 1993).

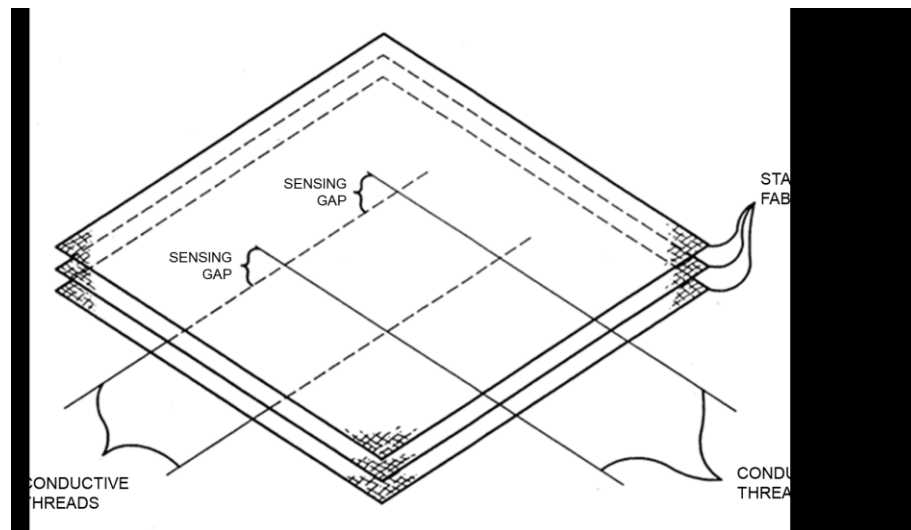


**Figure III.6.** Representation of the grid-like sensor system: the sensing threads are on a difference plane, so that they are perpendicular but not intersecting each other. A gap is formed between the wires that is the path with minimum resistance. At sensing gaps the resistance is measured.

## Flow Front Monitoring

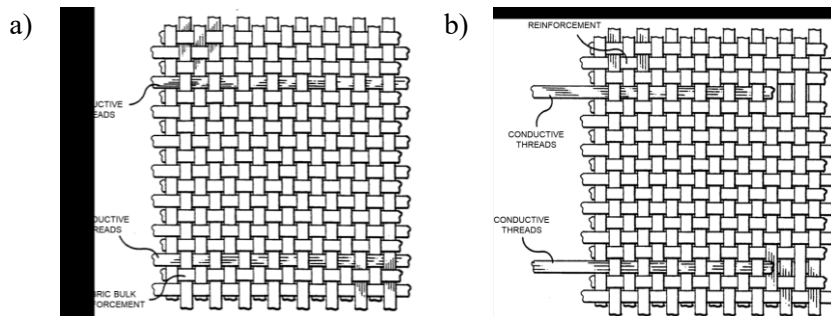


**Figure III.7.** a) Electrically conductive threads are woven into the reinforcement fabric; b) the end of each threads can be easily displaced into the fabric in order to allow the clamping and the connection with the measuring device.

In former case, the threads are usually conductive wires (basically copper that has the advantage of a nearly zero resistance and has a minimum disturbance on the acquired signal) that woven in an insulating cloth, a glass fibers fabric to form a skin layer (a single SMARTweave sensor grid) that is placed on the top and at the bottom of the laminate (Vaidya *et al.*, 2000). In the latter, the conductive thread usually is a tow of carbon fibers or coated-glass fiber. These are embedded into the reinforcement fabric layer and are integrated part of the composite laminated at the end of the manufacturing process. The other layers of reinforcement bulk work as insulator for the sensing gap.

The ends of each thread are connected to an acquisition data system via a multiplexer or switching device that allow to alternatively charge the excitation leads and the sense leads to monitor each the sensing junction. The change of resistance and capacitance at each junction may be registered. The data obtained allow drawing the information regarding the position of resin during filling stage and then calculate the flow front velocity, as well as the curing progress.

### 1.2.1 Principle of working

As above mentioned, when the resin infiltrates the fiber layer, it produces a resistance path,  $R_{jxy}$  (see figure III.5), between the two overlapping sense and excitation threads at the junction location. Different high resistance paths are formed between the excitation thread, take for example the  $V_{ext1}$  in figure 5, and the neighboring sense wires,  $V_{s1}$ ,  $V_{s2}$  and  $V_{s3}$ . The scanning software designates the excitation-sense pair and other sense inputs are not monitored, so that the sense voltage is measured at each excitation-sense node at time. To perform the measurement, the system applies a direct current (DC) voltage to the first excitation wire and monitors each analog sense  $V_{sxy}$  at time, collected

### Chapter 3

the information regarding the relative resistance,  $R_{jxy}$ . The other excitation leads,  $V_{ext2}$  and  $V_{ext3}$ , are not charged and are grounded to reduce the noises. Each excitation thread is grounded, determining an ancillary resistance  $R_e$ . Iteratively, the system de-charge the first lead and energize the second,  $V_{ext2}$ , and performs the sequential scan along the sense wires, as finished it pass to the third wire. When all nodes are monitored, the scanning iteration is repeated.

The sensing voltage  $V_s$  varies proportionally with the resistance  $R_j$ , which varies directly with the resin state. Therefore, continuously monitoring the output voltage the system is able to determine the resin cure properties and derive the process information, like gelation and optimal de-molding time. The eq.(2.3) describes the constitutive law of an ideal single node grid:

$$V_s = V_{ex} / (1 + R_j/R_e) \quad (III.3)$$

Starting from the initial ideal configuration, adding excitation and sense lines to the grid does not alter the value of the output voltage of  $V_s$ , conversely it modifies the value of reference resistance  $R_e$  resulting in a corresponding decrease of  $V_s$ . This drop of the output signal should be carefully taken into account by the sensing device because it could determine a misinterpretation of the resin cure state.

The figure III.8 describe a typical response of SMARTweave (Vaidya *et al.*, 2000).

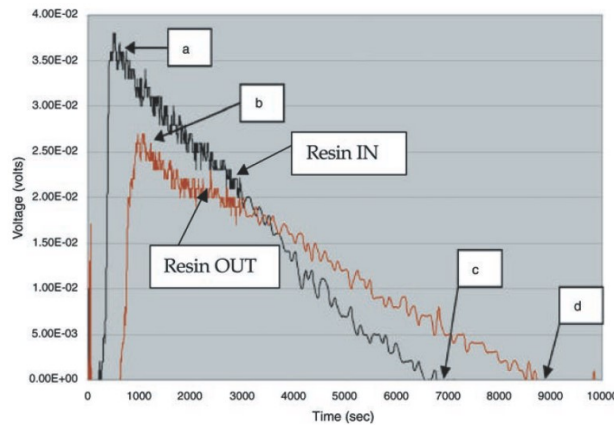


**Figure III.8.** Output voltage profile in a SMARTweave sensor: Resin IN and OUT refer to the voltage monitored at two distinct nodes, the inlet port and the vacuum point of the VARTM apparatus. Points a and c and points b and d refer to the peak values and zero voltage at inlet and vacuum point respectively.

## Flow Front Monitoring

The peak voltage in the curve indicates the arrival of the resin in the sensing junctions. As can be seen, there is a time lag between the two signals. This gap indicates the time required for the resin to move from the inlet point to the vacuum port. The decreasing profile of the voltage is related to the change in the resin state due to the curing progress. As the gelation of the resins occurs, the voltage approaches the zero values. The resin-IN curve reaches the zero earlier than the vacuum point suggesting that the resin curing at the inlet side is faster. This is probably because the resin at the inlet just entered into preform from the resin tank at the end of the impregnation stage and thus experienced a higher heat exposition (“bucket resin”) (Vaidya *et al.*, 2000).

This kind of sensor can be incorporated into the bulk reinforcement, into the vacuum bagging or into the other tools (i.e. the breather and the bleeder material). The compliant nature of the SMARTweave sensors make the suitable especially for one-side mold process, like VARTM, SCRIMP and Vacuum Bagging. Multi-planar sensing configuration, which consists in different sensing planes placed along the thickness of the composite part, can be used to monitor the resin advancement in case of 3D flow.

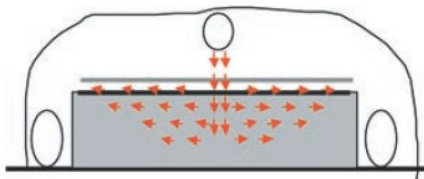


**Figure III.9.** Representation of the 3D flow of the resin in a VARTM process with center inlet port.

Different sensing grid planes are usually employed. One placed on the top of the lay-up, one on the bottom and one or more depending on the thickness of the part between the reinforcement layers. The use of a proper number of SMARTweave sensor provides a global knowing of resin position and cure state.

### 1.3. Ultrasonic sensors

Ultrasonic methods are widely employed for Non Destructive Test (NDT) problems, they also are successfully used for monitoring of the resin cure. Indeed, the mechanical properties measured by ultrasonic wave, i.e. viscosity as well as longitudinal and shear moduli, are sensitive to the extent and length of polymer chains that form during the curing as well as the mobility of the macromolecules. Therefore, measurements of the sound velocity and the attenuation of ultrasonic waves that propagate through the material can reveal the information on the physical and mechanical properties of the medium.

### Chapter 3

Two different methods are employed: the direct reflection and the direct transmission technique. The reflection method uses only one ultrasonic sensor that work as transmitter and receiver. The acquired signals are the reflected waves at the interface between different materials. In the direct transmission method, two sensors, one transmitter and one receiver, are employed. By means of an impulse generator, the first ultrasonic transducer, which work as transmitter, emit an acoustic signal and a short pulse propagates through the sample. The pulse is detected by the second sensor, the receiver. The signal is sent to an acquisition system that elaborate and analyses it, the data relative to running time and attenuation are extrapolate. The transmission method is commonly used in RTM processes(Rath *et al.*, 2000), because it has the advantage of no recording the disturbing echoes.

Ultrasonic sensors (Rath *et al.*, 2000; Schmachtenberg, Schulte Zur Heide & Töpker, 2005; Johnson, 1991) detect sound waves generated by an impulse generator on the opposite side of the mold. The arrival of the resin at sensor location as well as the changes in the resin state due to the progress of curing reactions are detected as change in the sound velocity of the wave and in variation in the attenuation coefficient.

Ultrasonic sound velocity is strictly related to the elastic modulus of the material and the sound velocity influences the elastic coefficients. As known, for a viscoelastic material the complex elastic modulus can be split in two contribution: in-phase with strain and out-of-phase components. The former part (the real part), called storage modulus, determines the reactive forces and the latter (the imaginary part) gives the dissipative forces and it is called loss modulus (Rath *et al.*, 2000). Measurements of the longitudinal wave absorption coefficients provide information about the phase velocities and the complex modulus (Staverman & Schwarzl, 1956):

$$L' = \rho c_L^2 \quad (\text{III.4})$$

$$L'' = \frac{2\rho c_L^3 \alpha_L}{\omega} \quad (\text{III.5})$$

Where  $L'$  and  $L''$  are respectively the real and the imaginary parts of the complex modulus,  $\omega$  is the frequency of the acoustic wave,  $c_L$  is the longitudinal wave velocity and  $\alpha_L$  is the attenuation.

As above mentioned, the running time and the amplitude of the ultrasonic waves are evaluated from the signal received by the second sensor. Using the delay time and the amplitude of the first transmitted pulse the longitudinal ultrasound velocity and the relative variation of the longitudinal wave attenuation can be calculated:

$$c_L = \frac{\tau}{x} \quad (m/s) \quad (\text{III.6})$$

$$\Delta\alpha_L = \ln\left(\frac{A}{A_0}\right) \frac{1}{x} \quad (Neper \text{ mm}^{-1}) \quad (\text{III.7})$$

## Flow Front Monitoring

Where  $\tau$  is the travelling time of the longitudinal wave,  $x$  is the thickness of material, representing the length of the ultrasonic path,  $A$  and  $A_0$  are respectively the current amplitude and the amplitude in the saturation part of the curve and  $\Delta\alpha_L$  is the relative variation of the attenuation coefficient for longitudinal waves. The attenuation coefficient equals the relative variation of the attenuation coefficient (assumed as material parameter) plus a constant. Figure III.10 shows the typical results of a measurement by the ultrasonic sensor, showing the sound velocity and the relative variation of attenuation in dependence of processing time

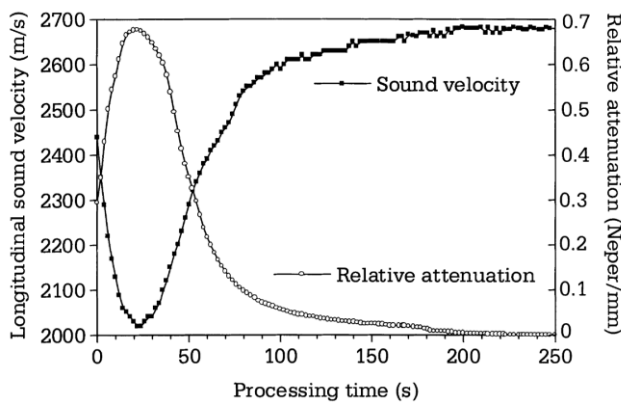


**Figure III.10.** Response of an ultrasonic sensor: longitudinal sound velocity and relative attenuation versus of processing time trends.

In this case, the behavior of an ultrasonic wave was depicted regarding to a curing of a thermosetting resin. The ultrasonic velocity initially decreases to a minimum and then increases up to a constant value. The initial reduction corresponds to a decreasing of the elastic modulus (also called “softening”) as the temperature of material increase (generally due to a preliminary contact with a preheated mold or during the initial curing stage when the part is placed into an oven). As the cross-linking reactions start as the cross-linking density increases, the sound wave propagates more rapidly through the material. The shape of the sound velocity curve reflects the rate of the chemical reaction. Indeed, the slope of sound velocity profile progressively reduces as the curing rate slows and the propagation speed approaches a steady value as the material is fully cured. The attenuation also depends on the processing time. It shows an initial growth up to a peak values corresponding to the softening of the material and then it decrease to a constant level. Due to the initial heating, the resin system softens reducing its viscosity and the polymer chains acquire a high mobility following the force generated by the ultrasound perturbation. As the amount of cross-links between the polymer chains and the weight of macromolecule increase their mobility decrease, the occurrence of glass transition causes as maximum in the attenuation (Rath *et al.*, 2000).

### Chapter 3

Schmachtenberg et al (Schmachtenberg, Schulte Zur Heide & Töpker, 2005) performed a RTM experimental comparing the response of pressure and ultrasonic sensors to monitor the preform impregnation and the subsequent resin curing stage (see figure III.11).

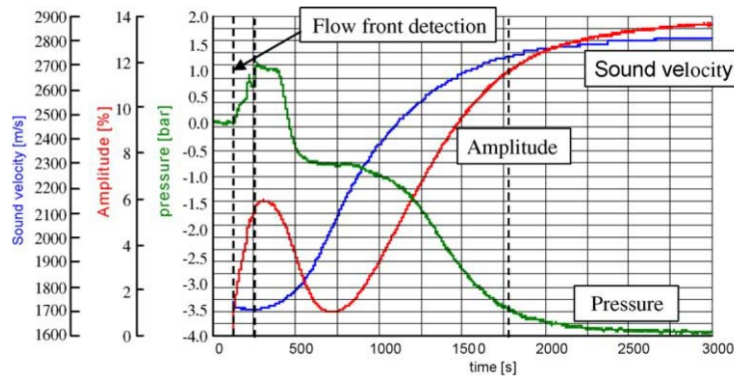


**Figure III.11.** *Ultrasonic measurement of preform impregnation and resin curing stage.*

The arrival of the resin in the sensor locations is detected by controlling both the transmission time and the amplitude. Indeed, when the preform is still dry the transmission of sound wave is not possible and a complete reflection is recorded at the beginning of the impregnation. As the infusion starts and the resin reaches the ultrasonic sensor, the system registers a high attenuation due to the impregnation of dry preform (corresponding to a rising in the pressure). As the infusion proceeds, the sensor measured and increasing in the amplitude due to the homogenization of the fiber wetting and a decreasing of the attenuation. As the mold cavity is completely filled with the resin, the subsequent phase takes place. The properties of the ultrasonic wave follow the behaviors above described.

In order to use the acoustic signal to monitor the evolution of composite manufacturing process a correlation between the thermal-mechanical parameters of the resin system and the measured parameters of the ultrasound wave have to be built. A quantitative relation between the sound velocity and the reaction conversion (degree of cure) for a resin sample can be constructed starting from the data obtained by isothermal differential scanning calorimetry (DSC) tests that provide data regarding the reaction conversion (curing as function of time) and the thermal properties of the resin.

#### **1.4. Fiber optic sensors**

The usage of Fiber optic sensors into LCM processes provide a non-invasive means to obtain real time information regarding the flow and the curing of the resin in order to monitor and control the progress of the

## Flow Front Monitoring

manufacturing process itself (Lim & Lee, 2000; Dunkers *et al.*, 2001; Melin *et al.*, 1999; Woo Il Lee, Loos & Springer, 1982).

Several monitoring methods, such as flow visualization techniques and thermocouple, implicate that the sensors have to be installed on the surface of the mold and hence are able to mainly monitor the flow along the mold wall. Conversely, the fiber optics sensors can be embedded into the dry preform without compromising the structural integrity of the composite part. Indeed the optic fibers have a small size and light weight, comparable with the reinforcement fibers themselves and the cladding layer are basically made of glass, so that they perfectly integrate with the surrounding fibers, especially in case of glass-fibers reinforcement. Therefore, they are appropriate to follow the resin flow within the bulk reinforcement, also in case of thick composite part.

Optical fiber consists of a core and a cladding. The core is the path of light and the cladding is the mechanical protection from outside impact. The laser light is transmitted through the optical fiber from one end and the intensity of the light at the opposite end is recorded. To detect the position of the resin within the preform and reconstruct the flow path short segments of the cladding should be removed from the optical fiber. Each of these bare spots act as sensor (see figure III.12) (Woo Il Lee, Loos & Springer, 1982).

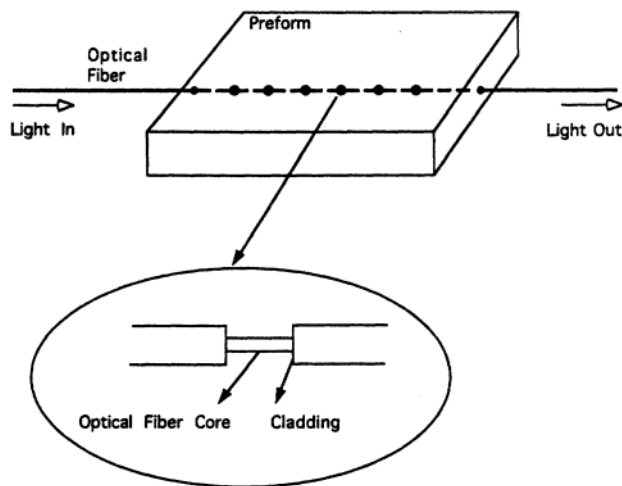


**Figure III.12.** Set-up of the optical fiber for measuring of the resin flow prior placing within the fiber preform

Before the resin reaches the bare spots along the optical-fiber sensor, a large light signal can be transmitted through the optical fiber (see Figures III.13). As the resin reaches the bare spots (the sensor), the light leaks through

### Chapter 3

these bare spots due to the different refractive indices of the resin and the cladding(Lim & Lee, 2000).

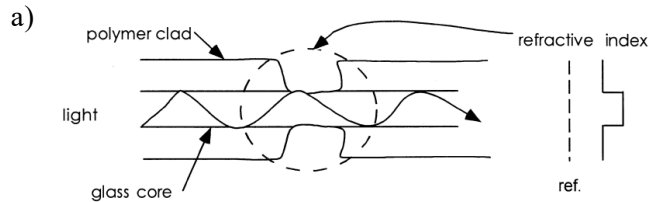


**Figure III.13a.** Behavior of transmitted light in an optical fiber before the resin reaches the sensing point.

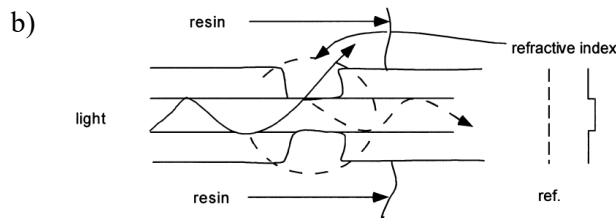


**Figure III.13b.** Behavior of transmitted light in an optical fiber after the resin reaches the bare spot.

Therefore, a significant and sudden drop in the intensity of the transmitted light occurs and the arrival of the resin front can be detected. A typical signal from the sensor is shown in figure III.14, the intensity of light sharply decreases as the resin front reaches the bare spots.

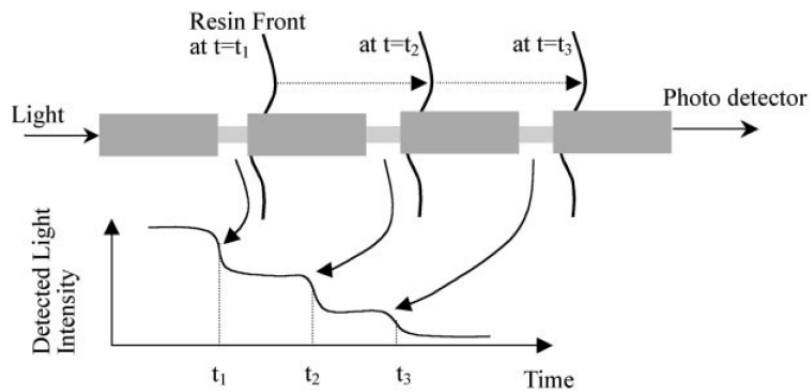


**Figure III.14.** Typical signal from the optical fiber sensor.

## Flow Front Monitoring

From the changes in the light intensity the rate of resin flow can be deduced. In addition, the optical fibers can be arranged to form a 3-dimensional grid embedded in the preform allowing to monitor the 3-D flow of the resin (see figure III.15).

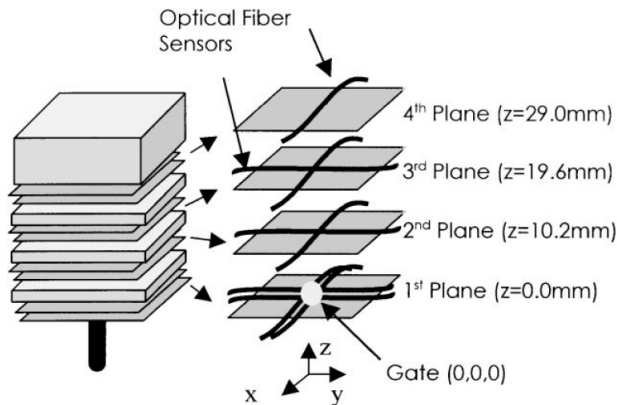


**Figure III.15.** The optical fibers can be placed on different planes along the thickness of the laminate between the stacked fibers layers. The arrival of the resin on each sensing point is detected and the 3-D path can be reconstructed. (Lim & Lee, 2000).

The optical fiber system are extremely sensitive to microbending when they are compressed between the preform layers inside the mold. It was observed that higher is the fiber volume fractions higher is the deterioration of the transmitted signal especially in the case of random mat. The effect of the bending reduce with the parallel unidirectional reinforcements. Moreover, it is likely that compressive stresses are induced in the optical fiber itself, affecting the acquired signal and resulting in a misinterpretation of the data (Dunkers *et al.*, 2001). Therefore, particular attention have to be paid during the calibration of the sensors. Moreover, to overcome this issue, the manufacturers often place over the sensor a glass sleeve, long enough to cover the entire fiber. These glass sleeves are not permanently fixed onto optical fiber so that slight movements along the optical fiber are allowed when they are placed in the mold and the liquid may flow inside them and reach the sensing point.

Both the transverse unidirectional mat and bi-directional weave cases are between these two extremes.

## Chapter 3

### 1.5. Temperature sensors

Temperature sensors (generally thermocouples) (Tuncol *et al.*, 2007) are used to measure the temperature of the mold cavity that changes due to (i) the arrival of the resin to a sensor if the inlet resin is either cooler or hotter than the mold walls, and/or (ii) the exothermic reaction which occurs with resin curing.

Thermocouples basically consist of two conductive wires that are joined each other at one of ends. The junction represents the sensing node that is attached to the medium of which the temperature will be measured. The other ends of the wire is connected to a device, thereby closing the electrical circuit. When the hot junction is heated, a small voltage difference is established between the wires due to an electromotive force. The voltage,  $V$ , is proportional to the temperature gradient between the temperature of the sensing junction,  $T_{hot}$ , and a temperature reference,  $T_{ref}$ , that is kept constant:

$$V = \alpha(T_{hot} - T_{ref}) \quad (\text{III.8})$$

Where  $\alpha$  is the Seeback coefficient. The main use of thermocouples in the manufacturing of fiber reinforced polymer (FRP) composite materials is related to the monitoring of the resin curing. Knowing the temperature history experienced by the resin allows to predict the degree of cure. The curing reaction of a thermoset resin system is exothermic and thus, the temperature rise due to the heat release during cure can be detected by the thermocouple sensors. Obviously, in order to use the temperature data to draw the time profile of the degree of cure, thermal and kinetics parameters of the resin and the tooling apparatus should be known.

The resin location and hence the flow front propagation can be also monitored if there is a significant temperature difference between the resin and mold walls. Indeed, the arrival of resin in a selected location of the mold is detected as a sharp drop in the temperature. This applies under either one of the following two conditions: (i) the thermoset polymer is heated prior to injection while the mold walls are kept initially at a lower temperature (generally room temperature); or (ii) the inlet thermoset polymer is at room temperature while the mold walls are heated.

A typical thermal history in a RTM process, (but it can be representative of a generic LCM process) is shown in figure III.16 (Johnson, Rudd & Hill, 1995).

## Flow Front Monitoring

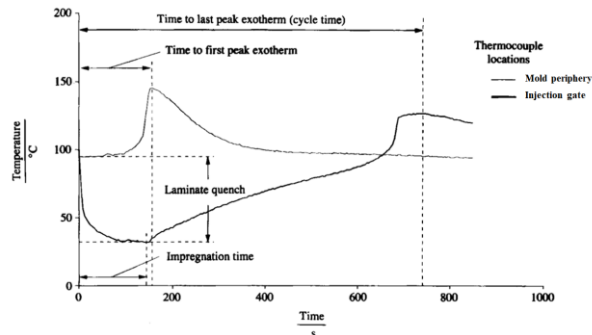


**Figure III.16.** *Temperature profiles during the resin infusion in a RTM process in two different location of the heated mold: resin inlet point and mold periphery.*

The sensor systems consists of several thermocouples embedded in selected locations of the mold, from the resin inlet gate to the ends of the molds. The number of thermocouples that should be employed to a correct estimation of resin flow path depends on the size and the shape complexity of the mold. The impregnation time can be represented by the period between the resin arrival at the injection gate, marked by a sudden fall in injection gate temperature, and a rise in the gate temperature. Indeed, when cold resin contacts the heated mold surface a sharp drop in temperature (mold quenching) occurs at that location.

The injection gate is continuously quenched by the resin until the end of impregnation, after that heat is recovered gradually at that location. The period available for fiber preform wetting is approximated by the time to the first exothermic peak which occurs near the mold periphery.

Also, the resin cures last at the injection gate, as marked by a sharp increase in temperature, due to the mold quench effect and a comparatively short residence time of the resin in that location of the mold (Johnson, Rudd & Hill, 1995, 1997). The use of thermocouples in a sensor system has significant advantages compared other sensor due to basically their limited cost and higher response speed. However, they present several shortcomings that limit their use especially if used in the LCM process

The response rate and accuracy of these sensors depend on the thermal properties of the mold and the resin, temperature difference between the inlet resin and the mold walls, and the flow rate (Schmachtenberg, Schulte Zur Heide & Töpker, 2005). The thermocouples are more useful in case of low thermal conductivity of mold material, high resin flow rate, high temperature difference between inlet resin and initial mold walls, and high specific heat of resin. Therefore they are unsuitable in case of metallic mold, but they could be used for flow monitoring with molds made of plastic material. However, the typical process conditions and parameters that commonly occur in LCM

## Chapter 3

processes are far from these, therefore the thermocouples should not be preferred over other sensor types and should be used with caution.

### ***1.4. Pressure sensors***

Pressure sensors (Di Fratta, Klunker & Ermanni, 2013) can be used for flow monitoring but not for curing. As the resin reaches a sensor location, the pressure at that point rises to the fluid pressure plus the initial static compaction pressure.

A pressure transducer is a transducer that converts pressure into an analog electrical signal. In a strain-gage base transducer, which is one of the most commonly used the conversion of pressure into an electrical signal is achieved by the physical deformation of strain gages which are bonded into the diaphragm of the pressure transducer and wired into a Wheatstone bridge configuration. Pressure applied to the pressure transducer produces a deflection of the diaphragm which introduces strain to the gages. The strain will produce an electrical resistance change proportional to the pressure. Accurate interpretation of resin arrival is usually difficult because of a slow rise in pressure. Moreover, placing pressure sensors at many discrete locations on the mold wall is expensive and hence their use is strongly limited, taking into account that these sensor are poorly reusable after a composite manufacturing cycle.

### ***1.6. Electric time-domain reflectometry (E-TDR)***

Electric time-domain reflectometry (E-TDR) method is used to measure the wetted regions of sensor wire by applying high speed pulses to the wire and detecting the reflection signals (Dominauskas, Heider & Gillespie, 2003, 2007) returning from the discontinuities with the transmission line. The reflection occur at different positions in the wire where the impedance of the sensing medium change (see figure III.17). The frequencies of the signals are in the microwave range, so the time scales are extremely fast.

## Flow Front Monitoring

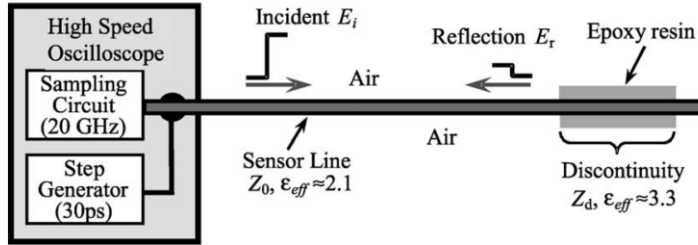


**Figure III.17.** Scheme of the E-TDR technique for flow monitoring:  $E_i$  and  $E_r$  are the voltage of emitted and reflected waves at a specific location respectively;  $Z_0$  is the characteristic impedance of the line;  $Z_d$  is the load or discontinuity impedance.

The generator emits a voltage with high-speed pulse ( $E_i$ ). It requires a finite time to travel down the line to a specific location (where is the discontinuity). The velocity of the voltage depends on the properties of the medium through which the voltage propagates summarized by the dielectric constant  $\epsilon_{eff}$  (or expressed by the medium impedance). If the impedance of the termination on the line is different from  $Z_0$ , a reflected wave,  $E_r$ , travel back to the source. The ratio of the reflected wave to the wave originating at the source (also called reflection coefficient) is related to the ratio between the two distinct impedance:

$$\frac{E_r}{E_i} = (Z_d - Z_0)/(Z_d + Z_0) \quad (\text{III.9})$$

The value that the ratio can take is affected by the resin system. The reflected voltage at each discontinuity was derived using the eq.(III.9) of the reflection coefficient. The time of flight can be calculated with the dielectric constant of the sensor in air and resin and the lengths of these regions. The E-TDR sensors that are used in LCM processes detect the arrival of the resin as a function of location of negative reflection (figure III.18a) (Dominauskas, Heider & Gillespie, 2003). As the liquid resin reaches the sensor a significant discontinuity on the emitted wave results, which can be used to detect the resin arrival.

Chapter 3

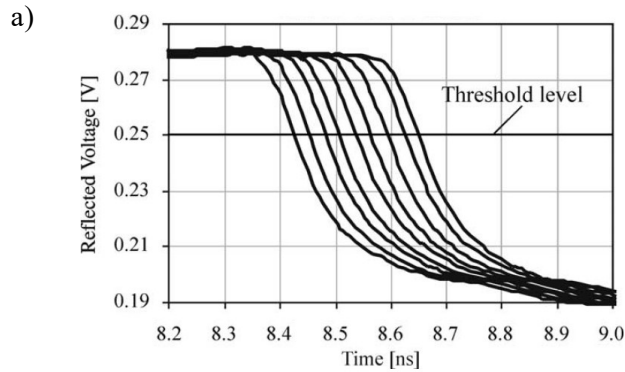


**Figure III.18a.** Example of planar E-TDR sensor response: voltage changes versus time trends.

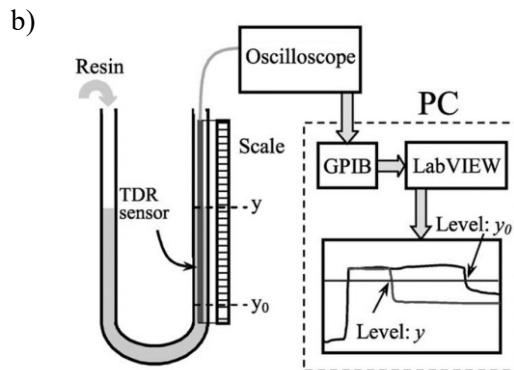


**Figure III.18b.** Example of planar E-TDR sensor response: resin level measurement

Initially, to calculate the resin location the speed of electromagnetic waves in the sensor is evaluated while it is not affected by the resin. A threshold value is calculated and it corresponds to the inflection point in the reflected voltage curve. The level of resin can be estimated by multiplying the initial speed with the arrival time of the inflection point. The gradual movement of the signal (i.e. the intersection point of the voltage curve with the threshold line) to the left of the diagram in figure 18a corresponds to the increase of the resin level from the  $y_0$  value to a higher  $y$  (see figure III.18b).

Different sensor configurations for a E-TDR sensors have been developed and tested (Dominauskas, Heider & Gillespie, 2003): planar transmission line geometry or two-wires configuration. The planar configuration (which the figures III.18 refer to) consists of a rectangular wave-guide in which the signal propagates (figure III.19a and III.19b). The sensor is a conductive strip (generally made using a printed circuit technology (PCB)) that is in direct contact with the resin. The planar sensor demonstrate a good capability to

## Flow Front Monitoring

detect the resin location with a high resolution. On the other hand, it has limitations in applications where it is necessary to embed the sensor in the fiber preform (for example VARTM processes). In this case, a flexible and small-case sensor should be preferred. The two-wire sensor consist of two conductive cables with an insulating external layer that prevent the direct contact with the resin liquid. It reduces the sensitivity of the sensor compared to the planar configuration. Conversely, the insulation of conductive wire allow employing this sensor with conductive preform where the transmission line would otherwise be shorted, resulting in large losses and limiting the maximum sensor length.

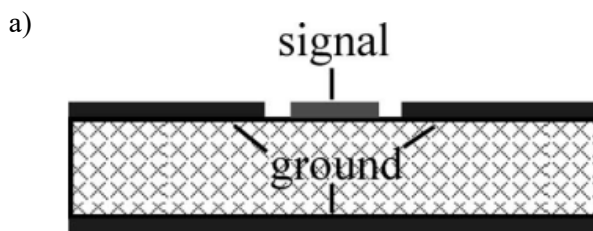


**Figure III.19a.** *Scheme of E-TDR planar sensor.*

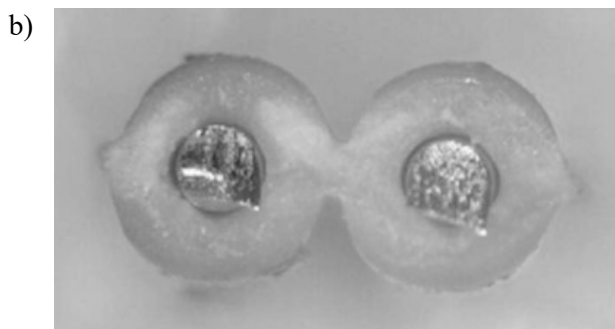


**Figure III.19b.** *Cross section of two wires sensor.*

The two wires type sensor was successfully used to monitor the flow front during the infusion of fibers preform (figures III.20) (Dominauskas, Heider & Gillespie, 2003).

### Chapter 3

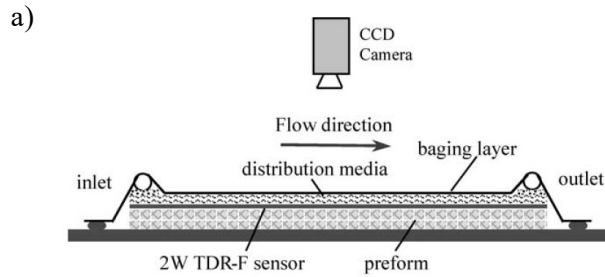


**Figure III.20a.** Scheme of the experimental setup for VARTM process.

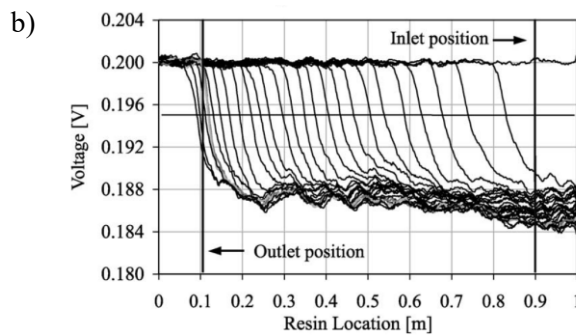


**Figure III.20b.** Response of the TDR-F sensor to the arrival of resin flow at the sensing locations.

The movement of the resin from injection line to the vent results in local dielectric changes of the transmission line. Initially, the flow rapidly fills out the preform, determining large gaps between the one measurement and the following. As the experiment progresses the flow slows down and the TDR response reflects the resin movement reducing the spatial gaps between the consecutive intersection points. The exact locations of the flow front can be calculated applying the threshold value procedure above described. The E-TDR embedded sensor can be also used in process scenarios that include sequential injections or injections with multiple injection points to simultaneously monitor multiple resin flow fronts. The resin arrival on the sensor is detected by means of a drop of the reflection voltage.

However, limitations in the accuracy and sensitivity of sensor occur when the flow fronts merge together due to the dispersive nature of the resin, transmission line losses, and multiple reflections. Indeed, the reflections cannot be fully separated and the simple threshold procedure to calculate the resin level is not easily employable. The threshold procedure can provide  $\pm 30$  mm distributed sensing accuracy with a 1 meter long sensor when multiple flow fronts exist.

This technique requires high speed equipment since reflections occur in the order of nanoseconds.

### **1.7. Dielectrical analysis (DEA)**

Dielectric analysis is based on the (McIlhagger, Brown & Hill, 2000; Hegg, 2005; Kim & Lee, 2002; Bang *et al.*, 2001; Rowe *et al.*, 1845) measurement of the dielectric properties, i.e. permittivity and ionic conductivity of the under test material. DEA can be employed during the in-situ monitoring of the composite manufacturing process. A dielectric material is placed between electrodes forming a capacitor and an alternating electric field is applied across the plates. Permittivity, which is a measure of the molecular alignment, loss factor, which is the energy required to align the dipoles, and the ionic conductivity, which occurs through impurity ions, can be determined from the output current (Abraham & Mcilhagger, 1998). Since the dielectric properties of the resin are strictly related to the viscosity, which is in turn a marker of the changes occurring in the material, these properties have been initially used to predict the degree of polymerization of the resin (Bang *et al.*, 2001; Lee & Kim, 2004).

The dedicated literature reports the usage of two types of sensing plates: (1) parallel-plate sensors placed on both sides of a mold (Hegg, 2005; McIlhagger, Brown & Hill, 2000); and (2) co-planar sensors (fringing effect field, FEF) placed on only one side of the mold (Rowe *et al.*, 1845; Vaidya *et al.*, 2000; Kim & Lee, 2002). In Skordos *et al.*'s study (Skordos, Karkanis & Partridge, 2000), a lineal sensor was used to monitor mold filling by measuring the total length of the region covered with resin on the sensor. Mounier *et al.* (Laurent-Mounier, Binétruy & Krawczak, 2005) used two parallel carbon fiber tows as electrodes of a lineal dielectric sensor to measure resin flow in a glass fabric preform. However, the single surface sensor suffers from a number of limitations that restricts its widespread use. First, the localized sensing region is considered the major limitation. Second, due to the low scanning depth, measurement through the thickness of a composite requires that the sensors should be placed at intervals within the fiber textile layers. Therefore, if such sensors remain embedded the components, they adversely affect the mechanical performance of the final part (McIlhagger, Brown & Hill, 2000). On the other hand, the parallel plate sensor consisting of two parallel plate shaped electrodes, between which the component is sandwiched, seems to be a more promising solution (Figure III.21).

### Chapter 3

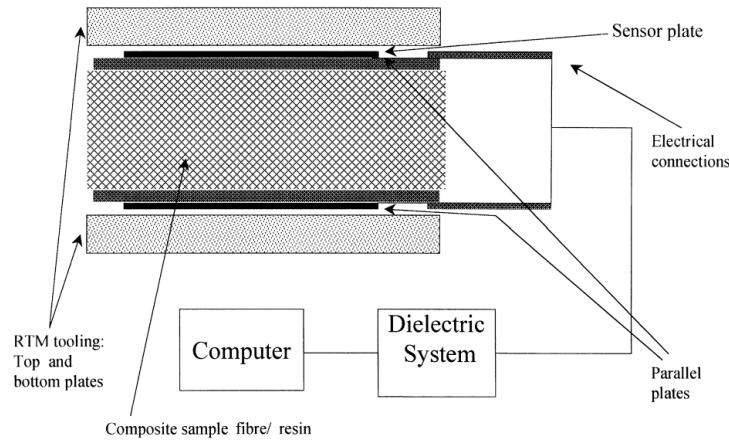


**Figure III.21.** Schematic representation of a parallel plate dielectric sensor integrated in a RTM tool.

The external electrodes can be placed outside of the composite laminate and should not compromise the mechanical integrity of the component. The bulk dielectric properties of the material can be evaluated.

Moreover, other advantages related to the usage of these sensors in the cure monitoring are worthy to be highlighted. The parallel plate sensor provide data having a good correlation with data from existing thermal analysis techniques such as differential scanning calorimetry (DSC) and dynamic mechanical analysis (DMA) (Abraham & Mcilhagger, 1998). The parallel plate configuration measures the average or bulk properties of the sample. This is considered to be more representative of overall cure than surface only measurements.

Three large parallel-plate sensors were used in Hegg et al. (Hegg, 2005; Yenilmez & Murat Sozer, 2009) and Rowe et al. (Rowe *et al.*, 1845) to monitor different regions in the mold. The dielectric sensors are capable of accurately measuring fill-front position and degree of cure. Some authors pointed out that the admittance signal from the sensors shows a linear dependence of on the fill-front positions. This type of sensor relies on fringing electric fields and allows continuous sensing of fill-front progression in one dimension (Skordos, Karkanis & Partridge, 2000). The sensing system designed by Rooney et al. (Rooney *et al.*, 1998) converts the capacitance to voltage and correlates this to flow-front position. This system is limited to sensing fill-front location and does not provide the ability to measure resin properties.

Flow Front Monitoring

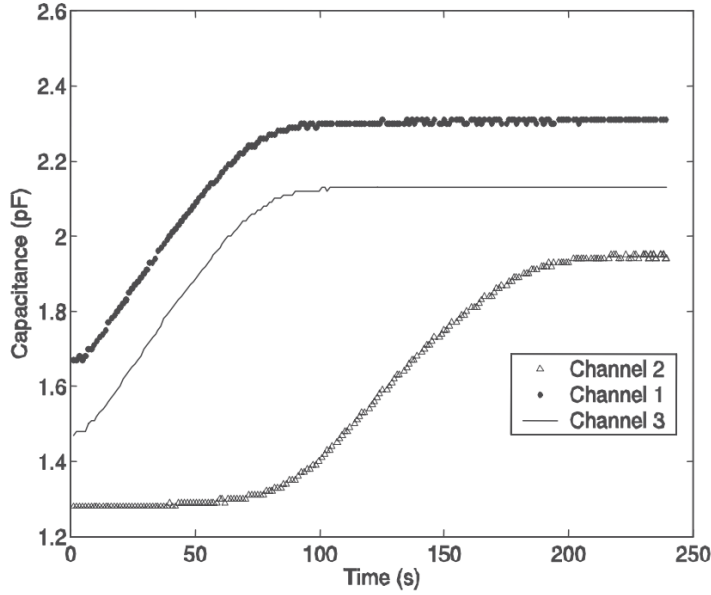
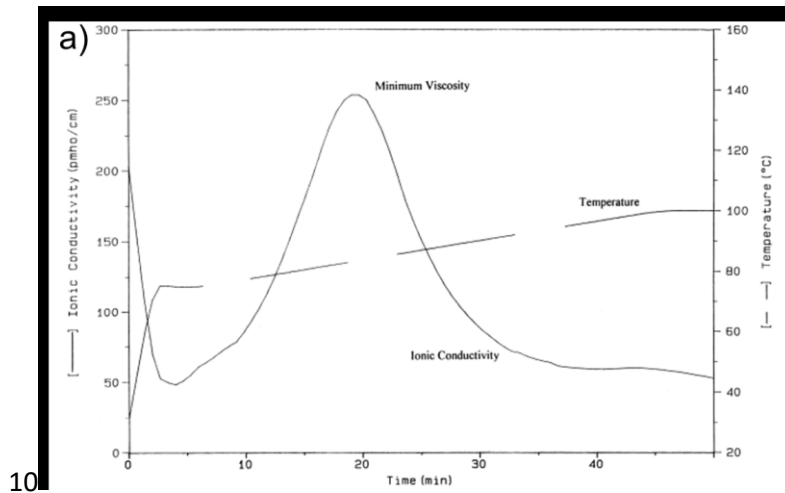


**Figure III.22.** Dielectric monitoring of the resin fill front: capacitance as function of time.

Similar to resistance, the capacitance of resin changes as it cures which permits monitoring of resin cure. Vaidya et al. (Vaidya *et al.*, 2000) and McIlhagger et al. (McIlhagger, Brown & Hill, 2000) used dielectric sensors for localized cure monitoring.



10

### Chapter 3

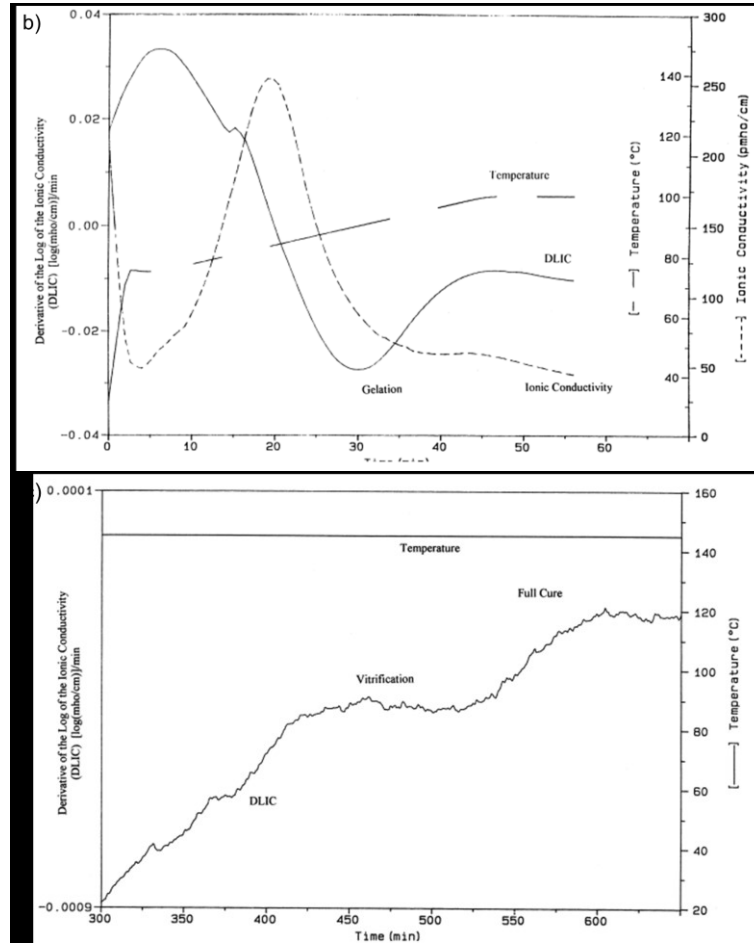


**Figure III.23.** Dielectric measurement: a) correlation of dielectric property with the viscosity of the resin; b) correlation between the gelation and the ionic conductivity ; c) vitrification/full cure estimate by means of the dielectric data.

As mentioned, DEA measures the two fundamental electrical characteristics of a material, the conductance and the capacitance as a function of time, temperature and frequency. Changes in the dielectric properties of a curing resin can be related to the salient chemical and rheological events of the process (McIlhagger, Brown & Hill, 2000). In DEA, the ionic conductivity is a measure of the ease with which ionic impurities can migrate through the resin and is thus directly related to viscosity. In particular, studies of the correlation between the data from DEA and other consolidated analysis techniques (i.e. DSC and DMA) confirmed that the maximum in the resin conductivity coincides with the point of minimum viscosity under isothermal or dynamic (thermal) conditions (figure III.23a) (Maistros & Partridge, 1998).

## Flow Front Monitoring

Gelation marks the first significant appearance of the crosslinking reaction and the gel point is a key parameter for the resin. The ionic conductivity can be related to the initiation of gelation states: “the inflexion point in the drop of the logarithmic ionic conductivity after the point of maximum flow provides the first evidence of a gelled material” (figure III.23b) (Maistros & Partridge, 1998). The gelation is characterized by the progressive formation of the molecular network thus resulting in a substantial increase in the crosslink density, glass transition temperature. Vitrification follows gelation and occurs as a consequence of the increasing average size of the molecules and by the network becoming tighter through crosslinking. The higher dimensions of the macromolecule and the increasing in the number of the cross-links reduce progressively the ions mobility of the polymeric material. The first point of inflexion following the maximum resin conductivity is taken as the onset of gelation (figure III.23b). Therefore, by evaluating the variation in the ionic conductivity calculating the derivative the evolution of the resin cure can be assessed (figure III.23c).

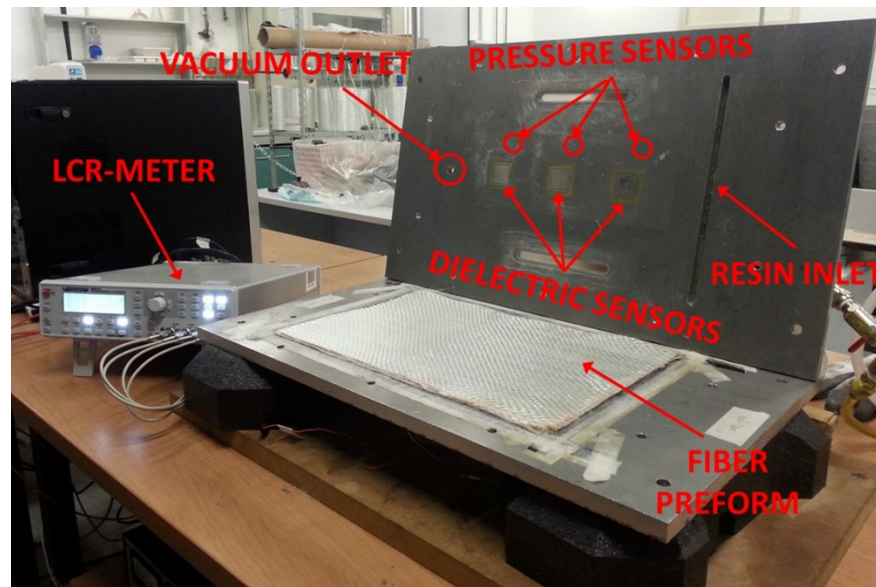
Since dielectric sensors have no need for direct contact with the resin, one side of the sensor can be placed over a non-metallic mold lid, and with this approach, sensors do not degrade the surface finish of the manufactured part. Nonetheless, the mould may need maintenance more often due to the non-metallic material used.

## Chapter 3

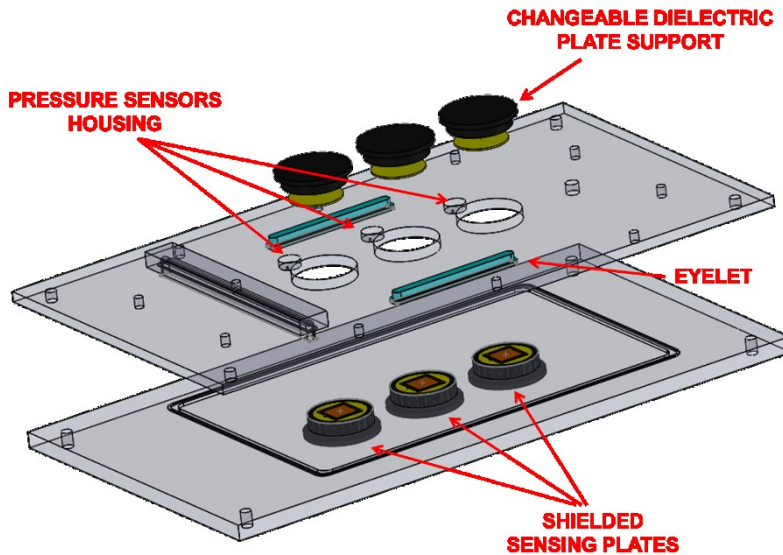
### 2. Experimental set-up for monitoring of the resin flow

#### 2.1 The LCM Mold

A laboratory scale sensing apparatus was designed and developed to reproduce a LCM manufacturing processes (figure III.24 and 25).

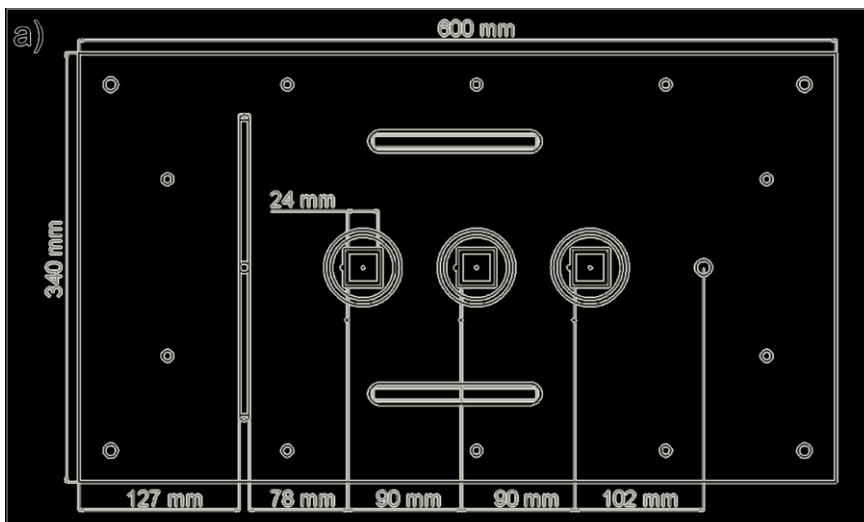


**Figure III.24.** *Experimental setup: sensed die and acquisition system used in the flow tests*



**Figure III.25.** 3D sketch of the sensing mold

The mold consists in two 10 mm thick aluminum sheets that were used as die and counter die to avoid thickness variations or inflections that affect the sensors geometrical configuration (distance) and consequently the measured capacitance. The size of the cavity was 380x240x3 mm<sup>3</sup>. The low depth of the cavity compared to the higher in-plane dimensions allows the establishing of 1D flow within the mold. The die was fixed on the working table and tightened by four peripheral bolts, while the distance and parallelism between the die was regulated using ten registration bolts.



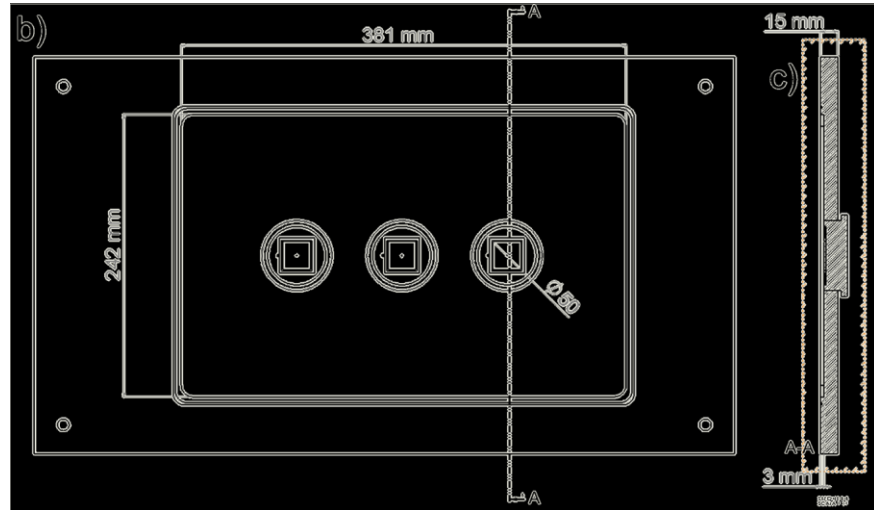


**Figure III.26.** Drawings of the mold: a) bottom view of upper die; b) top view of lower die; c) Section A-A.

Two eyelet transparent windows were also drilled on the upper mold in order to perform a visual observation of the flow advancement (see figure III.26a) independently from the measurements by means the sensors. A video camera was mounted above the transparent window during the infusion tests to record the progress of the experiment. The obtained data were used as validation and comparison with the sensors measurements. Two holes were also placed in the counter die at the edges of cavity to be used as fluid inlet and the vacuum port. In correspondence of inlet vent, a rectangular cave was milled and a distribution media was placed to achieve a one-dimensional flow. This is a simple case that can unlikely occur in actual manufacturing process, however is very useful to for the experimental work to tune up the numerical model and determine the permeability.

The mold was instrumented with dielectric and pressure sensor to continuously monitor the advancement of the resin during the impregnation.

## 2.2. Dielectric Sensors

The sensing unit of DEA consists of two electrodes. The parallel plate sensor is the most straightforward sensor type. Since the resin in the composite is a dielectric, the electrodes and the composite form a capacitor. The material under test is sandwiched between two parallel plates that are connected to an alternate excitation voltage. The material's bulk dielectric properties can be analyzed by modelling the dielectric with an equivalent circuit of a capacitor and a resistor in parallel, whose values rely on resin and reinforcement properties. Conversion of the measured data to the material's dielectric

properties (complex dielectric constant, conductivity and impedance) using this method can be easily achieved.

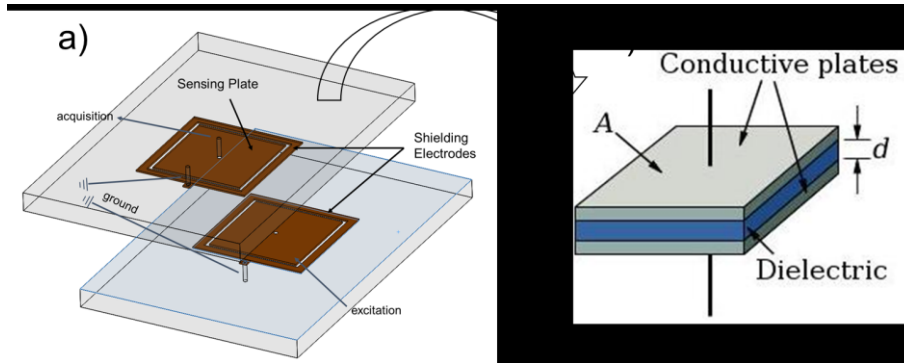


**Figure III.27.** a) 3D scheme of the designed shielding sensor; b) operating principles of a parallel plate dielectric sensors.

The application of this sensor to the monitoring of the preform filling and impregnation is based on the simple assumption that capacitance variations are imputable to variations of the dielectric material between the two parallel-plates, i.e. the actual volume fractions of reinforcement, fluid and air/vacuum. These variations are firstly induced by the arrival of the unsaturated flow and vanish as soon as the preform between the plates is fully saturated.

Capacitance of a parallel-plate capacitor is ideally given by the well-known equation:

$$C = \varepsilon_0 \varepsilon_r \frac{A}{d} \quad (\text{III.10})$$

Being  $A$  the plate's area,  $d$  their mutual distance,  $\varepsilon_0$  vacuum permittivity and  $\varepsilon_r$  relative permittivity of the dielectric material.

The distance between the plates should remain constant throughout the process for a reliable measurement. This leads to an issue in a production environment (e.g. Resin Transfer Moulding or Vacuum Assisted RTM) where the plates are susceptible to the external pressure applied on the laminate or to the resin pressure during the filling that lead to a variation on a continuous variation of laminate thickness and therefore the equipment requires continuous re-calibration. Besides, the  $A/d$  ratio ( $A$ : area of the plate,  $d$ : distance between the plates) should be big for enough sensitivity, making this method inappropriate for a composite with either complicated or thick shape. However, because of this method requires the presence of the electrodes on both sides of the mold, its usage is more difficult for manufacturing techniques using single-sided molds. In addition, the sensors are vulnerable to external electric fields and are affected by non-uniform regions of the electric field due to the fringing effect that could occur at plate's edges. The detected

### Chapter 3

capacitance could deviate from the theoretical value (as calculated by eq.(III.10)). When the sensors are employed for monitoring the resin flow, this phenomenon could also lead to an increase of capacitance before the actual arrival of the resin on the edge of sensing plate, resulting in a misleading interpretation of the data. To eliminate both the effects a conductive shields was placed around the sensing and the excitation plate reducing its size with respect to the exciting plate. The dielectric sensors have a reduced sensitivity to the external fields and fringing effect.

Three dielectric sensors were adopted: the  $mm \times 24$  mm sensing plate area is surrounded by a 2 mm wide shield with 1 mm gap filled by non-conductive material. Both plates and shield were made of copper that was deposited on a thin cylindrical plates made of an insulating material. Each as printed sensor plate was mounted on a PVC support (see figure III.25). The supports can be easily extract from the mold, allowing to replace the sensor in case of damage or failure. In addition, they further insulate the sensing plate from the potential disturbances exerted by the metallic mold. The supports and the sensor plate are embedded in holes machined into the rigid aluminum die (see figure III.25). The three shielded dielectric sensors (hereinafter labelled as S1, S2 and S3) were then embedded in the die. The first sensor was placed at 80 mm by the inlet vent. Then, the sensors distance from each other 90 mm (see figure III.26).

### 2.3 Pressure Sensors and data acquisition devices

Three holes (labelled P1, P2 and P3 in the following) were drilled in the counter die in correspondence of the edge of dielectric sensors (see figures III.24, 25 and 26) to accommodate the piezoelectric pressure sensors (Honeywell-SSDRNT100PAAA3) for liquid pressure acquisition within the mold cavity.

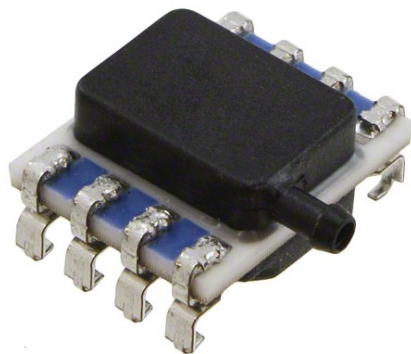


**Figure III.28.** Pressure sensor: *Honeywell SSDRNT100PAAA3*

## 2.4. Data acquisition devices

Pressure data were collected using a National Instruments PCI 6132 data acquisition system interfaced with the sensors via a NI BNC-2110 connector. An in-house program was implemented to manage acquired data in the Labview suite. The data were compared with the capacitance measurements and used to calibrate the dielectric sensors. During the infusion tests, to avoid damages to the pressure sensors an un-reactive liquid was employed. Indeed, the solidification of the catalyzed resin, after the infusion of the preform would be caused the breakage of the sensor.

A LCR meter (Hameg HM8118) was connected to the dielectric sensor to acquire the signal from three sensors.



**Figure III.29.** HM8118 LCR Bridge/Meter

The instrument provide directly the measurements of capacitance and resistance without the need to convert the volt signal to the quantities of interest. The conventional LCR meters, however, can detect only one channel at time, therefore a switch system with three channel was developed and built. The switch consists in three couple of relays, each pair is connected to a dielectric sensor allowing to isolate the signal of a sensors from the others. The channel switch frequency was set to acquire three consecutive measurements for the same sensor before changing the sensor controlled. It allows to compensate the signal noises due to the high frequency alternate current employed for the measure and the instability of the signal and reconstruct the actual trend of capacitance and resistance.

## 2.5. Materials

### 2.5.1 Glass fiber reinforcement

The dry preforms employed are made of glass fibers that are commercially available. Two distinct configurations for the preform have considered in the experimental campaign. In the first infusion tests, a plain weave 0–90 e-glass fabric with grammage of 250 g/m<sup>2</sup> was employed. The preform consists of

### Chapter 3

four layers of the glass fabric, stacked in the mold cavity, a volume fraction of approximately 20%. Was obtained The resulted high porosity and permeability, due to the reduced “packaging density” of the dry preform, determine an easy flowing of the resin through the fibers bulk, with a consequent reduction of the time required for the impregnation. This was useful in the first tests to speed up the process.

The second preform was made of eight layer of twill e-glass fabric (390 g/m<sup>2</sup>). A volume fraction of 40% was obtained. Fabrics were carefully stratified up in order to prevent the formation of undesired race tracking channels.

For each fabric, the preform in-plane dimension was 370×210 mm<sup>2</sup>, according to the dimension of the mold cavity. The dimension of the preform in the flow direction was slightly smaller than the cavity, because of a few free spaces between the inlet and the vacuum vent location and the edges of the preform are required to ensure the correct resin propagation through the reinforcement and the establishing of the mono-dimensional flow.

#### 2.5.2 Resin liquid system

The resin system is a two-part system comprising the unsaturated polyester resin (ESI Resin GP UK OTL) and the hardener (Curox M-312). The employed resin is well suited for hand lay-up and spray techniques and cures at room temperature. Table III.1 lists the main properties of the employed resin.

**Table III.1.** *Properties of the Polyester Resin.*

Property	Value	Unit
Viscosity, 20 s <sup>-1</sup> , 23 °C	300 - 800	mPa · s
Density	≈ 1100	Kg/m <sup>3</sup>
Gel time from 25 to 35 °C	18-30	min
Peak temperature	105 - 135	°C
Glass transition temperature	93	°C
Cure time (room temperature)	24	h
Flash point	≈ 33	3

The long cure time required, approximately 24 hours at room temperature, and the low viscosity allow using the mentioned resin system for the Resin Infusion tests without affecting the filling and reinforcement impregnation. An un-reactive liquid (mineral oil) with a similar viscosity was also used in the first experimental trials to testing the apparatus. The relative results was used to compare the data from the pressure and the dielectric sensors with the outcomes of the numerical simulation.

# Chapter 4: EXPERIMENTAL RESULTS

## 1. Infusion test of un-heating resin

### *1.1. Materials and Experimental procedure*

Two different test cases, hereinafter Test 1 and Test 2, were reproduced. In first trial, Test 1, a dry preform made of four layer of glass fabrics with  $250 \text{ g/m}^2$  of grammage was considered, with a vacuum level of 0.80% (corresponding to an internal absolute pressure of 20 kPa) within the mold. Mineral oil was employed, instead of resin, in order to collect also pressure data without damaging the pressure sensors. In this test case, the flow was monitored using both dielectric and pressure sensors, to compare the detection of the flow front arrival by means of both sensing methods, as well as to validate the numerical macro scale model. In Test 2, the unsaturated polyester resin catalyzed with 1% in weight of hardener was employed. As mentioned, the resin system was a two-component mixture comprising the unsaturated polyester resin (ESI Resin GP UK OTL) and the hardener (Curox M-312). The reinforcement consisted of eight layers of the  $390 \text{ g/m}^2$  glass fiber twill, while the same vacuum conditions have been applied. The catalyzed resin was cured at room temperature in order to obtain a fully cured laminate for the subsequent microscopy analysis to assess the presence of defects and voids and to evaluate the actual fiber volume fraction. The curing stage was also monitored by means of the dielectric sensors and the degree of cure profiles of the resin in the sensing locations were estimated. Several samples were extracted in distinct selected locations of the laminates, i.e. in proximity of the sensed zone. Microscopy observations were finally processed using image analysis tools to quantitatively assess experimental predictions.

## Chapter

### 1.2 Result of the Test 1

Figure III.1 reports the pressure profiles the evolution of intra-tow, extra-tow, and total resin volume fraction as well as the normalized capacitance values as measured by the dielectric sensors. Capacitance values were normalized, for each sensor, assuming the minimum and maximum capacitance in correspondence of absence of resin (with only the reinforcing fibers between the conductive plates) and full saturation conditions for each working fluid.

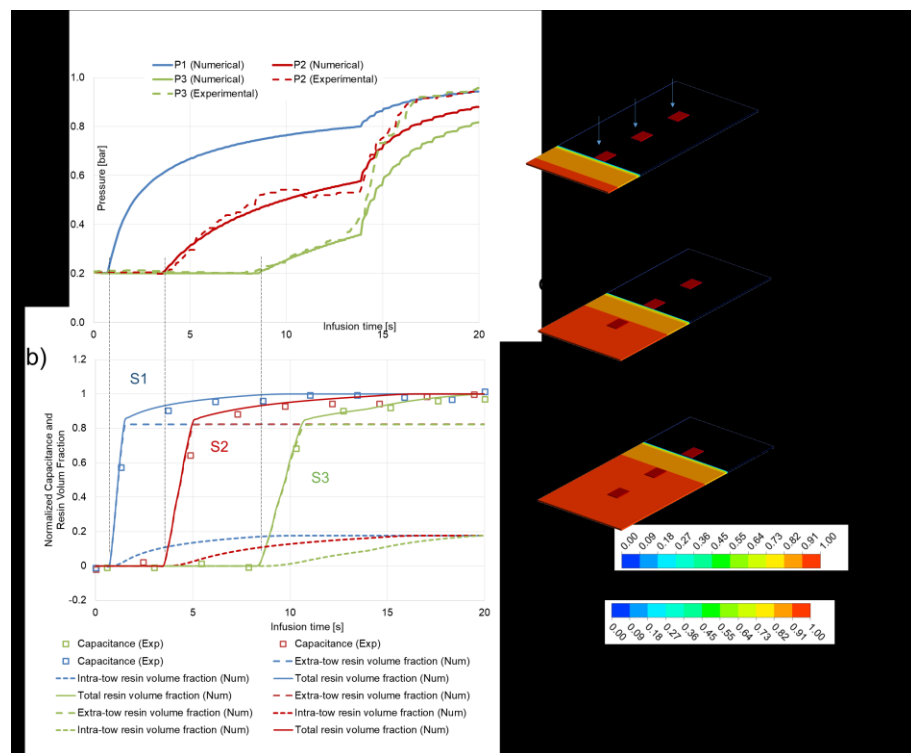


**Figure III.1.** Experimental and numerical results of the Test 1: a) pressure profiles; b) normalized capacitance and (extra-tow, intra-tow, and total) resin volume fractions; resin volume fraction when the resin arrive at the sensing locations c) S1, d) S2, and e) S3.

At the beginning of the test, the applied vacuum pressure was measured in the mold at sensor locations and computed by the macro scale model (Figure III.1 a). Then, as the impregnating fluid approached the pressure measurement points, a continuous pressure increase was detected. This trend was observed until the unsaturated front reached the vacuum port that corresponded to a prompt increase in pressure, which sharply tended to the atmospheric value.

## Experimental Results

Figure III.1a highlights also the good overlap between the prediction of the numerical model and the experimental data collected by the pressure sensors. Observing Figures III.1a and b it is evident that pressure sensors reacted as they were exposed to the resin, i.e. at the arrival of the unsaturated flow front at the sensors location. Figures III.1c, d, and e show the contour plots of the resin volume fraction in the preform at the three time instants, respectively 0.9, 3.5 8.3 s after the inlet opening, corresponding to the first detection by the dielectric sensors. It can be argued that pressure sensors can be effectively used to detect the arrival of the unsaturated flow front (Di Fratta, Klunker & Ermanni, 2013). However, no significant and reliable information can be gained as far as saturation is regarded. On the other hand, a satisfactory correlation between the total volume fraction of resin, which depends on impregnation and saturation and the normalized capacitance profiles. Experimental dielectric measurements and simulations outcomes highlighted the absence of capacitance variations before the arrival of the unsaturated front.

The profile of the normalized capacitance, in the examined case, exhibits two distinct parts. The former, characterized by relatively major slope, is representative of the macro-flow, while the latter, showing a very gradual increase, is indicative of the saturation micro-flow. In fact, the difference between the bulk and the tow permeability causes a flow velocity in the inter-tow region significantly higher with respect to the micro-flow front velocity. This induces the complete filling of the unreinforced zone surrounding the fiber bundles, constituting, in the considered case, the 82% of the total volume available for fluid flow, in a very short amount of time. At dielectric sensor locations, the following estimations of the time required for a complete impregnation (not saturation) were obtained: 0.6 s, 1.4 s, and 2.5 s, respectively for S1, S2, and S3. These narrow time intervals, combined with the fluid and fabric properties, as well as with the low pressure at the flow front, were not sufficient to induce the penetration of a significant quantity of liquid mass in the fiber tow. However, following the complete impregnation of the inter-tow region, a micro-flow toward the center of the tow is materialized, causing a further continuous (but relatively slower) increase in capacitance, until the full saturation is locally achieved. Afterwards, since no further variations in fluids (resin and air) volume fractions are possible, a stable unitary value is reached. The full saturation was achieved after 8.6 s (7.5 s since the first detected variation) for the sensor S1, 15.3 s (11.8 s since the first detected variation) for the sensor S2, and 19.2 s (10.9 s since the first detected variation) for the sensor S3. Finally, good agreement was observed between the numerically predicted saturation (total resin volume fraction equal to one) and the stabilization at the unitary value of the experimentally measured normalized capacitance, confirming the intriguing capability of the dielectric system for unsaturated as well as saturated flow monitoring. Comparing the pressure and the dielectric techniques, it is apparent that the

## Chapter

former solution failed in saturation monitoring, whereas the latter provided very useful data.

### 1.2. Result of the Test 2

Figure III.2 graphically summarizes the collected and simulated data related to second testing campaign, in which catalyzed resin was used as working fluid and the vacuum was applied until the full saturation of the preform. As aforementioned, pressure sensors were removed from the sensed die in order to avoid damages. Consequently, no data relative to the pressure profiles were reported.

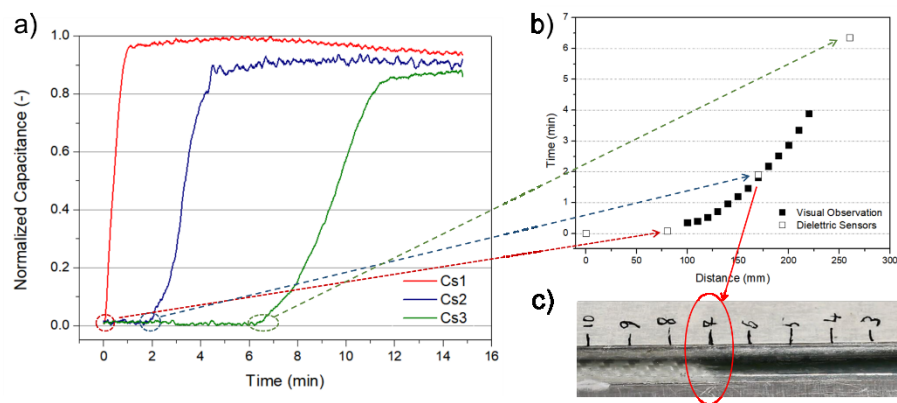


**Figure III.2.** Visual and experimental comparison of measure fill-front position.

The working fluid used in Test 2, even if it still in the unreacted state, exhibits viscosity values higher than the mineral oil used in Test 1, thus a slower advancement of the unsaturated flow front was expected. The sensors S1, S2, and S3 were reached in 6 s, 2 min, and 6.5 min, respectively. If compared to the previous case, it was more evident the beginning of a micro-flow before the complete development of the macro-flow at each dielectric sensor location. Finally, the flow front approached the vacuum port after approximately 8 min since the beginning of the impregnation. Figure III.2.b shows that the fill-front measurement by the sensor system is in good agreement with the positions recorded by the video camera. The maximum difference between the visual and experimental data is approximately 5 mm. The error is mainly observable in the region between the sensors, where the measurements are less accurate due to fringing field effects. In the absence of fringing field effects, the sensors would record fill-front progression only when the liquid is directly between the sensing electrodes of the parallel-plate.

## Experimental Results

Since the exact position of the sensors on the mold is known a priori, a measurable change in sensor signal directly corresponds to the position of the resin flow front. However, the fringe effect causes the sensor to measure fill-front progression before the liquid is directly underneath the sensor (Hegg, 2005).

On the other hand, the measurement of fill-front position works equally well, indeed the sensor response is strong in both cases and the data agreed with the visual observation (see Figures III.2). This suggests that the simultaneous usage of the shielding electrodes surrounding the sensing plates and of the insulating support has proved to be an effective solution to make the sensors less sensitive to the disturbances.

The full saturation condition was achieved after 6 min, 10 min and 14 min from the opening of the inlet, respectively for S1, S2, and S3. A delay between the unsaturated saturated flow fronts at the last sensing location (i.e. S3), near the vacuum vent of 8 minutes were evaluated.

Also in this case, results highlighted how a dielectric sensing system is capable to detect the preform saturation in the case of a “regular” front advancement (as experienced by sensors S1 and S2), as well as in the case of unexpected pressure variations due to the working setup, as detected by the sensor S3.

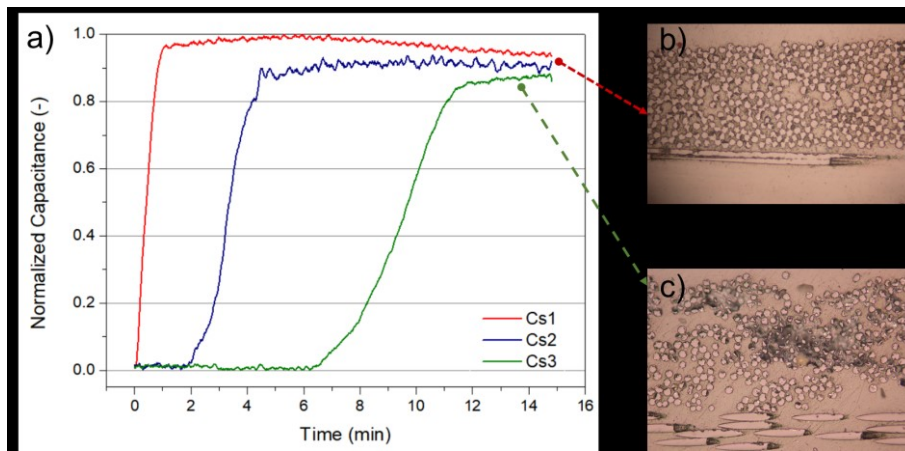


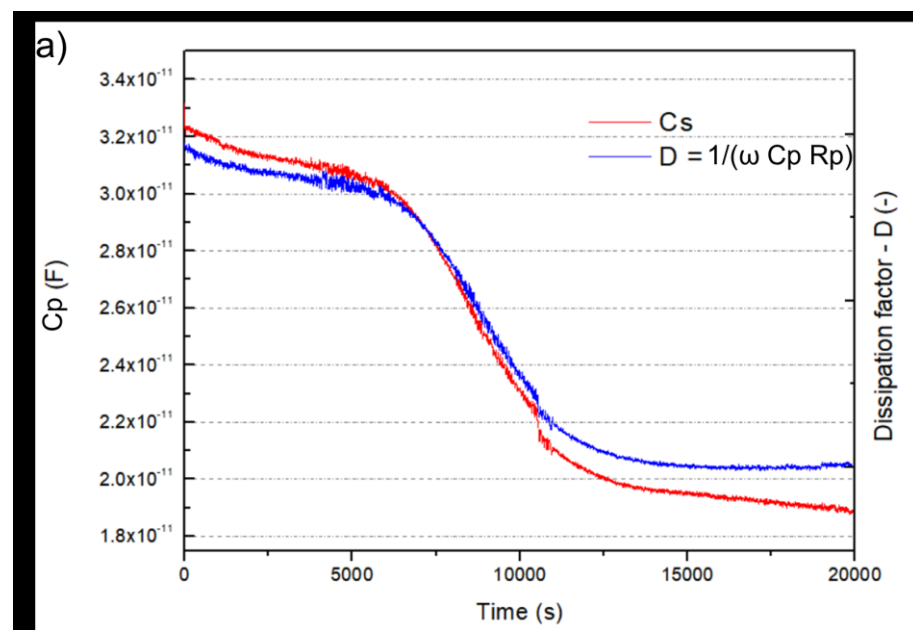
**Figure III.3.** a) Normalized capacitance profiles, b) microstructure of a sample extracted in the region of the sensor S1, with evidence of the full saturation; c) microstructure of a sample extracted in the region of the sensor S3, with evidence of voids and unsaturated zones.

As the laminate was fully cured, it was demolded and several samples were cut to a microscopical analysis. Microstructure observations, reported in Figures III.3b and c, depicting the cross section of representative samples extracted from the material between the S1 and S3 plates, evidence that the

## Chapter

intra-tow region at the sensor S1 was completely saturated, leading to a coherent interphase between the fibre and the matrix. Differently, large resin free zones within the fibre bundle can be observed in Figure III.3c. From the same figure, it is apparent that the inter-tow zone is substantially void free. The void content, measured by image analysis, was equal to 5.2 %, 6.0 %, and 5.5%.

After the filling process is complete, the sensors measured the curing process of the resin. Figure III.4 the profile of the degree of cure as evaluated from the dielectric data (Hussain, Chen & Hojjati, 2007).



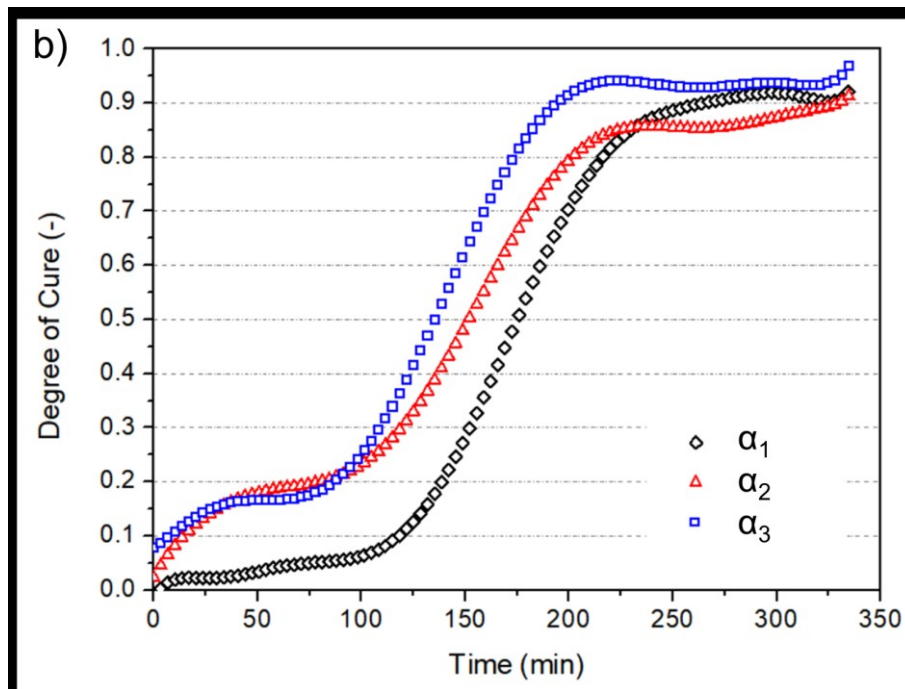


**Figure III.4.** a) Capacitance ( $C_s$ ) and dissipation factor ( $D$ ) during the curing stage at the sensor S1; b) resin degree of cure profiles evaluated in the sensing locations S1, S2 and S3 within the mold.

In dielectric analysis (DEA), the ions and dipoles that are present in the materials induce conductive and capacitive characteristics. When applying an electric field to the sample, the ions, that initially had a random orientation, start to move towards an electrode of opposite polarity while the dipoles try to align with the electric field. The resulting signal is obtained during the process by measuring the change in amplitude and phase shift in regards to the mobility of the ions and the alignment of the dipoles. From the amplitude and phase, permittivity,  $\epsilon'$ , the loss factor,  $\epsilon''$ , as well as complex permittivity,  $\epsilon^*$  (see eq.(II.1)), can be estimated.

During the cure process, as the polymers starting from the liquid state become solids, the mobility of ions and rotation of dipoles become more and more limited. Since ion conductivity and the ion mobility are related to the material's viscosity, they are a good indicator of the viscosity change during the cure process. By measuring the change in the dielectric loss factor, which in turn is mainly contributed by the ion conductivity at low frequencies, the degree of cure of materials can be calculated (Hussain, Chen & Hojjati, 2007). Taking into account a parallel plate dielectric sensor and modelling the dielectric medium as an equivalent circuit with capacitor and a resistor in parallel, the dissipation factor can be defined as:

## Chapter

$$D = \frac{1}{\omega C_p R_p} = \tan\left(\frac{\epsilon''}{\epsilon'}\right) \quad (\text{III.1})$$

Where  $\omega$  is the frequency of the electric fields. The dissipation factor is shown to be decreasing with cure time in Figure III.4a. In the presence of an electric field, the changes in transitional mobility of ions and the rotational mobility of dipoles become more apparent with increasing cure time. The decrease in dissipation factor (and then of the loss factor) is due to the ion and dipole mobility becoming more restricted as the sample turns into solids. The loss factor, in particular, is dominantly characterized by the ion mobility migrating from one electrode to the other with opposite polarity. The measurement of loss factor as a function of cure temperature and time allows for the calculation of degree of cure:

$$\alpha = \frac{\log_{10} \epsilon''_0 - \log_{10} \epsilon''(t)}{\log_{10} \epsilon''_0 - \log_{10} \epsilon''_{inf}} \quad (\text{III.2})$$

Here  $\epsilon''_{inf}$  is dielectric loss factor at infinity,  $\epsilon''(t)$  corresponds to dielectric loss factor at time  $t$  and  $\epsilon''_0$  is dielectric loss factor at the beginning. The degree of cure at three sensor location is shown in Figure III.4b.

## 2. In-line preheating infusion test: Resonance cavity 1

### 2.1. Materials and Experimental procedure

Eight layers of twill 2/2 e-glass fabric, with 390 gr/m<sup>2</sup> in grammage, were used as reinforcement resulting in a fibers volume fraction of approximately 0.4. Un-reactive liquid (mineral oil) with viscosity equivalent to the polyester resin was employed as working fluid to avoid damage to the pressure sensor and variations of the dielectric properties during the test due to a potential premature onset of cure during the heating. Dynamic viscosity and density of the liquid were 0.3 Pa·s and 1.1 kg/l respectively. A pressure gradient of 90 kPa (corresponding to a measured pressure in the cavity before the start of the test of 10 kPa) was set as driving force. Low resin viscosity, coupled with the low fibers volume fraction as well as high pressure difference allow to obtain a relative short test time. The in-line microwave system mounting the first resonance cavity (150 mm in length) was used to preheat the resin flow (figure III.5). The magnetron operated at a nominal frequency of 2.45 GHz with a power of 2 kW. A thermocouple was used to measure the temperature of resin at the exit of cavity and before entering into the mold as well as correlate the power absorbed by the stream (evaluated as difference between the nominal power of generator and reflected power) and the temperature gradient. The PTFE tube within the resonance cavity was filled with the operating fluid

## Experimental Results

before the start of the test. It allows that the first resin that enter within the mold was at the operating temperature and prevents unheated liquid from impregnating the preform. A small delay of ten second between the turning on of the microwave generator and the opening of the inlet valve was set. The maximum increase of temperature obtained for the working fluid adopted during the infusion tests was approximately  $10^{\circ}\text{C}$  with a magnetron output power of 2 kW. Therefore, two distinct test cases were considered and compared: the one carried out at room temperature (approximately  $23^{\circ}\text{C}$ ), the other connecting the microwave system in line with the LCM and pre-heating the resin up to  $33^{\circ}\text{C}$ . The same conditions of LCM process, i.e. pressure gradient, resin as well as fiber preform, was used for both experimental cases.

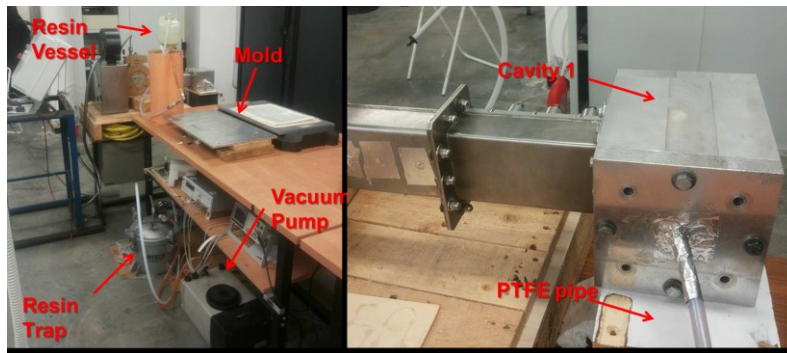


**Figure III.5.** *Experimental set-up for the microwave in-line preheating tests with cavity 1*

### 2.1 Experimental results

Figure III.6 and 7 report the data for unheated and preheated resin flow test in terms of pressure and capacitance trends.

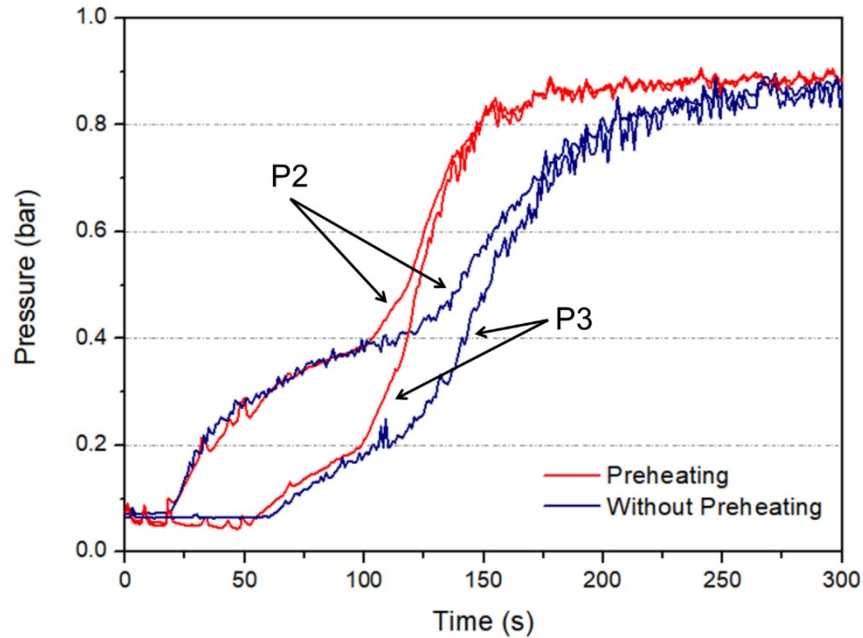


**Figure III.6.** Pressure profiles at locations P2 and P3: comparison between the no-heating and preheating infusion tests

As for the results exposed in the previous section, distinct phases of impregnation can be observed from the pressure profile (Figure III.6, related to the pressure sensors P2 and P3). From 0 to 19 seconds, the pre-form is dry, the measured pressure is approximately 10 kPa (vacuum condition in mold cavity). The sensor reacted as it comes into contact with the resin, it corresponds to a sharp increase of resin pressure, approximately from 19 to 32 s. The pressure increases as the mold filling progresses, up to a value of 500 kPa at 133 s from the beginning of the infusion. The sensor 3, located near the vacuum vent, presented a similar trend. The sensor reacted with a delay of approximately 40 seconds, when the resin reached the location of the sensor.

At 133 s, the pressure profiles in each location starts to rise more rapidly pointing out that the unsaturated resin flow have reached the vacuum vent (as previously argued). It determines the rapid increasing of the pressure within the whole mold cavity. Indeed, the Pressure/Time curves of sensors 2 and 3 joined and reached a steady state value of approximately 900 kPa at the same time at the end of impregnation (after 400 seconds) (Grimsley *et al.*, n.d.)[].

## Experimental Results

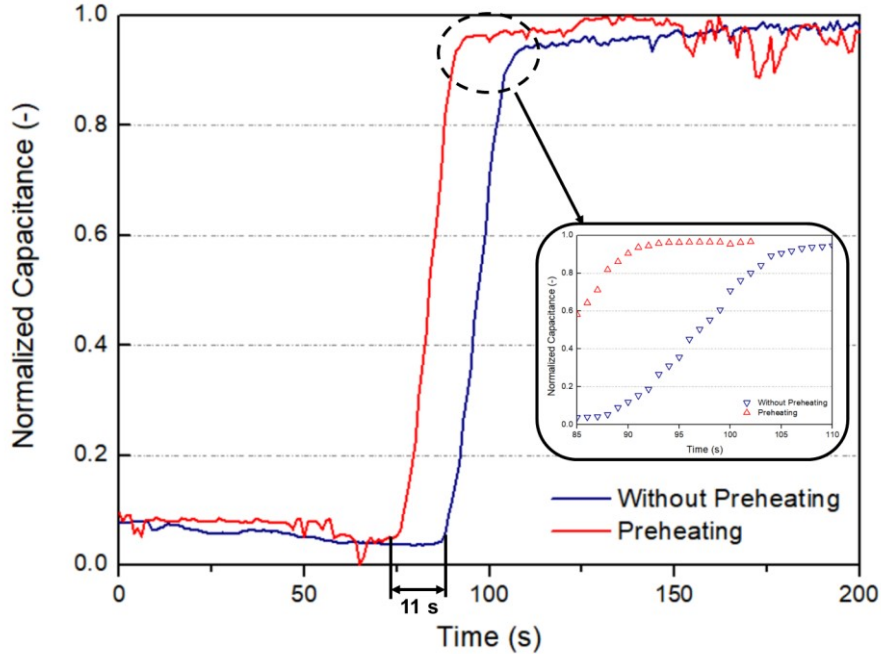


**Figure III.7.** Normalized Capacitance measure by sensor S3: comparison between preheating and un-heating resin infusion test.

The capacitance variation during the impregnation test confirms the observed phenomenon (Figure III.7). As can be seen, no capacitance variations were observed until the flow reached the sensing area, indicated also by the pressure increase. Then, the dielectric sensor exhibited a continuous increase. In the first part of the curve, the capacitance linearly changed, the slope depends on the macro flow that characterizes the initial phase of pre-form impregnation (Carlone & Palazzo, 2014). The high amount of liquid fraction that occupies the sensing area explains the high variation of capacitance in a relative short time (approximately 20 seconds). Then, the capacitance continued to grow until the unsaturated flow front entirely overcame the sensor (Carlone & Palazzo, 2014). As the saturated front approached the sensing area, the capacitance profile became asymptotic and tend to a steady state value corresponding to any other variation of the medium between the two electrodes. This pointed out that the saturated flow front entirely overcomes the sensor.

Observing the pressure measurement, the advantages deriving from the use of microwave system concern mainly the second phase of impregnation, i.e. the flow of the resin in the inter-tows regions. Indeed, in the initial phase of infusion no remarkable improvements in filling time were detected. Both preheated and unheated pressure profiles started to increase almost at the same time for each pressure sensor. A small gap of 8 seconds was observed on the third pressure sensor as resin flow front arrival at the location P3. On the other

## Chapter

hand, the pre-heating seems to be more effective during the second stage of infusion, mainly dominated by the microflow of the resin from the gap space between the fiber bundles into the fiber tows. Indeed the lower viscosity, resulting from the resin temperature increase of 10 °C, allowed to achieve a significant reduction in the cycle time. The pressure, relative to the pre-heating test, rose more rapidly than the unheated test, and reached a steady state value 60 seconds before the pressure profile in the unheated route. Both of the pressure sensors showed the same trends as the second stage of the infusion was established, as occurred for the unheated test.

The data from the dielectric sensors allowed to better evaluate the effect of microwave heating system, proving a major sensitivity also during the primary stage of the infusion. The pre-heated resin reached the sensing location in advance of 11 seconds compared to the resin at room temperature.

Then, the both capacitance profiles linearly increased with the same slope, confirming how the pre-heating did not significantly affect the impregnation in this early stage. At the end of the ramp, the capacitance profile of pre-heated and unheated resin flow were slightly different. The tangent of the pre-heated curve presented a higher slope of approximately one degree ( $1^\circ$ ) than the unheated one. The gap remained unvaried until a steady state value of capacitance was reached. This resulted in an advance of 30 seconds for the saturation in the pre-heated test. Comparing the pressure and capacitance measurements with the visual observation, the required times of early impregnation of dry pre-form and the subsequent saturation for both pre-heating and room temperature tests have been evaluated.

Knowing the location of the pressure and dielectric sensor, the fill front progression can be estimated (Figure III.8). The collected data point out that the pre-heating allows to obtain a time reduction of approximately 15 % (from 88 seconds to 76 seconds of process time) for the unsaturated flow (see figure III.7) as pointing out by the response of the dielectric sensor and a decreasing of the time required to the resin flow to reach the vacuum vent of approximately 15 s. A reduction of 20 % for the saturation (from 175 seconds to 145 seconds of process times) of pre-form in the sensing area have been observed.

## Experimental Results

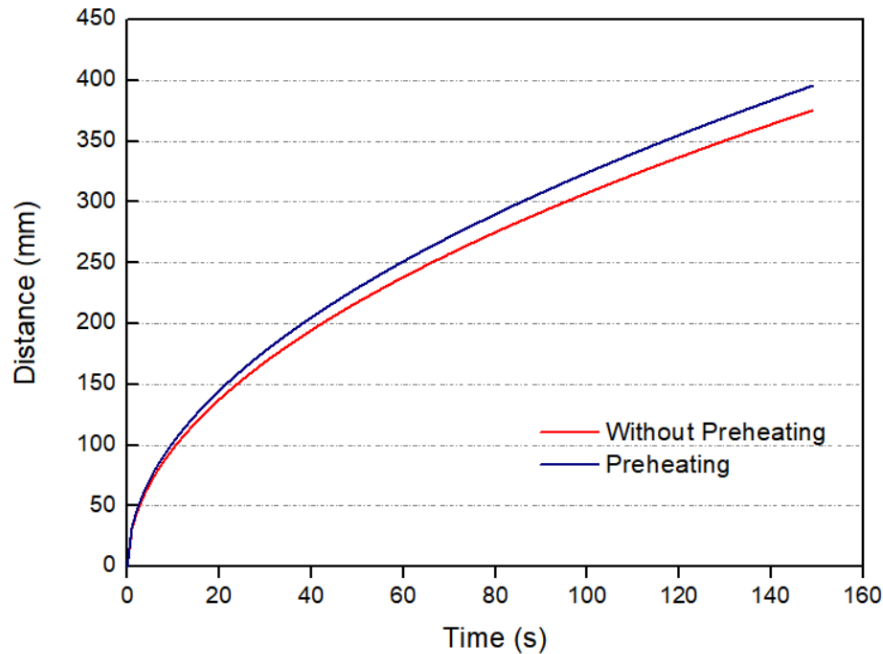


**Figure III.8.** *Un-heated and preheated resin flow front advancement.*

The experimental tests performed on the first configuration of the microwave heating system allow to argue that the in-line preheating system is able to improve the infusion of the fiber reinforcement. Taking into account the small gradient temperature of only 10 °C obtained by means of the shorter cavity 1, a reduction of 15 s of the filling time represents an intriguing and promising result. On the other hand, the system needs to be improved. Indeed, the heating required a power 2000 W from the microwave generator, pointing out that the tested configuration, despite its effectiveness, is not cost-effective. The following tests on the other two configuration aimed to overcome this drawback.

### **3. In-line preheating infusion test: Resonance cavity 2**

#### **3.1. Materials and Experimental procedure**

For the microwave heating tests performed adopting the second resonance cavity the preform was made of eight layers of twill 2/20 e-glass fabric, the same used for the tests described in the previous section. The fibers volume fraction reached approximately 0.4. The polyester resin catalyzed with the 1% in weight of the hardener was employed as working. The properties of the hardener-resin system are listed in the table III.1. A pressure gradient of 80 kPa (corresponding to a measured pressure in the cavity before the start of the

## Chapter

test of 20 kPa) was set as driving force. The in-line microwave system mounts the second resonance cavity 1 m in length (figure III.9). Two thermocouples was used to measure the temperature of resin at the exit of cavity and before entering into the mold as well as evaluate the temperature gradient achieved.

Two distinct test cases were considered varying the parameter of the microwave system:

1. Test A: according to the preliminary test on the cavity 2 (see chapter 2 paragraph 6.2) the power was initially set at 1500 W to heat the resin at high rate, then set at 500 W, as the resin flow rate drops. At the beginning of the test, the high power of the microwave coupled with the higher length of the cavity could result in an overheating of the resin, when it is stopped in the PTFE tube. For this reason a proper strategy was adopted using a twin stream circuit at the exit of the cavity as described in chapter III paragraph 6.2 (see figure III.9). At the start of the trials the heated resin was sent to a secondary reservoir. As the output temperature was stable at the proper value, the connection valve between microwave and LCM systems was opened (the valve to the reservoir was simultaneously closed) and the resin flowed into the mold.
2. Test B: the power of magnetron was set at 200 W for the entire duration of the trial. In this test case, the same procedure described previously in this chapter, paragraph 3.1 was adopted.

The same conditions of LCM process, i.e. pressure gradient, resin as well as fiber preform, were used for both experimental cases. The achieved maximum temperature of the adopted working fluid for both Test A and B ranged between 55 – 60 °C and 50 – 55 °C. As for the experimental analysis on the cavity 1, for both Test A and Test B two distinct trials were performed: one carried out at room temperature (approximately 25°C), the other connecting the microwave heating system in line to the LCM.



**Figure III.9.** *Experimental set-up of the microwave in-line preheating tests with cavity 2*

### ***3.1 Experimental results***

Figure III.10 shows the results of the Test A as comparison between the un-heating and the preheating trials. The resin fill front propagations were reported. During the preheating trial, the starting temperature was 29°C, while the temperature at the exit of the cavity stabilized at 60 °C. Observing the flow front profiles, the resin preheating provided a significant reduction the filling time at the early stage of the infusion. Indeed, the preheated flow was constantly in advance with respect to the unheated flow. At 100 mm from the inlet vent (a third of the total length of the cavity), the first dielectric sensor revealed an advance of almost 60 s. After that, a sharply increase in the slope of the space/time profile for the preheated flow was detected. It corresponded to the increasing of the time required for the resin to flow through the fibers bulk. The earned advance of the preheating flow on the un-heated one progressively reduced until at 200 mm from the inlet, the crossover of the two profiles occurred. The space/time profile started to increase exponentially. After that, no detections of the preheated resin flow front were acquired. The sensor S3 did not react during the whole tests and no further progression of the flow front was visually observed pointing out that the resin suddenly stopped before arriving at the vacuum vent. The image of the cured laminate (reported also in figure III.10) after the demolding clearly indicates the arrest of the resin flow and the incomplete impregnation of the fiber preform. This occurrence is due to the premature curing of the resin due the heat provide by the microwave system. The temperature of 60°C experienced by the resin was too high and overcame the onset temperature of the resin itself. In the early stage of the infusion, the effect of the increased temperature was reducing the viscosity of the resin allowing it to flow more freely through the dry preform. It composed with the high flow rate regime characterizing the earlier infusion caused the significant advance of the preheating flow on the un-heating one. However, as the flow rate reduced the exposition time of the resin to the electromagnetic field dramatically increased. The high amount of supplied energy promote the curing of the resin and the gelification occurred rapidly, resulting in a too rapid increasing of the viscosity.

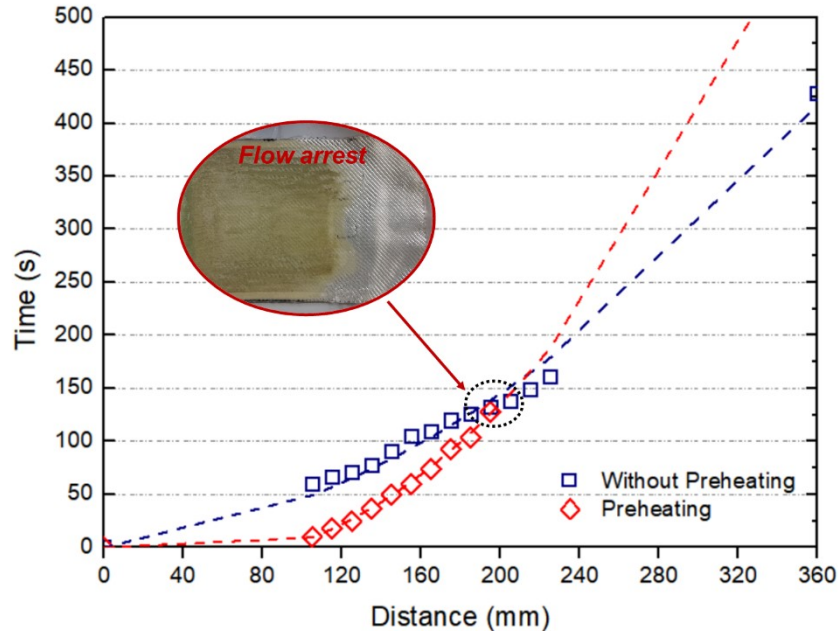


**Figure III.10.** Result of the Test A: resin flow front progression for unheating and preheating trials

The performed trial with the Test A configuration failed. It was probably due to the too high power provided by the microwave generator. The following experimental campaign (i.e. Test B case) was performed reducing the nominal power.

In the Test B trial, the microwave generator constantly supplied 200 W of power. Starting from a temperature of 31 °C, measured at the entrance of the resonance cavity, the output temperature ranged between 52 and 55 °C. Figures III.11 shows the results of the Test B trials. As can be seen, the preheating of the resin resulted in an advance of the fill front with respect to the unheating flow. In the early stages of the infusion no significant results are observable. The unheated and preheated flow reaching the S1 location at the same time. This outcome agree with what was observed in the tests of cavity 1, pointing out as the preheating is almost ineffective when the resin flow is dominated by the macroflow through the fibers bundles and the flow rate is relatively high. As the mold filling progresses, after the resin reached the third of the cavity length the preheating flow earned an increasing advance on the unheated one. At the half of the mold (approximately at 180 mm from the inlet vent) the preheating flow is in advance of 20 s. It further increased up to 40 s detected at S3 location.

## Experimental Results

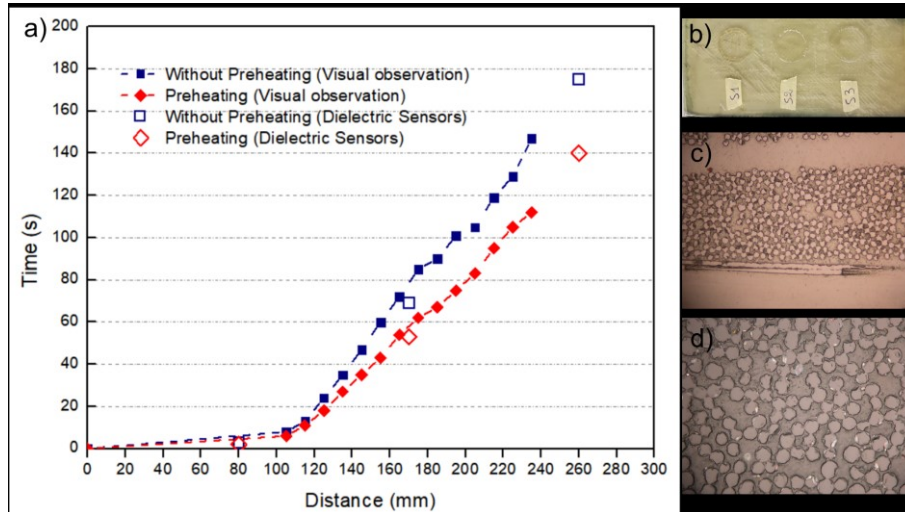


**Figure III.11.** Result of the Test B: a) resin flow front progression for unheating and preheating trials; b) image of the composite laminate manufactured; micrographies of the laminate cross section in different location c) S1 and d) S3.

The microwave heating proved to be able to improve the impregnation of the fibers. Indeed, the micrographies of the laminate cross-sections (figure III.11c and d) show that the S1 and S3 was completely saturated, leading to a coherent interphase between the fiber and the matrix. Both inter-tow and intra tow zones are substantially void free, pointing out the improvement provided by the preheating with respect to the infusion at room temperature (as observable in figure III.3 where voids in the intra tow region are clearly visible).

The result of the Test B proved that the cavity 2 is a suitable solution for the in-line preheating. Compared to the cavity 1, it allowed to obtain a significant reduction of the mold filling time, up to approximately 40 seconds at the location of the third dielectric sensor, corresponding to a total reduction slightly below the 30 % requiring a power of only 200 W. The configuration with the cavity 2 appears to be a suitable and cost-effective solution for the in-line resin preheating infusion process. However, despite the promising results provided by the developed system, it presents a disadvantage related to the impossibility of any regulation. Indeed, only setting the microwave power at 200 W successful results can be obtained. Higher power levels will result in the excessive heating of the resin and increasing risk of premature curing. Moreover, the system does not allow to set lower power than the 200 W. Therefore the as configured microwave system is strictly limited to the process parameters adopted. Variation in, for example, driving pressure, resin volume fraction, preform permeability cause changes in the resin flow that the system

## Chapter

cannot afford. The development of the cavity 3 aimed to overcome this drawback.

### **4. In-line preheating infusion test: Resonance cavity 3**

#### ***4.1. Materials and Experimental procedure***

The same materials and process conditions used for the tests with the cavity 2 are employed for the cavity 3. Therefore, a preform made of eight layers of twill 2/20 e-glass fabric was carefully placed into the mold cavity, resulting in a fibers volume fraction of 0.4. A mixture of polyester resin and 1 % in weight of hardener was employed as working fluid. The pressure gradient was set at 80 kPa as driving force. The in-line microwave system, mounting the third resonance cavity (approximately 600 mm length), was connected to the LCM apparatus to preheat the resin flow (Figure III.12). Two thermocouple placed at the exit of cavity and before entering into the mold were used to measure in real time the temperature and evaluate the temperature gradient achieved. Also for the cavity 3, two distinct test cases were considered and compared: the first performed at room temperature without using the microwave heating system, the second connecting the microwave system in line with the LCM and preheating the resin. The same conditions of LCM process, i.e. pressure gradient, resin as well as fiber preform, were used for both experimental cases.

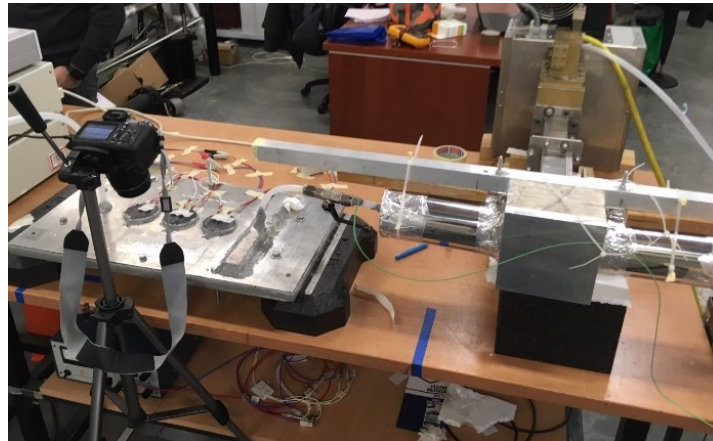


**Figure III.12.** *Experimental set-up of the microwave in-line preheating tests with cavity 3*

#### ***4.2. Experimental results***

Observing the results of the preliminary tests (described chapter 2, paragraph 6.3), the cavity 3 allows to obtain a certain temperature gradient

## Experimental Results

with different working conditions (microwave power vs. flow rate), thus a different strategy to heat up the resin was designed (see figure III.13).

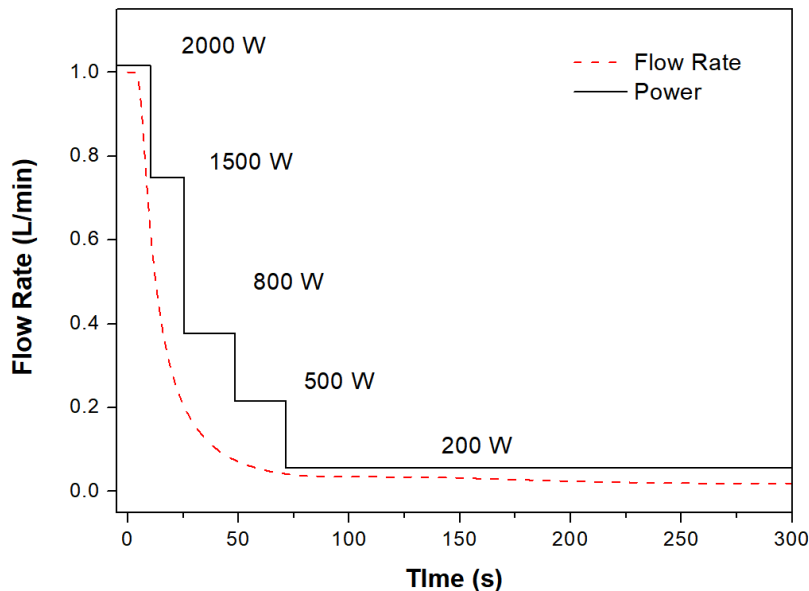


**Figure III.13.** Microwave heating strategy

According to the flow rate profile evaluated in the un-heating trial, the microwave power was continuously varied during the infusion, setting a proper automatic cycle (“recipe”). The power was set at the maximum level at the early beginning of the infusion, when the flow rate experienced the highest values (approximately 1 L/min). As the flow rate drops, the power was progressively reduced step by step up to 200 W (the minimum level that can be supplied by the generator), when the resin flow was completely developed and the flow rate stabilized. The procedure already used for the cavity 1 and for the Test B with the cavity 2 was adopted. The risk of the resin overheating is averted due to the reduced length of the cavity 3.

Figure III.14 reports the resin flow front profiles for the unheating and preheating tests. Similarly to what happened in the Test B with the cavity 2, the preheating and unheating flows evolved almost in the same way at the beginning of the infusion. Then at 100 mm from the inlet vent, the two profiles started to diverge each other and the preheating flow resulted in advance of approximately 15 s on the unheated flow. Compared to the cavity 2, where the unheating and preheating flows started to diverge only at 140 mm for the inlet, in this case the preheating flow earlier achieves a significant advancement. It is probably due to the higher power supplied at the beginning of the infusion (see figure III.13) with respect to the 200 W in the cavity 2-Test B. After that, the time gradient between the two flows progressively increased, stabilizing at 40 s in the middle zones of the mold cavity. When the flows reached the sensing

Chapter

location S3, the preheated flow resulted in advance of approximately 100 s. It points out that the microwave preheating allowed to save more than 1 minute of the cycle time.

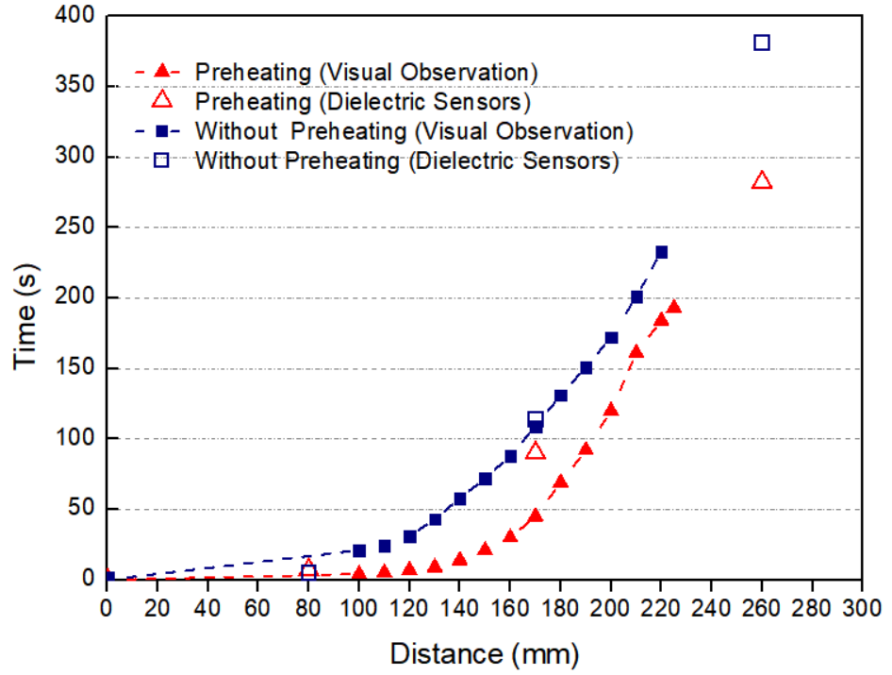


**Figure III.14.** Resin flow front progression for un-heating and preheating trials.

# CONCLUSIONS

The following is a summary of the major conclusions derived from this thesis.

- An in-line microwave resin preheating system has been installed within a prototype RI laboratory scale facility. The resin preheat temperature can be controlled precisely using the microwave resin preheating system.
- Different configurations of the microwave system have been developed and tested, varying the length of the cylindrical applicator. Three dimensions are considered: 150 mm, 600 mm and 1 meter. All three evaluated solutions allowed to effectively apply the microwave preheating technique.
- The intermediate configuration of the microwave system proved to be the optimal and cost-effective solution to reduce the cycle time. It also is suitable for different process conditions, allowing to regulate the microwave heating parameter to different resin infusion process condition
- Preheating of the resin at constant temperature during infusion minimizes the cycle time. Reductions in cycle time up to 30% were achieved using the preheating techniques for the given molding parameters. The principal reasons for the cycle time reduction is the improved resin flow through the mold. The resin preheat temperature is optimized when increases in this temperature do not produce a corresponding cycle time reduction due to premature gelification.
- Microwave resin preheating reduce the amount of residual voids within the laminate at macro- and micro scale: complete saturation can be achieved in the inter-tows and intra-tows zones. The quality of the laminate can be enhanced using the microwave preheating.

### Conclusions

- A non-invasive sensing strategy, based on parallel-plate dielectric and pressure sensors embedded into the mold, was developed to monitor the position of unsaturated and saturated resin flow front in two distinct cases: unheated resin and pre-heated resin.
- The realized and tested dielectric system can be effectively used to detect not only the arrival of the unsaturated flow front, but also the tow saturation in the sensed region. What is more, they are capable to detect incomplete saturation, lack of impregnation and other flow anomalies attributable, for instance, to pressure variations or flow stop conditions. Dielectric sensors seem excellent candidates for the inclusion in active monitoring and control systems for this kind of application. Nevertheless, in authors' opinion, further work is needed in order to investigate the uncertainty of such sensors and generalize their applicability to flexible or geometrically complex dies

# BIBLIOGRAPHY

- Abraham, D. & Mcilhagger, R. (1998) *Glass fibre epoxy composite cure monitoring using parallel plate dielectric analysis in comparison with thermal and mechanical testing techniques*. 811–819.
- Bang, K.G., Kwon, J.W., Lee, D.G. & Lee, J.W. (2001) Measurement of the degree of cure of glass fiber-epoxy composites using dielectrometry. *Journal of Materials Processing Technology*. [Online] 113 (1–3), 209–214. Available from: doi:10.1016/S0924-0136(01)00657-4.
- Barooah, P., Berker, B. & Sun, J.Q. (2003) *Lineal Sensors for Liquid Injection Molding of Advanced Composite Materials*. (JANUARY 1998), 1–29.
- Becker, D. & Mitschang, P. (2015) Influence of preforming technology on the out-of-plane impregnation behavior of textiles. *Composites Part A: Applied Science and Manufacturing*. [Online] 77, 248–256. Available from: doi:10.1016/j.compositesa.2015.05.001.
- Bickerton, S. & Advani, S.G. (1999) Characterization and modeling of race-tracking in liquid composite molding processes. *Composites Science and Technology*. [Online] 59 (15), 2215–2229. Available from: doi:10.1016/S0266-3538(99)00077-9.
- Boey, F.Y. & Yue, C.Y. (n.d.) The Effect of Microwave and Thermal Curing on the Interfacial Properties of an Epoxy-Glass Composite,. In: *Proceedings of the Deformation and Fracture of Composites Conference, Manchester, England*,. pp. 1–8.
- Boey, F.Y.C., Gosling, L. & Lye, S.W. (1993) Processing Problems and Solutions for an Industrial Automated Microwave Curing System for a Thermoset Composite. In: *The 9th International Conference on Composite Materials, Madrid, Spain*. 1993 pp. 651–656.
- Bradley, J.E., Diaz-Perez, J., Gillespie Jr., J.W. & Fink, B.K. (1998) On-line process monitoring and analysis of large thick-section composite parts utilizing SMARTweave in-situ sensing technology. *International SAMPE Symposium and Exhibition (Proceedings)*. 43 (1).
- Carlone, P. & Palazzo, G.S. (2014) Unsaturated and Saturated Flow Front Tracking in Liquid Composite Molding Processes using Dielectric Sensors. *Applied Composite Materials*. [Online] 22 (5), 543–557.

- Available from: doi:10.1007/s10443-014-9422-3.
- Costigan, P.J. & Birley, A.W. (1988) Microwave preheating of sheet moulding compound. *Plastics and Rubber Processing and Applications*. 9, 233–240.
- Danideh, A. & Sadeghzadeh, R.A. (2013) Cpw-fed slot antenna for mimo system applications. *Indian Journal of Science and Technology*. [Online] 6 (1), 3872–3875. Available from: doi:10.1002/mop.
- Danisman, M., Tuncol, G., Kaynar, A. & Sozer, E.M. (2007) Monitoring of resin flow in the resin transfer molding (RTM) process using point-voltage sensors. *Composites Science and Technology*. [Online] 67 (3–4), 367–379. Available from: doi:10.1016/j.compscitech.2006.09.011.
- Dominauskas, A., Heider, D. & Gillespie, J.W. (2007) Electric time-domain reflectometry distributed flow sensor. *Composites Part A: Applied Science and Manufacturing*. [Online] 38 (1), 138–146. Available from: doi:10.1016/j.compositesa.2006.01.019.
- Dominauskas, A., Heider, D. & Gillespie, J.W. (2003) Electric time-domain reflectometry sensor for online flow sensing in liquid composite molding processing. *Composites Part A: Applied Science and Manufacturing*. [Online] 34 (1), 67–74. Available from: doi:10.1016/S1359-835X(02)00232-4.
- Drzal, L.T., Hook, K.J. & Agrawal, R.K. (1991) Enhanced Chemical Bonding at the Fiber-Matrix Interphase in Microwave Processed Composites. In: *Microwave Processing of Materials II Materials Research Society Symposium Proceedings*. 1991 pp. 449–454.
- Dunkers, J.P., Lenhart, J.L., Kueh, S.R., Van Zanten, J.H., et al. (2001) Fiber optic flow and cure sensing for liquid composite molding. *Optics and Lasers in Engineering*. [Online] 35 (2), 91–104. Available from: doi:10.1016/S0143-8166(00)00110-X.
- Fink, B.K., Gillespie, J.W., Walsh, S., DeSchepper, D.C., et al. (1995) Advances in resin transfer molding flow monitoring using SMARTweave sensors. In: *In: Proceedings of ASME, international mechanical engineering congress and exposition. San Francisco, CA, 1995*. 1995 pp. 999–1015.
- Di Fratta, C., Klunker, F. & Ermanni, P. (2013) A methodology for flow-front estimation in LCM processes based on pressure sensors. *Composites Part A: Applied Science and Manufacturing*. [Online] 47 (1), 1–11. Available from: doi:10.1016/j.compositesa.2012.11.008.
- Gebart, B.R., Gudmundson, P. & Lundemo, C.Y. (1992) An Evaluation of Alternative Injection Strategies in RTM. In: *The Society of Plastics Industry. The 47th Annual Conference, Composites Institute*. 1992 pp. 1–8.
- Grieser, T., Rieber, G. & Mitschang, P. (n.d.) Production of continuously formed high performance preforms for FRPC profiles. In: *ECCM 2012 - Composites at Venice, Proceedings of the 15th European Conference*

## Experimental Results

- on Composite Materials*. Venice. p.
- Grimsley, B.W., Hubert, P., Song, X. & Langley, N. (n.d.) *Flow and Compaction During Vacuum Assisted Resin Transfer Molding Process*.
- Hawley, M.C. & Wei, J. (1991) Processing of Polymers and Polymer Composites in a Microwave Applicator. In: *Microwave Processing of Materials II Materials Research Society Symposium Proceedings*. 1991 pp. 413–420.
- Hegg, M.C. (2005) Remote Monitoring of Resin Transfer Molding Processes by Distributed Dielectric Sensors. *Journal of Composite Materials*. [Online] 39 (17), 1519–1539. Available from: doi:10.1177/0021998305051083.
- Hill, D.J. (1993) *Microwave Preheating of Thermosetting Resin for Resin Transfer Moulding*. University of Nottingham.
- Von Hippel, A.R. (1995) *Dielectric Materials and Applications*. Arthur R. Von Hippel (ed.). Artech House (December 1, 1995).
- Hussain, F., Chen, J. & Hojjati, M. (2007) Epoxy-silicate nanocomposites: Cure monitoring and characterization. *Materials Science and Engineering A*. [Online] 445–446, 467–476. Available from: doi:10.1016/j.msea.2006.09.071.
- Johnson, D.O. (1991) Ultrasonic cure monitoring of advanced composites. *The Journal of the Acoustical Society of America*. [Online] 90 (6), 3386–3386. Available from: doi:10.1121/1.401372.
- Johnson, M.S. (1995) *The application of microwave preheating in resin transfer moulding*. [Online] (I). Available from: <http://etheses.nottingham.ac.uk/1752/>.
- Johnson, M.S., Rudd, C.D. & Hill, D.J. (1995) Cycle Time Reductions in Resin Transfer Moulding Using Microwave Preheating. *Proceedings of the Institution of Mechanical Engineers, Part B: Journal of Engineering Manufacture*. [Online] 209 (6), 443–453. Available from: doi:10.1243/PIME\_PROC\_1995\_209\_108\_02.
- Johnson, M.S., Rudd, C.D. & Hill, D.J. (1997) The effect of microwave resin preheating on the quality of laminates produced by resin transfer molding. *Polymer Composites*. [Online] 18 (2), 185–197. Available from: doi:10.1002/pc.10273.
- Kamal, M.R. & Sourour, S. (1973) Kinetics and thermal characterization of thermoset cure. *Polymer Engineering and Science*. [Online] 13 (1), 59–64. Available from: doi:10.1002/pen.760130110.
- Karbhari, V.M., Slotte, S.G., Steenkamer, D.A. & Wilkins, D.J. (1992) Effect of material, process, and equipment variables on the performance of resin transfer moulded parts. *Composites Manufacturing*. [Online] 3 (3), 143–152. Available from: doi:10.1016/0956-7143(92)90077-8.
- Ken Han, K., Lee, C.W. & Rice, B.P. (2000) Measurements of the permeability of fiber preforms and applications. *Composites Science and*

- Technology*. 60, 2435–2441.
- Kendall, K.N., Rudd, C.D., Owen, M.J. & Middleton, V. (1992) Characterization of the resin transfer moulding process. *Composites Manufacturing*. [Online] 3 (4), 235–249. Available from: doi:10.1016/0956-7143(92)90111-7.
- Kim, H.G. & Lee, D.G. (2002) Dielectric cure monitoring for glass/polyester prepreg composites. *Composite Structures*. [Online] 57 (1–4), 91–99. Available from: doi:10.1016/S0263-8223(02)00072-7.
- Kuentzer, N., Simacek, P., Advani, S.G. & Walsh, S. (2006) Permeability characterization of dual scale fibrous porous media. *Composites Part A: Applied Science and Manufacturing*. [Online] 37 (11), 2057–2068. Available from: doi:10.1016/j.compositesa.2005.12.005.
- Laurent-Mounier, A., Binétruy, C. & Krawczak, P. (2005) Multipurpose carbon fiber sensor design for analysis and monitoring of the resin transfer molding of polymer composites. *Polymer Composites*. [Online] 26 (5), 717–730. Available from: doi:10.1002/pc.20104.
- Lawrence, J.M., Hsiao, K.T., Don, R.C., Simacek, P., et al. (2002) An approach to couple mold design and on-line control to manufacture complex composite parts by resin transfer molding. *Composites - Part A: Applied Science and Manufacturing*. [Online] 33 (7), 981–990. Available from: doi:10.1016/S1359-835X(02)00043-X.
- Lawrence, J.M., Neacsu, V. & Advani, S.G. (2009) Modeling the impact of capillary pressure and air entrapment on fiber tow saturation during resin infusion in LCM. *Composites Part A: Applied Science and Manufacturing*. [Online] 40 (8), 1053–1064. Available from: doi:10.1016/j.compositesa.2009.04.013.
- Lee, D.G. & Kim, H.G. (2004) Non-Isothermal in Situ Dielectric Cure Monitoring for Thermosetting Matrix Composites. *Journal of Composite Materials*. [Online] 38 (12), 977–993. Available from: doi:10.1177/0021998304040563.
- Lim, S.T. & Lee, W. Il (2000) An analysis of the three-dimensional resin-transfer mold filling process. *Composites Science and Technology*. [Online] 60 (7), 961–975. Available from: doi:10.1016/S0266-3538(99)00160-8.
- Lindsey, K.A. (1994) *Interfacial Properties of Composites Produced by Resin Transfer Moulding*. University of Nottingham,.
- Lundstrom, T.S. & Gebart, B.R. (1994) Influence from process parameters on void formation in resin transfer molding. *Polymer Composites*. [Online] 15 (1), 25–33. Available from: doi:10.1002/pc.750150105.
- Maistros, G.M. & Partridge, I.K. (1998) Monitoring autoclave cure in commercial carbon fibre/epoxy composites. *Composites Part B: Engineering*. [Online] 29 (3), 245–250. Available from: doi:10.1016/S1359-8368(97)00020-6.
- Marand, E., Baker, K.R. & Graybeal, J.D. (1992) Comparison of reaction

## Experimental Results

- mechanisms of epoxy resins undergoing thermal and microwave cure from in situ measurements of microwave dielectric properties and infrared spectroscopy. *Macromolecules*. [Online] 25 (8), 2243–2252. Available from: doi:10.1021/ma00034a028.
- McIlhagger, A., Brown, D. & Hill, B. (2000) Development of a dielectric system for the on-line cure monitoring of the resin transfer moulding process. *Composites Part A: Applied Science and Manufacturing*. [Online] 31 (12), 1373–1381. Available from: doi:10.1016/S1359-835X(00)00050-6.
- Melin, L.G., Levin, K., Nilsson, S., Palmer, S.J.P., et al. (1999) A study of the displacement field around embedded fibre optic sensors. *Composites Part A: Applied Science and Manufacturing*. [Online] 30 (11), 1267–1275. Available from: doi:10.1016/S1359-835X(99)00036-6.
- Meredith, R.J. (1998) Engineers' Handbook of Industrial Microwave Heating. *IEE London UK ISBN*. [Online]. p.382. Available from: doi:10.1049/PBPO025E.
- Metaxas, A.C. & Meredith, R.J. (1983) *Industrial Microwave Heating*. [Online]. Available from: doi:10.1049/ep.1983.0309.
- Methven, J.M. & Ghaffariyan, S.R.. (1992) A Preliminary Assessment of the Microwave Assisted Pulwinding of Composite Re-Bars. In: *The Plastics and Rubber Institute. The 5th International Conference on Fibre Reinforced Composites, March 1992*. 1992 pp. 1–4.
- De Meuse, M.T. & Ryan, C.L. (1993) The microwave processing of polymeric materials. *Advances in Polymer Technology*. [Online] 12 (2), 197–203. Available from: doi:10.1002/adv.1993.060120207.
- Michaud, V. & Mortensen, A. (2001) Infiltration processing of fibre reinforced composites: Governing phenomena. *Composites - Part A: Applied Science and Manufacturing*. [Online] 32 (8), 981–996. Available from: doi:10.1016/S1359-835X(01)00015-X.
- Modi, D., Johnson, M., Long, A. & Rudd, C. (2009) Analysis of pressure profile and flow progression in the vacuum infusion process. *Composites Science and Technology*. [Online] 69 (9), 1458–1464. Available from: doi:10.1016/j.compscitech.2008.05.026.
- Patel, N., Perry, M.J. & Lee, L.J. (1991) Influence of RTM and SRIM Processing Parameters on Molding and Mechanical Properties. In: *Proc. Conf. Advanced Composites Materials: New Developments and Applications, Detroit, MI USA, September 1991*. 1991 pp. 105–113.
- Perry, M.J., Xu, J., Ma, Y., Wang, T.J., et al. (1992) Monitoring and Simulation of Resin Transfer Molding. In: *The Society of the Plastics Industry. Proceedings of the 7th Annual Conference of the Composites Institute*. 1992 pp. 1–13.
- Peterson, R.C. & Robertson, R.E. (1991) Flow Characteristics of Polymer Resin Through Glass Fiber Preforms in Resin Transfer Molding. In:

- Advanced Composite Materials: New Developments and Applications Conference Proceedings, Detroit, MI USA*. 1991 pp. 203–208.
- Pillai, K.M. & Advani, S.G. (1998a) A Model for Unsaturated Flow in Woven Fiber Preforms during Mold Filling in Resin Transfer Molding. *Journal of Composite Materials*. [Online] 32 (19), 1753–1783. Available from: doi:10.1177/002199839803201902.
- Pillai, K.M. & Advani, S.G. (1998b) Numerical simulation of unsaturated flow in woven fiber preforms during the resin transfer molding process. *Polymer Composites*. [Online] 19 (1), 71–80. Available from: doi:10.1002/pc.10077.
- Pillai, K.M. & Munagavalasa, M.S. (2004) Governing equations for unsaturated flow through woven fiber mats. Part 2. Non-isothermal reactive flows. *Composites Part A: Applied Science and Manufacturing*. [Online] 35 (4), 403–415. Available from: doi:10.1016/j.compositesa.2004.01.001.
- Rath, M., Doring, J., Stark, W. & Hinrichsen, G. (2000) Process monitoring of moulding compounds by ultrasonic measurements in a compression mould. *NDT and E International*. [Online] 33 (2), 123–130. Available from: doi:10.1016/S0963-8695(99)00029-8.
- Rooney, M., Biermann, P.J., Carkhuff, B.G., Shires, D.R., et al. (1998) Development of in-process RTM sensors for thick composite sections. In: *Proceedings of the 1998 American Control Conference. ACC (IEEE Cat. No.98CH36207)*. [Online]. 1998 IEEE. pp. 3875–3878 vol.6. Available from: doi:10.1109/ACC.1998.703374.
- Rowe, G.I., Yi, J.H., Chiu, K.G., Tan, J., et al. (1845) Fill-front and cure progress monitoring for vartm with auto-calibrating dielectric sensors. *Mechanical Engineering*. 1–14.
- Rudd, C.D. & Kendall, K.N. (1991) Modelling Non-Isothermal Liquid Moulding Processes. In: *Proceedings of the 3rd International Conference on Automated Composites, The Hague, Netherlands*. 1991 pp. 1–5.
- Rudd, C.D. & Kendall, K.N. (1992) Towards a Manufacturing Technology for High-Volume Production of Composite Components. *Proceedings of the Institution of Mechanical Engineers, Part B: Journal of Engineering Manufacture*. [Online] 206 (2), 77–91. Available from: doi:10.1243/PIME\_PROC\_1992\_206\_060\_02.
- Rudd, C.D., Owen, M.J. & Middleton, V. (1990) Effects of process variables on cycle time during resin transfer moulding for high volume manufacture. *Materials Science and Technology*. [Online] 6 (7), 656–665. Available from: doi:10.1179/mst.1990.6.7.656.
- Schledjewski, R. & Grössing, H. (2017) *Liquid Composite Molding: A Widely Used Group of FRPC Processing Techniques, but still a Challenging Topic*. [Online] 879, 1715–1720. Available from: doi:10.4028/www.scientific.net/MSF.879.1715.

## Experimental Results

- Schmachtenberg, E., Schulte Zur Heide, J. & Töpker, J. (2005) Application of ultrasonics for the process control of Resin Transfer Moulding (RTM). *Polymer Testing*. [Online] 24 (3), 330–338. Available from: doi:10.1016/j.polymertesting.2004.11.002.
- Schubel, P.J. (2010) Technical cost modelling for a generic 45-m wind turbine blade produced by vacuum infusion (VI). *Renewable Energy*. [Online] 35 (1), 183–189. Available from: doi:10.1016/j.renene.2009.02.030.
- Skordos, A.A., Karkanis, P.I. & Partridge, I.K. (2000) A dielectric sensor for measuring flow in resin transfer moulding. *Measurement Science and Technology*. [Online] 11 (1), 25–31. Available from: doi:10.1088/0957-0233/11/1/304.
- Slade, J., Pillai, K.M. & Advani, S.G. (2001) Investigation of unsaturated flow in woven, braided and stitched fiber mats during mold-filling in resin transfer molding. *Polymer Composites*. 22 (4), 491–505.
- Smyth, C.P. (1955) Dielectric Materials and Applications. *Journal of the American Chemical Society*. [Online] 77 (6), 1714–1714. Available from: doi:10.1021/ja01611a117.
- Sozer, E.M., Bickerton, S. & Advani, S.G. (2000) On-line strategic control of liquid composite mould filling process. *Composites Part A: Applied Science and Manufacturing*. [Online] 31 (12), 1383–1394. Available from: doi:10.1016/S1359-835X(00)00060-9.
- Staverman, A.J. & Schwarzl, F. (1956) Linear Deformation Behaviour of High Polymers. In: *Theorie und molekulare Deutung technologischer Eigenschaften von hochpolymeren Werkstoffen*. [Online]. Berlin, Heidelberg, Springer Berlin Heidelberg. pp. 1–125. Available from: doi:10.1007/978-3-662-01378-6\_1.
- Strand, N.S. (1980) Fast microwave curing of thermoset parts. *Modern plastics*. 57 (10), 64–67.
- Tinga, W.R. & Nelson, S.O. (1973) Dielectric Properties of Materials for Microwave Processing -Tabulated. *Journal of Microwave Power*. 8 (1) pp.23–65.
- Tuncol, G., Danisman, M., Kaynar, A. & Sozer, E.M. (2007) Constraints on monitoring resin flow in the resin transfer molding (RTM) process by using thermocouple sensors. *Composites Part A: Applied Science and Manufacturing*. [Online] 38 (5), 1363–1386. Available from: doi:10.1016/j.compositesa.2006.10.009.
- Vaidya, U.K., Jadhav, N.C., Hosur, M. V., Gillespie, J.W., et al. (2000) Assessment of flow and cure monitoring using direct current and alternating current sensing in vacuum-assisted resin transfer molding. *Smart Materials and Structures*. [Online] 9, 727–736. Available from: doi:10.1088/0964-1726/9/6/301.
- Verleye, B., Lomov, S. V., Long, A., Verpoest, I., et al. (2010) Permeability prediction for the meso-macro coupling in the simulation of the

- impregnation stage of Resin Transfer Moulding. *Composites Part A: Applied Science and Manufacturing*. [Online] 41 (1), 29–35. Available from: doi:10.1016/j.compositesa.2009.06.011.
- Walsh, S. (1993) *In-situ sensors method and device*.
- Weimer, C., Preller, T., Mitschang, P. & Drechsler, K. (2000a) Approach to net-shape preforming using textile technologies. Part I: edges. *Composites Part A: Applied Science and Manufacturing*. [Online] 31 (11), 1261–1268. Available from: doi:10.1016/S1359-835X(00)00073-7.
- Weimer, C., Preller, T., Mitschang, P. & Drechsler, K. (2000b) Approach to net-shape preforming using textile technologies. Part II: holes. *Composites Part A: Applied Science and Manufacturing*. [Online] 31 (11), 1269–1277. Available from: doi:10.1016/S1359-835X(00)00074-9.
- Woo Il Lee, Loos, A.C. & Springer, G.S. (1982) Heat of Reaction, Degree of Cure, and Viscosity of Hercules 3501-6 Resin. *Journal of Composite Materials*. [Online] 16 (6), 510–520. Available from: doi:10.1177/002199838201600605.
- Woo Il Lee & Springer, G.S. (1984) Microwave Curing of Composites. *Journal of Composite Materials*. [Online] 18 (4), 387–409. Available from: doi:10.1177/002199838401800405.
- Yenilmez, B. & Murat Sozer, E. (2009) A grid of dielectric sensors to monitor mold filling and resin cure in resin transfer molding. *Composites Part A: Applied Science and Manufacturing*. [Online] 40 (4), 476–489. Available from: doi:10.1016/j.compositesa.2009.01.014.
- Young, W.-B. & Tseng, C.-W. (1994) Study on the Pre-Heated Temperatures and Injection Pressures of the RTM Process. *Journal of Reinforced Plastics and Composites*. [Online] 13 (5), 467–482. Available from: doi:10.1177/073168449401300506.

# Appendix A: NUMERICAL SIMULATION OF THE RESIN FLOW

The appendix A is devoted to the numerical simulation of the resin flow through the fiber preform during the resin infusion. The back ground regarding the models developed and the approaches adopted by the researchers in the recent years were briefly described. Then, the development of a suitable numerical model of the resin flow was depicted.

## 1. Modelling of the resin flow in the liquid composite molding

**processes.**

The process modelling and simulation activities have paid a key role in the achievement of a more deep knowledge of the phenomena involved in the manufacturing of the composite materials. Resin flow through the fibrous reinforcement is commonly described as a fluid flow through a porous medium. In the relatively simple case of homogeneous porosity and permeability, the flow rate is dictated by the Darcy's law, stating the proportionality between the front velocity and the applied pressure gradient:

$$\mathbf{v}_s = -\frac{K}{\mu} \cdot \nabla p \quad (\text{A.1})$$

Being  $v_s$  fluid superficial velocity, which implicitly accounts for the volume porosity,  $K$  the permeability tensor,  $\mu$  the resin viscosity and  $\nabla p$  is the pressure gradient. Modelling the resin as an incompressible fluid, the set of equations to be solved is completed by the mass conservation:

$$\nabla \cdot \mathbf{v} = 0 \quad (\text{A.2})$$

## Appendix A

The reliability of impregnating flow simulation mainly depends on the adopted permeability values for the preform. As far as advanced composite materials are regarded, it is relevant to consider that in the case of the commonly used reinforcement architectures, such as woven or stitched fabrics, the aforementioned conditions are not satisfied. Textile permeability is generally an anisotropic and non-homogeneous property, which depends on the fabric structure and material. Indeed, the preform materials are constituted by fiber bundles (also called tows), which are themselves porous materials (Slade, Pillai & Advani, 2001; Ken Han, Lee & Rice, 2000).

In particular, micron sized pores can be individuated within each tow (intra-tow porosity) and millimeter sized pores between the tows (inter-tow porosity). This leads to a dual scale nature of the medium and to the establishment of macro and micro flows, exhibiting distinct impregnation rates. As a direct consequence, a single permeability value, or tensor, is not sufficient to describe both flows, since two phenomena, namely impregnation and saturation, must be accounted for. The dual-scale nature of many textiles has brought to the need for methodologies to assess simultaneously the inter-tow or macro flow, as well as the intra-tow or micro flow. The research activity was devoted to the development of a numerical multi-scale model of the vacuum assisted resin transfer molding (VARTM), a.k.a. resin infusion, process (Michaud & Mortensen, 2001; Pillai & Advani, 1998a).

Many efforts have been spent in the last years to develop a comprehensive model that is able to predict the real behavior of the resin during the preform impregnation. Among the different solution proposed, a suitable approach consists in modifying the mass balance equation of macro flow (eq.(A.2)) adding a negative sink term that accounts for the adsorption of resin from the inter-tow region into the tows due to their delayed impregnation. Satisfactory agreement between numerical and experimental results was claimed using this approach. Some authors adopted a rigorous mathematical approach and derived the equations of mass and momentum balance for the resin flow through the dual-scale preform leading to an integral expression for sink term applicable for any realistic dual-scale porous medium. The proposed model can also be extended to deal with the flow of a reactive liquid adding the effect of temperature and cure reaction in the governing equations, taking into account also heat convection and diffusion phenomena in the writing of the mass balance and sink term equations (Pillai & Munagavalasa, 2004; Lawrence, Neacsu & Advani, 2009).

However, significant simplifications had to be done. Indeed, in a first case, a simple cylindrical geometry of the tow was assumed, while the tow's cross section is no longer a circle when a compacted preform is considered, but rather an ellipsoid. In another case, a more realistic hypothesis of a rectangular shape was proposed. According to this assumption the flow through the smaller side surfaces can be neglected and only the flow through the upper and bottom surfaces is considered. The flow into the fiber bundles can be

therefore modelled as a one-dimensional flow and the flow rate used as sink term in macro-scale simulation.

## 2. The developed model of the micro-scale resin flow

The preform impregnation and saturation were simulated on the macroscale introducing a sink term  $S$  in eq.(A.2) and modifying eq.(A.1) introducing the pressure drop attributable to the micro flow, yielding:

$$\nabla \cdot \mathbf{v}_s = -S \quad (\text{A.3})$$

$$\mathbf{v}_s = -\frac{K_b}{\mu} \cdot \nabla p \quad (\text{A.4})$$

In the above equations  $K_b$  represents the bulk (or inter-tow) permeability tensor of the preform, whose porosity was defined assuming the fiber tows as solid element in macro-scale flow simulation. The bulk permeability and the mass flow rate through the fiber tows were not analytically derived, but assessed, for the used preform, by means of numerical flow simulations of inter- and intra-tow flows at the meso-scale.

A representative volume element (RVE) of the textile architecture was modelled at the meso-scale, using a reverse approach starting from post processing microstructure observation of composite laminates for permeability and saturation rate assessment. In particular, several samples were extracted by manufactured composite panel. Low magnification cross sectional images were acquired using an optical microscope. The obtained contours were finally used to generate the solid model of the RVE (see figure A.1).

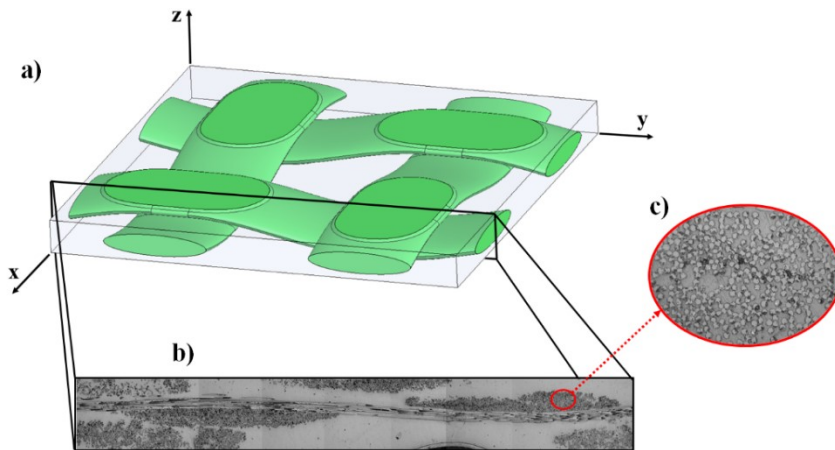


**Figure A.1.** *Microscopy observation of the manufactured laminates and 3D solid model of the representative volume element.*

## Appendix A

The intra-tow porosity was measured using high magnification images of the cross section of the intra-tow region as the ratio between the area occupied by the fibers and the overall analyzed area (Figure A.1c).

The basic assumption behind the used approach is that the macro- and micro- flow rate significantly differs, meaning that, in the same location, tow saturation is delayed with respect to the complete filling of macro-pores. Consequently, in the simulated RVE it is possible to separate the inter-tow and intra-tow flows and split the analysis in two distinct simulations. In both cases, a laminar flow condition, consistent with the relatively low Reynolds number characterizing this kind of processes, was enforced, neglecting body forces and capillary effects (Lawrence, Neacsu & Advani, 2009). Moreover, because of a unidirectional impregnation process was considered, only in plane bulk permeability value (unique due to the geometry of the RVE) is required. The bulk permeability was computed modelling the fiber tows as solid (impenetrable) material, therefore meshing only the inter-tow region. Steady-state mono-phase simulations, i.e. modelling the resin as the only fluid flowing through the computational domain, were launched, imposing a predefined pressure gap (1 kPa) between the inlet and outlet boundary, as indicated in Figure A.2. It should be noted that the definition of the pressure gap was definitely arbitrary. In fact, each variation in the pressure difference implies a proportional variation of the mass flow rate, thus leaving the permeability value unchanged. Periodic boundary conditions were applied on opposite surfaces closing the domain along the in-plane directions, while no slip conditions were imposed on the surfaces normal to the out-of-plane direction (Verleye *et al.*, 2010).

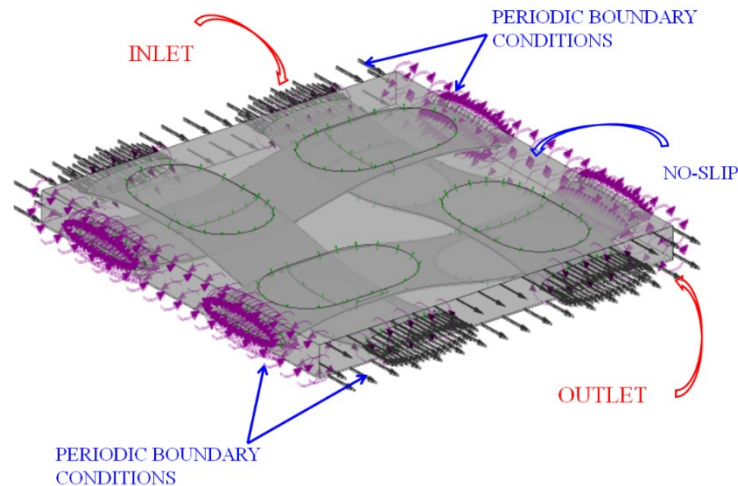


**Figure A.2.** Schematic of the domain and the applied boundary conditions

The equation describing the sink term was formulated post-processing numerical outcomes provided by transient multi-phase simulations in the same

computational domain. At the macro-scale, this term affects the continuity equation, introducing, with the negative sign, the rate of mass “disappearing” from the inter-tow region and penetrating in the intra-tow region. Consequently, the sink term equation can be derived, at the meso-scale, estimating the amount of mass moving from the fluid zone to the porous one.

The transient simulation was organized into two consecutive main steps, assuming the initial conditions as follows:

- the inter-tow region is completely filled by the liquid phase and no air presence is allowed; the liquid is assumed stationary at a uniform pressure given by the average value between the inlet and outlet pressures;
- in the intra-tow region, no liquid phase is initially allowed (zero saturation) and the only existing and stationary fluid is compressible air at the pressure imposed during the process by the vacuum pump.

The first step evaluates the pressure and velocity fields established in the inter-tow region before the beginning of any intra-tow flows. Afterwards, in the second step, a conservative interface flux condition was activated at the surfaces separating the fluid and the porous regions, in order to allow the liquid to penetrate inside the porous subdomain (Kuentzer *et al.*, 2006). A comprehensive simulation campaign was launched varying the initial average pressure in the RVE, providing, for each case, the mass flow rate for a set of pressure and saturation values. Finally, a regression analysis was carried out in the MATLAB environment on numerical outcomes. Polynomial and non-polynomial forms for the sink term were tested, in order to derive an analytical formulation to be applied in the equations regulating the macro scale model. Afterwards, the governing equation of the macro-scale model were modified to include relevant information to predict resin macro flows. The model was validated by comparison with data acquired during a properly designed unidirectional infusion test.

### 3. Results of the simulation

Figure A.3 shows the result the flow simulation in meso-scale level. The streamlines of the resin flowing through the representative volume element are depicted. A prevalent flow can be observed in the unreinforced region between the two bundles parallel to the impregnation direction. On the other hand, the overlapping between crossing fiber tows actually represents a tangible obstacle, related to the materializing of a low permeability zone, opposing to the flow. In the relatively larger unreinforced zones, the local velocity profile appears, with reasonable approximation, flat with negligible transversal flows. On the contrary, when a transverse bundle is approached, the reduction of the high permeability section available for resin flow induces an increase in the velocity of the impregnating fluid.

## Appendix A

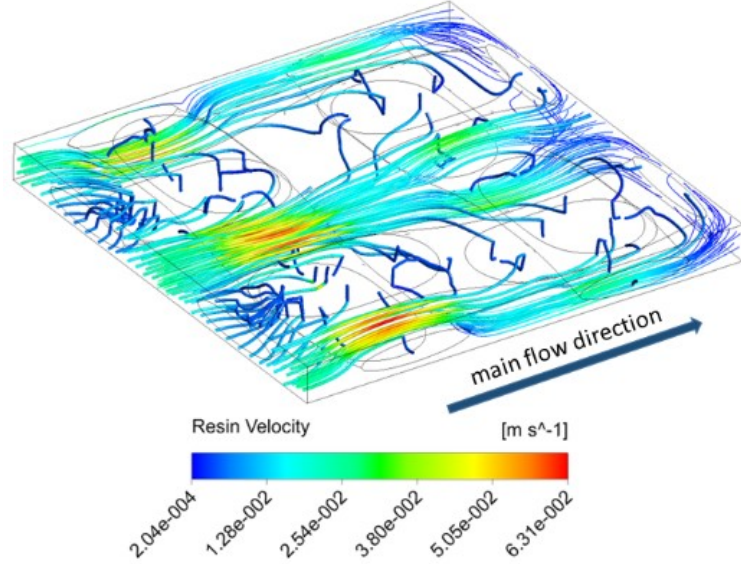


**Figure A.3** Streamlines of the inter-to flow in the representative volume element.

The bulk permeability value, along the main flow direction, was inferred post processing the fluid velocity field at the inlet (or outlet) surfaces, according to the following discretization of the Darcy law (eq.(A.1)):

$$Q = - \frac{K_b A (p_{in} - p_{out})}{\mu L} \quad (A.5)$$

being  $Q$  the liquid flow rate,  $K_b$  the bulk permeability along the main flow direction,  $\mu$  the liquid viscosity,  $L$  and  $A$  the length and the cross section of the RVE,  $p_{in}$  and  $p_{out}$  the inlet and outlet pressures, respectively. The application of Eq. 7 to simulation results provided, for the modelled preform, a bulk permeability  $K_b$  equal to  $6.089 \text{ E-}9 \text{ m}^2$ . The computed permeability value is several orders of magnitude higher than the tow transverse permeability, estimated from the consolidated analytical model as  $9 \text{ E-}13 \text{ m}^2$ , assuming 0.5 as fiber volume fraction within the tow, according to the performed microstructure analysis. The remarkable difference in permeability clearly indicates that, considering the same fluid properties and the same applied pressure gradients, the liquid flow through the inter-tow region (macro-flow) is significantly faster than the flow through the intra-tow region (micro-flow). This confirms the assumption according to which the fiber bundles were modelled as impenetrable solid material.

The bulk permeability is the dominant parameter regulating the macro-flow, on the contrary the sink term  $S$  plays a key role to explain the occurrence of micro-flows and the formation of uncoherent matrix-reinforcement

## Numerical Simulation Of The Resin Flow

interface (Pillai & Advani, 1998b). The sink term is modelled as a function of saturation index  $s$ , indicating the volume fraction of micro pores filled by the resin within the tow, and the average liquid pressure  $p$  in the surrounding inter-tow region. The reliability of the simulation results on the macroscale relies not only on the trustable bulk permeability estimation, but also on the correct description of this term. The explicit form of  $S$  will vary depending on different parameters, such as preform type, tows and fibers arrangement, as well as the impregnation history (i.e. pressure values establishing during the filling, residual air percentage, and so on). The amount of resin drawn off by the tow from the macro flow region depends also on the micro permeability of the tow, that is many order of magnitude smaller than the macro permeability (Pillai & Munagavalasa, 2004). Once the tows are fully saturated the sink term disappears and the preform behaves as a single scale medium.

Figure A.4 shows a representative result of the simulation launched, depicting the variation of the sink term with the saturation for a given value of average liquid pressure in the RVE. Please note that the very first part of the sink term curve, exhibiting a positive slope, represents a numerical error attributable to the first simulation step finalized to the computation of the redistribution of the liquid pressure. Thus, it was not included in the regression analysis. After the re-equilibrium of the liquid pressure, a continuous reduction of the liquid mass penetrating into the porous region, and consequently of the sink term, is detected as the saturation increases.

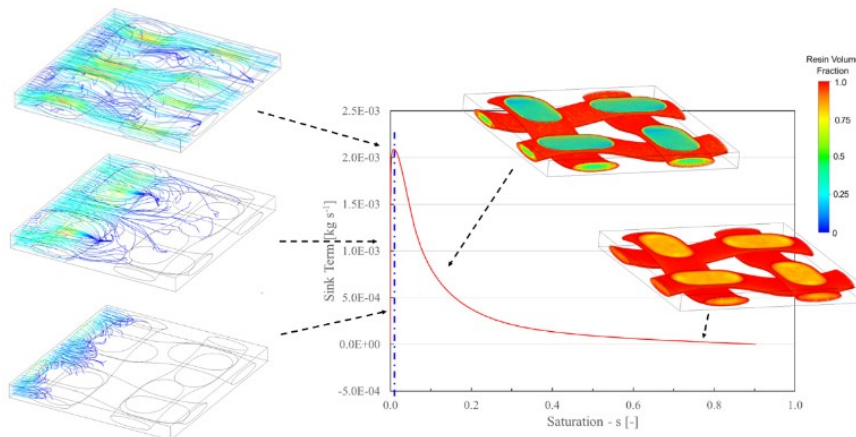


**Figure A.4.** Sink term variation as a function of the saturation

The reduction of the sink term with the saturation can be intuitively explained considering that at higher saturation levels corresponds to higher resin mass already present in the peripheral zone of the porous region that must be pushed toward the center of the tow, under vacuum condition, by the incoming fluid. Moreover, the presence of liquid resin within the tow implies a reduction of the pressure gradient at the saturating flow front, thus, according

## Appendix A

to the Darcy law, the micro-flow slowing is well motivated. As apparent from Figure A.4, the sink term reduces with the saturation until a null value is reached when  $s$  approaches the unit value. Different simulation trials of resin flow in RVE domain were performed varying the average liquid pressure, a linear dependence of the numerically predicted sink term on the average liquid pressure for distinct saturation levels has been observed.

Figure A.5 shows the dependence of the numerically predicted sink term on the average liquid pressure for distinct saturation levels. The plot highlights that this relationship is linear with reasonable approximation. The lines, fitting the points characterized by the same saturation level, exhibit increasing slopes as the saturation decreases, congruently with the profile reported in Figure A.4 and converge to the null value of the sink term for an abscissa value equal to the applied vacuum pressure. In fact, as the liquid pressure in the inter-tow region matches the applied vacuum pressure, the pressure gradient vanishes and, congruently with the Darcy law, the flow front velocity vanishes.

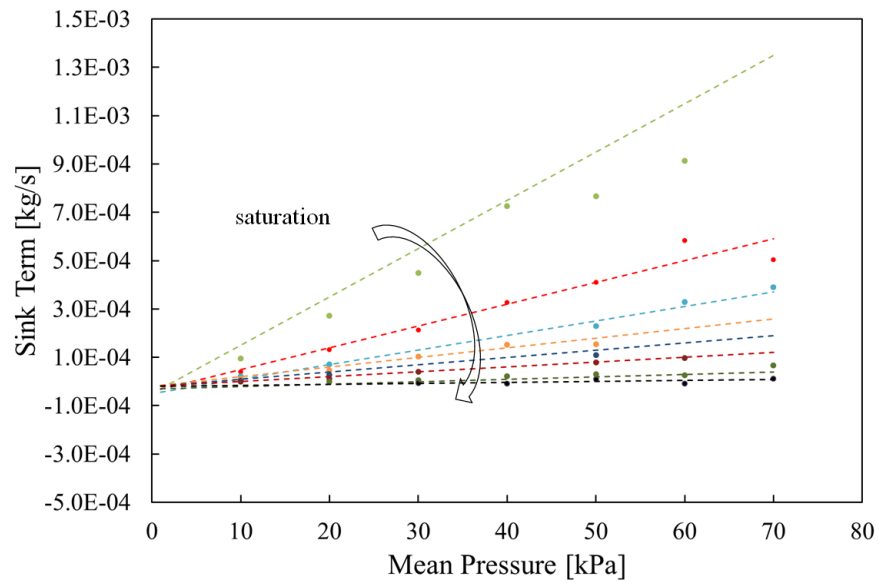


**Figure A.5.** Sink term as a function of the inter-tow liquid pressure

Taking such observations into account, the following form for the sink term was proposed:

$$S = S(s, p) = m(s)(p - p_0), \quad (\text{A.6})$$

Modelling the sink term as a family of straight lines, nulling when the liquid pressure matches the applied vacuum pressure and with saturation dependent angular coefficient  $m(s)$ . Different forms for the relationship  $m(s)$  were hypothesized. The earlier attempt was assuming a low order polynomial

## Numerical Simulation Of The Resin Flow

form for  $m(s)$ , to high order polynomial model. Acceptable data fitting was achieved adopting a polynomial order higher than 5 with a correlation index major than 0.99. Higher order polynomials did not significantly improve the quality of the solution (see figure A.6).

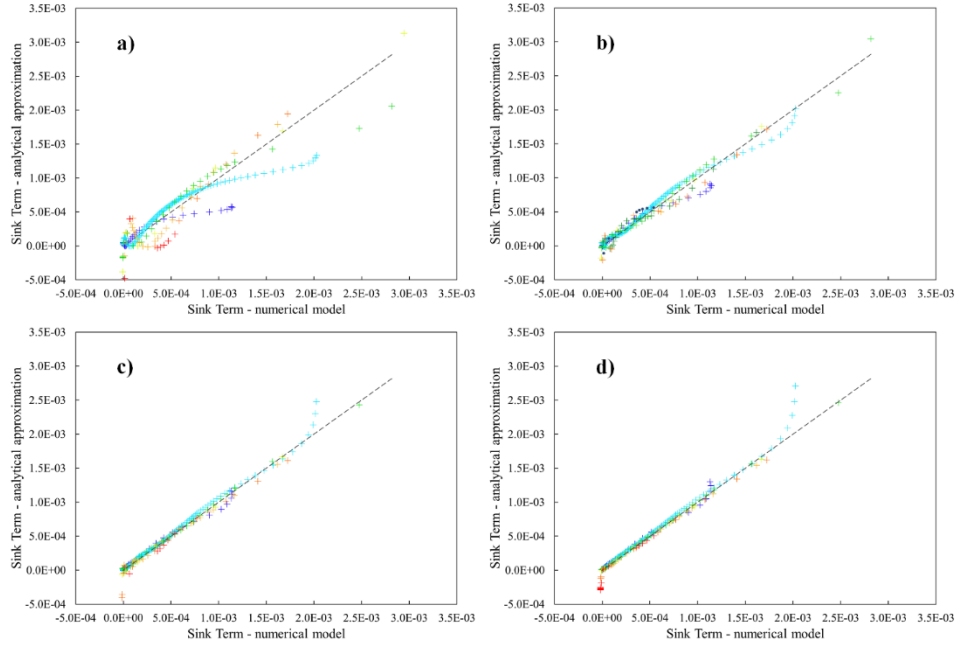


**Figure A.6.** Results of the regression analysis for the angular coefficient  $m(s)$ : a) third order polynomial model, b) fifth order polynomial model, c) seventh order polynomial model, d) exponential model.

However, the polynomial form is negatively affected by oscillations of the prediction when the plateau of the curve is approached, causing the computation of negative values for  $S$ . It could determine on the macroscale level an unrealistic mass generation term, when the tow reaches a high saturation level. In addition, it also could result in a non-null value of  $S$  at full tow saturation. To address such problems, an alternative form based on an exponential regression model is proposed, according to the following equation:

$$m(s) = c_1 \exp(-k_1 s) + c_2 \exp(-k_2 s) \quad (\text{A.7})$$

Being  $c_1$ ,  $c_2$ ,  $k_1$ , and  $k_2$  constant values obtained by fitting simulation data and dependent on the architecture, geometrical features and size, and material properties of the porous domain. The values of the parameter for the RVE considered, for the hypotheses and the boundary conditions adopted are listed in the table A.1

## Appendix A

**Table A.1.** *Sink term parameters*

$c_1$ [Pa <sup>-1</sup> s <sup>-1</sup> ]	$k_1$	$c_2$ [Pa <sup>-1</sup> s <sup>-1</sup> ]	$k_2$
2.846 E-5	4.24	7.091e-5	17.66

Once assessed the proper form for the sink term, the simulation of the resin macro-flow was performed according to the eqs.(A.3),(A.4) and (A.7).